AFIT/GAE/ENY/91D-18

APPLICATION OF MIXED H_2/H_∞ OPTIMIZATION

THESIS

John J. Kusnierek
Captain, USAF
AFIT/GAE/ENY/91D-18

REPORT DOCUMENTATION PAGE

Form Approved
OMB No. 0704-0188

1. AGENCY USE ONLY (Leave blank)	2. REPORT DATE	3. REPORT TYPE AND DATES COVERED
	December 1991	Master's Thesis

4. TITLE AND SUBTITLE

Application of Mixed H_2/H_∞ Optimization

5. FUNDING NUMBERS

6. AUTHOR(S)

John J. Kusnierek, Captain, USAF

7. PERFORMING ORGANIZATION NAME(S) AND ADDRESS(ES)

Air Force Institute of Technology, WPAFB OH 45433-6583

8. PERFORMING ORGANIZATION REPORT NUMBER

AFIT/GAE/ENY/91D-18

9. SPONSORING / MONITORING AGENCY NAME(S) AND ADDRESS(ES)

WL/FIGC
Wright-Patterson AFB, OH 45433

10. SPONSORING / MONITORING AGENCY REPORT NUMBER

11. SUPPLEMENTARY NOTES

12a. DISTRIBUTION / AVAILABILITY STATEMENT

Approved for public release; distribution unlimited

12b. DISTRIBUTION CODE

13. ABSTRACT *(Maximum 200 words)*

A non-conservative optimization technique is utilized to examine the problem of minimizing the 2 norm of one transfer function subject to an ∞-norm bound on another transfer function. For single exogenous input/single exogenous output systems this nonconservative mixed solution is shown to be up to 5% better in a specific example. For single exogenous input/two exogenous output systems the mixed solution is shown to be up to 27% better than a previous technique for a specific example. Finally, a two exogenous input/two exogenous output practical system is examined to demonstrate the utility of this mixed optimization technique.

14. SUBJECT TERMS

Control Theory, White Noise, Linear Systems, Mathematical Filters

15. NUMBER OF PAGES

121

16. PRICE CODE

17. SECURITY CLASSIFICATION OF REPORT	18. SECURITY CLASSIFICATION OF THIS PAGE	19. SECURITY CLASSIFICATION OF ABSTRACT	20. LIMITATION OF ABSTRACT
Unclassified	Unclassified	Unclassified	UL

AFIT/GAE/ENY/91D-18

APPLICATION OF MIXED H_2/H_∞ OPTIMIZATION

THESIS

Presented to the Faculty of the School of
Engineering of the Air Force Institute
of Technology
In Partial Fulfillment of the
Requirements for the Degree of
Master of Science in Aeronautical Engineering

John J. Kusnierek, B.S.
Captain, USAF

November 1991

Acknowledgements

I'd like to thank my advisor, Captain D. Brett Ridgely, for his help and guidance in doing this thesis. I'd also like to thank Maj. Curtis Mracek for his great help sorting out software problems. Dr. Brad Leibst deserves a thank you as well for his excellent help educating me about Matlab and related state space issues. Of my sponsors in the Controls Analysis Group, Captain Andy Sparks was especially helpful regarding the Bernstein & Haddad solution. Finally, I thank my wife Imaculada and sons John & Chris for their support while completing this thesis.

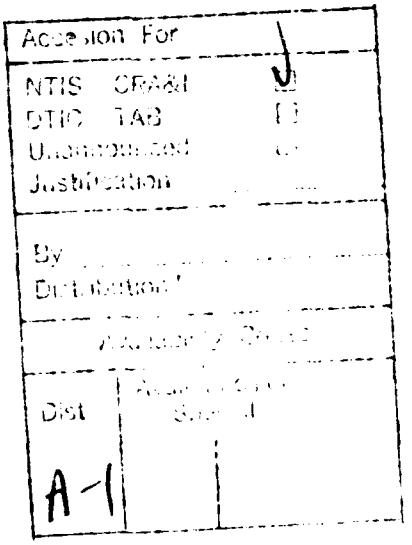

Table of Contents

List of Figures

Application of Mixed H_2/H_∞ Optimization

Abstract

A nonconservative optimization technique is utilized to examine the problem of minimizing the 2 norm of one transfer function subject to an ∞-norm bound on another transfer function. For single exogenous input/single exogenous output systems this nonconservative mixed solution is shown to be up to 5% better than a previous technique in a specific example. For single exogenous input/two exogenous output systems the mixed solution is shown to be up to 27% better than a previous technique for a specific example. Finally, a two exogenous input/two exogenous output practical system is examined to demonstrate the utility of this mixed optimization technique.

Application of Mixed H_2/H_∞ Optimization

Chapter I. Introduction

1.1 Background

The designer of a Single-Input-Single-Output (SISO) or Multiple-Input-Multiple-Output (MIMO) system must contend with two major factors in the design process. First, the design must minimize the energy of the output errors in the face of input noises. Second, the design must minimize the output errors given a non-noise bounded energy input that would affect robustness. Noise sensitivity will be called performance in this work, and using the LQG techniques in modern control theory is easily handled. LQG by itself however usually exacerbates robustness problems. LQG/LTR addresses robustness in an unstructured manner, but an acknowledged shortcoming in modern control design has been the lack of visibility into performance/robustness trade-offs.

Recent efforts have focused on characterizing this problem with the 2-norm as a measure of performance and the ∞-norm as a measure of robustness. These are usually referred to as H_2/H_∞ Optimization problems and they can be formulated in a variety of different ways. The formulation for this thesis can be stated as maximizing performance at a

given robustness level. Numerous approaches to this problem currently exist, but only one is non-conservative. The non-conservative approach was first forwarded in 1991 by Ridgely [1] and will be referred to as the Mixed Solution throughout this thesis.

The Mixed Solution has only recently become available and allows H_2/H_∞ trade-offs to be made for a wide class of systems. The robustness design parameter can be used to handle a variety of problems such as unmodeled dynamics, sensor bias and disturbances, excessive gain scheduling, and input disturbances.

1.2 Purpose

The purpose of this thesis is to demonstrate the use of the Mixed Solution and compare results to other techniques. First, the Mixed Solution will be compared to the H_∞ Central controller for a system with a single exogenous input and a single exogenous output (1I1O). Then, the Mixed Solution will be compared to the technique forwarded by Bernstein and Haddad [5] for a system with one exogenous input and two exogenous outputs (1I2O). Finally, a physically motivated system with two exogenous inputs and two exogenous outputs (2I2O) will be examined using the Mixed Solution to demonstrate the practical aspects of this technique (no other two-in two-out techniques exist for comparison). Various plants will be used.

1.3 Overview

In Chapter 2, various aspects of control theory and the role of H_2 and H_∞ theory are discussed. In Chapter 3, the procedure and analysis techniques required to obtain a Mixed Solution are discussed. In Chapter 4, problem synthesis, description, and results for the 1I1O system are discussed. Likewise in Chapter 5, the 1I2O system is covered and in Chapter 6 the 2I2O system. Chapter 7 contains a summary and conclusions followed by recommendations for further study.

The software package PRO-MATLAB was used for this thesis. FORTRAN 77 (UNIX) was also utilized.

Chapter II. Mixed H_2/H_∞ Control Theory

2.1 Singular Values, H_2 Norm, and H_∞ Norm

The basic analysis tool in multivariable control design is the singular value versus frequency plot. The singular values of a matrix A are related to the eigenvalues of A as follows

$$\sigma_i(A) = [\lambda_i(A^*A)]^{1/2} \tag{2.1}$$

with $\sigma_i(A)$ = ith singular value
λ_i = ith eigenvalue
A^* = complex conjugate transpose of A
$A \in C^{m \times n}$

The largest singular value is denoted $\bar{\sigma}$ and the smallest is denoted $\underline{\sigma}$. These two scalars are a measure of the size (gain) of a transfer function matrix at a given frequency. Thus, $\bar{\sigma}$ and $\underline{\sigma}$ are frequency dependent. In SISO systems, $\bar{\sigma} = \underline{\sigma}$ and a plot of $\bar{\sigma}$ verses frequency is just the Bode magnitude plot. The 2-norm is related to the area under the σ vs ω (frequency) curve and is given by

$$\|G(j\omega)\|_2^2 = \frac{1}{2\pi}\int_{-\infty}^{\infty} tr\,[G^*(j\omega)\,G(j\omega)]\,d\omega \tag{2.2}$$

By Parseval's Theorem it can be seen that this is the transfer function's total energy output. This nicely

characterizes the energy of a system in the presence of white noise.

The ∞-norm of a transfer function is given by

$$\|G(j\omega)\|_\infty = \sup_\omega \bar{\sigma}\ [G(j\omega)] \tag{2.3}$$

and is a measure of the maximum gain of the transfer function. Thus, a singular value plot with a large spike, and hence large ∞-norm, would not be considered robust at the spike's frequency because any excitation at the frequency of the spike causes a potentially disastrous gain. Another way of looking at the ∞-norm this is through the small gain theorem. Suppose we have

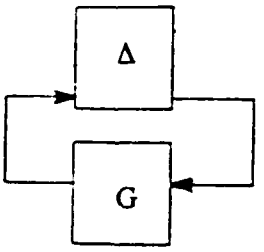

Figure 2.1 Small Gain Block Diagram

with G and $\Delta \in RH_\infty$. Then this system is closed loop stable if

$$\|\Delta\|_\infty \cdot \|G\|_\infty < 1 \tag{2.4}$$

If $\|G\|_\infty < \gamma$ then

$$\|\Delta\|_\infty < \frac{1}{\gamma} \tag{2.5}$$

is sufficient to guarantee stability of the system. Thus, the smaller γ ($\|G\|_\infty$) is, the larger $\|\Delta\|_\infty$ can be and still have guaranteed system stability. If we think of Δ as a system disturbance or uncertainty and G as a nominal closed-loop system, then keeping γ low will maximize the system's disturbance tolerance or robustness.

2.2 Motivation and Characterization

Any physical system will have noise and uncertainty in it. Thus, it makes sense to want to minimize the system's sensitivity to noise and maximize its robustness. In this thesis, this problem, called mixed H_2/H_∞ optimization, is formulated as:

infimize $\|T_{zw}\|_2$	subject to the constraint
K stabilizing	that $\|T_{ed}\|_\infty \leq \gamma$

With a system as shown in Figure 2.2, T_{zw} indicates the z to w transfer function while T_{ed} the e to d transfer function.

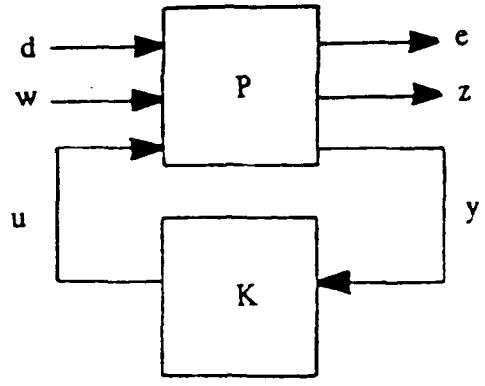

Figure 2.2 Standard Problem Block Diagram

The w input will normally be white noise while the d input will be bounded energy disturbances. The following definitions are helpful:

γ_o = inf $\|T_{ed}\|_\infty$
K stabilizing

α_o = inf $\|T_{zw}\|_2$
K stabilizing

K_{2opt} = K required to achieve α_o

γ_2 = $\|T_{ed}\|_\infty$ when $K = K_{2opt}$

For clarity in the following discussion, consider $T_{zw} = T_{ed}$. First, it can be seen that minimizing $\|T_{zw}\|_2$ will produce a system of finite (and probably low) bandwidth in

order to minimize the area under the plot. However, minimizing $\|T_{ed}\|_\infty$ typically produces a closed-loop system of infinite bandwidth, as the low frequency energy is forced to higher and higher frequencies. Thus, mixed H_2/H_∞ optimization has competing objectives.

When $\|T_{zw}\|_2$ is at α_o, the resulting controller (K_{2opt}) is unique. Thus, K_{2opt} will produce a finite $\|T_{ed}\|_\infty$ (γ_2) which is as large as $\|T_{ed}\|_\infty$ will ever get in the mixed H_2/H_∞ problem. As $\|T_{ed}\|_\infty$ approaches γ_o, $\|T_{zw}\|_2$ goes to infinity since the closed-loop bandwidth (and thus area under the curve) typically becomes infinite. A typical trade-off would look like that in Figure 2.3.

No matter how large γ gets, $\|T_{ed}\|_\infty$ will never exceed γ_2. In fact, it really makes no sense to talk about mixed H_2/H_∞ solutions with $\gamma>\gamma_2$ since there is no trade-off, and the solution is just trivially K_{2opt}. The above plot has been shown [1] to be monotonically decreasing for the Mixed Solution.

Of key importance is that, for $\gamma>\gamma_o$, the controller that gives $\|T_{ed}\|_\infty \leq \gamma$ is not unique. An infinite number of stabilizing controllers can achieve $\|T_{ed}\|_\infty \leq \gamma$. Thus, for $\gamma_o<\gamma<\gamma_2$, the family of stabilizing controllers will contain a controller such that $\|T_{zw}\|_2$ is a minimum given $\|T_{ed}\|_\infty \leq \gamma$. In (1:120) it is shown that this minimum is achieved with a controller such that $\|T_{ed}\|_\infty = \gamma$. The curve given by a plot such as in Figure 2.3 is, for the Mixed Solution, a true

trade-off; that is, for a given γ level (and controller order), no other controller exists that will give a lower $\|T_{zw}\|_2$. Currently, only the Mixed Solution can make this claim, since other methods involve overbounds of varying tightness.

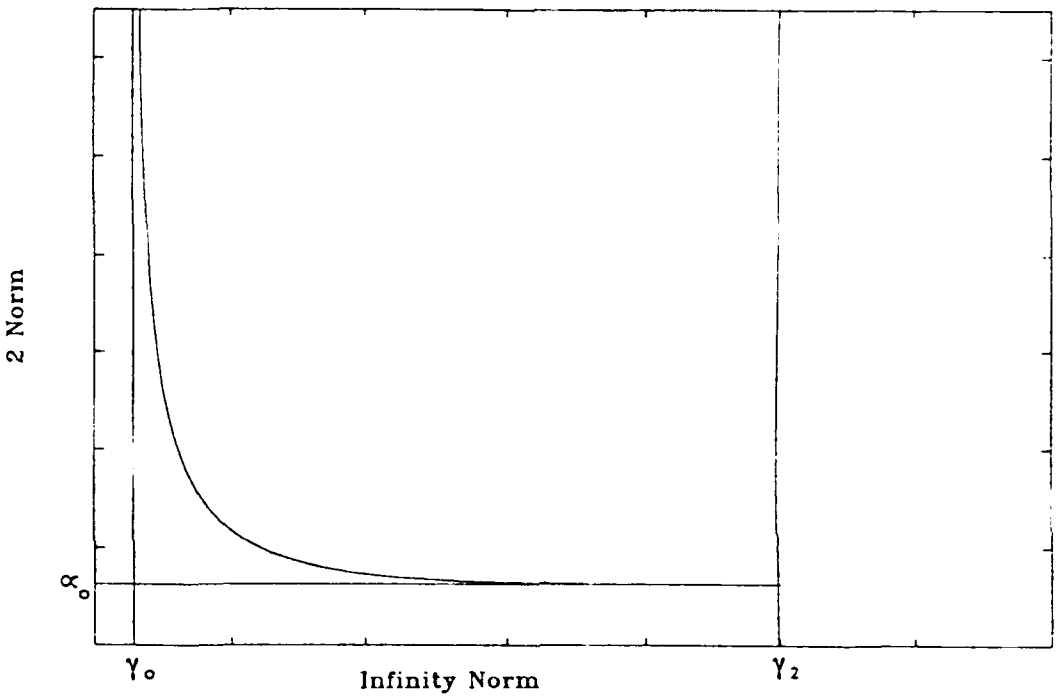

Figure 2.3 Typical Performance/Robustness Trade-off

2.3 Mixed H_2/H_∞ Control Theory [1]

Recall that the mixed H_2/H_∞ problem is

$$\text{infimize } \|T_{zw}\|_2 \quad \text{subject to } \|T_{ed}\|_\infty \leq \gamma$$

We are trying to find a controller K that accomplishes the above.

This is a linear time invariant feedback control system. Also note that this may be an output feedback

controller or a full state feedback controller. The exogenous inputs in the d vector represent commands, disturbances, etc. into the plant P. The regulated output in the e vector is the system response that will be associated with the ∞-norm. The exogenous inputs in the w vector represent white noises coming into the plant P. The regulated output in the z vector is the system response that will be associated with the 2-norm. The output y is fed to the controller K which generates the u input into P. The plant can be represented in partitioned transfer function form as

$$P = \begin{bmatrix} P_{ed} & P_{ew} & P_{eu} \\ P_{zd} & P_{zw} & P_{zu} \\ P_{yd} & P_{yw} & P_{yu} \end{bmatrix} \tag{2.6}$$

which yields:

$$e = P_{ed}d + P_{ew}w + P_{eu}u \tag{2.7}$$

$$z = P_{zd}d + P_{zw}w + P_{zu}u \tag{2.8}$$

$$y = P_{yd}d + P_{yw}w + P_{yu}u \tag{2.9}$$

Using a lower linear fractional transformation, the transfer

functions T_{zw} and T_{ed} are:

$$T_{zw} = P_{zw} + P_{zu}K\,[I - P_{yu}K]^{-1}\,P_{yw} \tag{2.10}$$

$$T_{ed} = P_{ed} + P_{eu}K\,[I - P_{yu}K]^{-1}\,P_{yd} \tag{2.11}$$

Note that the characteristic equation and hence system stability is determined by the $[I-P_{yu}K]^{-1}$ term. There are, of course, "cross transfer functions" T_{ew} and T_{zd}, but neither of them is directly addressed in the mixed problem. They really don't need to be included, since any concern about these cross transfer functions should be taken care of through modeling.

A state space realization of P is given by

$$P = \left[\begin{array}{c|ccc} A & B_d & B_w & B_u \\ \hline C_e & D_{ed} & D_{ew} & D_{eu} \\ C_z & D_{zd} & D_{zw} & D_{zu} \\ C_y & D_{yd} & D_{yw} & D_{yu} \end{array}\right] \tag{2.12}$$

which results in:

$$\dot{x} = A_x + B_d d + B_w w + B_u u \tag{2.13}$$

$$e = C_e x + D_{ed} d + D_{ew} w + D_{eu} u \tag{2.14}$$

$$z = C_z x + D_{zd} d + D_{zw} w + D_{zu} u \tag{2.15}$$

$$y = C_y x + D_{yd} d + D_{yw} w + D_{yu} u \tag{2.16}$$

Note that D_{zw} must be zero or the 2-norm of T_{zw} will be infinite for any controller. D_{ed} and D_{yu} are assumed to be zero for convenience. Further, the plant must satisfy the following conditions:

1) (A, B_u) stabilizable and (C_y, A) detectable

2) $D_{eu}^T D_{eu}$ full rank and $D_{yd} D_{yd}^T$ full rank

3) $D_{zu}^T D_{zu}$ full rank and $D_{yw} D_{yw}^T$ full rank

4) $\begin{bmatrix} A - j_w I & B_u \\ C_e & D_{eu} \end{bmatrix}$ full column rank for all w

5) $\begin{bmatrix} A - j_w I & B_d \\ C_y & D_{yd} \end{bmatrix}$ full row rank for all w

6) $\begin{bmatrix} A - j_w I & B_u \\ C_z & D_{zu} \end{bmatrix}$ full column rank for all w

7) $\begin{bmatrix} A - j_w I & B_w \\ C_y & D_{yw} \end{bmatrix}$ full row rank for all w

Condition 1 must be satisfied or there exists no stabilizing controllers. Conditions 2) through 7) come from various aspects of the individual H_2 and H_∞ problems which are assumed to be met in the mixed H_2/H_∞ problem [1].

The compensator K is given in state space by:

$$\dot{x}_c = A_c x_c + B_c y \tag{2.17}$$

$$u = C_c x_c + D_c y \tag{2.18}$$

Again, to avoid an infinite $\|T_{zw}\|_2$, D_c must equal zero. This does not result in loss of generality [1]. This thesis assumes that the order of the controller equals the order of the plant. It as been shown [4] that the optimal controller has an order higher than that of the plant (possibly infinite). It is often true that higher order controllers gain little in performance.

Closing the P-K loop results in:

$$\dot{\tilde{x}} = \tilde{A}\tilde{x} + \tilde{B}_d d + \tilde{B}_w w \tag{2.19}$$

$$e = \tilde{C}_e \tilde{x} + D_{ew} w \tag{2.20}$$

$$z = \tilde{C}_z \tilde{x} + D_{zd} d \tag{2.21}$$

where

$$\tilde{A} = \begin{bmatrix} A & B_u C_c \\ B_c C_y & A_c \end{bmatrix} \tag{2.22}$$

$$\tilde{B}_d = \begin{bmatrix} B_d \\ B_c D_{yd} \end{bmatrix} \tag{2.23}$$

$$\tilde{B}_w = \begin{bmatrix} B_w \\ B_c D_{yw} \end{bmatrix} \tag{2.24}$$

$$\tilde{C}_e = [C_e \quad D_{eu} C_c] \tag{2.25}$$

$$\tilde{C}_z = [C_z \quad D_{zu} C_c] \tag{2.25}$$

Note that closed loop system stability is determined by $\tilde{A}$. Now,

$$\|T_{zw}\|_2^2 = tr\,[Q_2 \tilde{C}_z^T \tilde{C}_z] \tag{2.27}$$

where Q_2 is the solution to the Lyapunov equation

$$\tilde{A} Q_2 + Q_2 \tilde{A}^T + \tilde{B}_w \tilde{B}_w^T = O \tag{2.28}$$

Also, $\|T_{ed}\|_\infty \leq \gamma$ if there exists a $Q_\infty = Q_\infty^T \geq 0$ satisfying

$$\tilde{A} Q_\infty + Q_\infty \tilde{A}^T + \gamma^{-2} Q_\infty \tilde{C}_e^T \tilde{C}_e Q_\infty + \tilde{B}_d \tilde{B}_d^T = O \tag{2.29}$$

with $\hat{A}$ stable. $\hat{A}$ is stable if $(\tilde{A}, \tilde{B}_d)$ is stabilizable.

From here, the problem can be cast as a Lagrange Multiplier Problem with $J = \|T_{zw}\|_2^2 = tr\ [Q_2\tilde{C}_z^T\tilde{C}_z]$ (minimizing the square of the function is the same as minimizing the function). The constraints are the Lyapunov Equation 2.28 and the Ricatti Equation 2.29.

$$\mathcal{L} = tr\ [Q_2\tilde{C}_z^T\tilde{C}_z] + tr\{[\tilde{A}Q_2 + Q_2\tilde{A}^T + \tilde{B}_w\tilde{B}_w^T]\mathbf{X}\} \tag{2.30}$$

$$+ tr\{[\tilde{A}Q_\infty + Q_\infty\tilde{A}^T + \gamma^{-2}Q_\infty\tilde{C}_e^T\tilde{C}_eQ_\infty + \tilde{B}_d\tilde{B}_d^T]\mathbf{Y}\}$$

The first order necessary conditions for a minimum are found by evaluating.

$$\frac{\partial\mathcal{L}}{\partial A_c} = \frac{\partial\mathcal{L}}{\partial B_c} = \frac{\partial\mathcal{L}}{\partial C_c} = \frac{\partial\mathcal{L}}{\partial\mathbf{X}} = \frac{\partial\mathcal{L}}{\partial\mathbf{Y}} = \frac{\partial\mathcal{L}}{\partial Q_2} = \frac{\partial\mathcal{L}}{\partial Q_\infty} = O \tag{2.31}$$

These necessary conditions represent a set of 7 matrix equations. These matrix equations, however, do not lend themselves to an immediate solution. Numerical techniques must be used. The particular technique used in this thesis is covered in Chapter 3.

Chapter III. Analysis and Procedure

3.1 Solution Technique [1]

The objective is to generate a $\|T_{zw}\|_2$ versus $\|T_{ed}\|_\infty$ curve for a given system. This entails selecting a γ ($\gamma_o < \gamma < \gamma_2$) and solving the mixed problem. The 7 necessary conditions mentioned in Chapter 2 are coupled and highly nonlinear. No known analytic solution exists, so a numerical technique must be used.

In order to facilitate a numerical solution, the performance index is changed to

$$J = (1-\mu)\, tr[Q_2 \tilde{C}_z^T \tilde{C}_z] + \mu\, tr[Q_\infty \tilde{C}_e^T \tilde{C}_e] \tag{2.36}$$

where μ is a numerical convergence parameter. At $\mu = 1$, the problem reverts to the minimum entropy problem with a well known and easily obtainable solution. In [1:134], it is shown that as $\mu \to 0$ the solution does converge to the mixed H_2/H_∞ solution.

The choice of numerical technique is critical, since there are a large number of unknowns, the problem is highly nonlinear, and computation of second derivatives (fourth order tensors) is unwieldly. In connection with research in this area, a Davidon-Fletcher-Powell (DFP) algorithm had

already been coded up in Fortran. The code was modified to include a Ricatti solver and to allow for increased problem size.

The DFP problem is formulated [8] as minimizing a scalar function F given a vector of unknowns X. The direction, S, in which to move the unknowns is given as a function of the gradient $\nabla F(x)$

$$S = H \cdot \nabla F(x)$$

where H is the second derivative matrix. H does not have to be analytically derived; it can be approximated adequately. The step size K is determined by minimizing F(X + KS) by numerical means. Equality boundaries are enforced by artifically setting F(X + KS) to a large number (10^{16}) if the boundary is violated. This has the effect of causing the step to back away from the boundary.

In this particular problem, the boundary constraints are determined by four of the seven necessary condition equations

$$\tilde{A}Q_z + Q_z\tilde{A}^T + \tilde{B}_w\tilde{B}_w^T = O \tag{3.1}$$

$$\tilde{A}^T\mathbf{X} + \mathbf{X}\tilde{A} + (1-\mu)\,\tilde{C}_z^T\tilde{C}_z = O \tag{3.2}$$

$$\tilde{A}Q_\infty + Q_\infty\tilde{A}^T + \gamma^{-2}Q_\infty\tilde{C}_e^T\tilde{C}_eQ_\infty + \tilde{B}_d\tilde{B}_d^T = O \tag{3.3}$$

$$[\tilde{A} + \gamma^{-2}Q_\infty\tilde{C}_e^T\tilde{C}_e]^T\mathbf{Y} + \mathbf{Y}[\tilde{A} + \gamma^{-2}Q_\infty\tilde{C}_e^T\tilde{C}_e] + \mu\,\tilde{C}_e^T\tilde{C}_e = O \tag{3.4}$$

As shown in [1:143,144] the Q_z, Q_∞, X and Y solutions must be positive semidefinite. Also, for $\mu \neq 0$, $(\tilde{A} + \gamma^{-2}\,Q_\infty\tilde{C}_e^T\tilde{C}_e)$ must be stable. Note that $\tilde{A}$ contains the controller A_c, B_c, and C_c matrices, and thus contains all the unknowns. The number of unknowns is

$$(\#\text{ states})^2 + (\#\text{ inputs})(\#\text{ states}) + (\#\text{ outputs})(\#\text{states})$$

Convergence is checked by observing the change in F with respect to the last iteration's F. With ε as the convergence criteria, this can be formulated as

$$\frac{\nabla F^T H \nabla F}{\|F(x)\|} < \epsilon \tag{3.5}$$

The flow diagram for this algorithm is given in Figure 3.1. This problem does not have guaranteed convexity, so a good starting point is critical. The starting point here is a guess at the controller. In addition to satisfying $\|T_{ed}\|_\infty \leq$

γ, the start point controller must satisfy Equations 3.1 through 3.4. Typically, when starting a new problem, this would be chosen to be the H_∞ central controller, although any admissible "nearby" controller is acceptable.

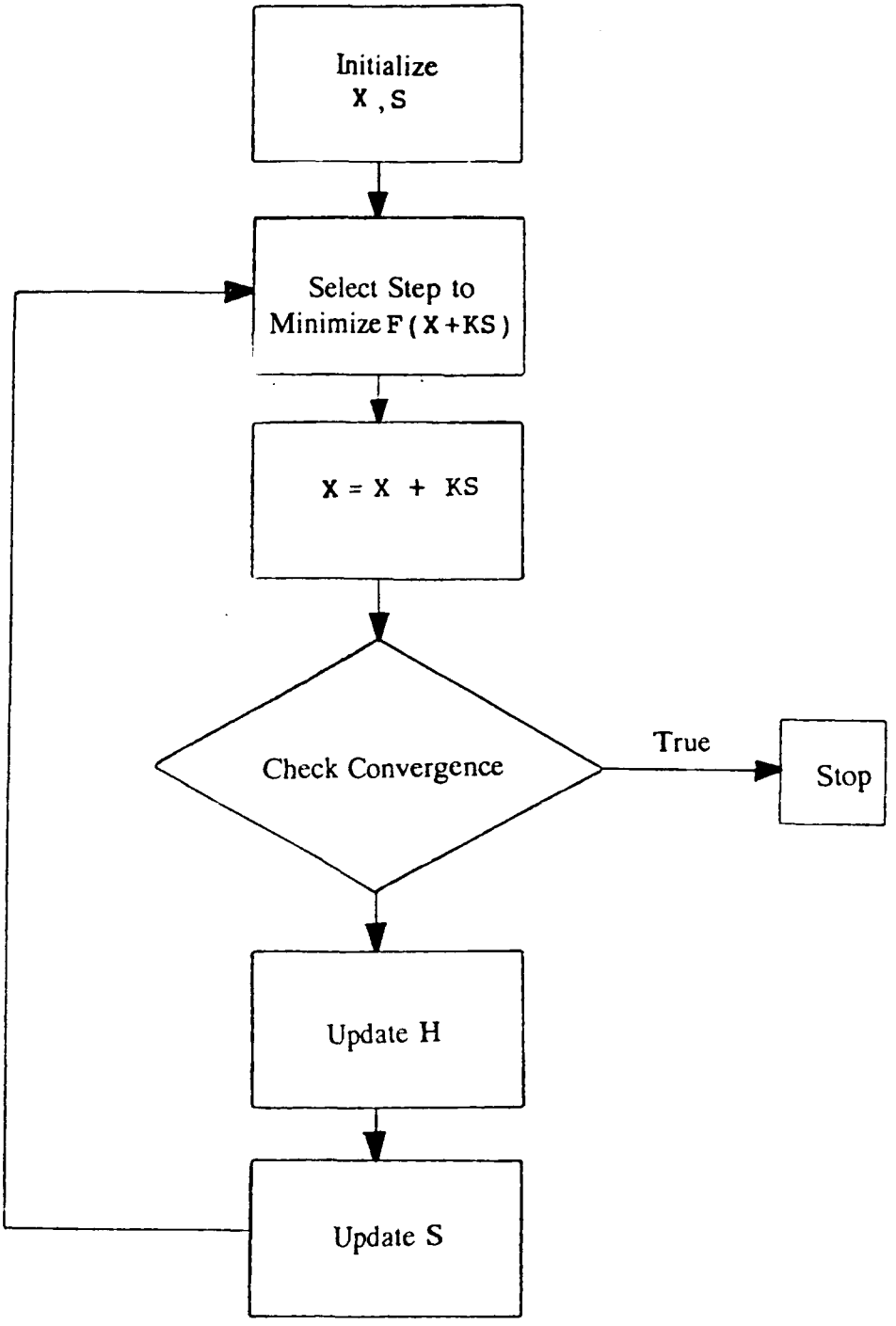

Figure 3.1 DFP Flowchart

3.2 Procedure

Matlab is used to initially characterize the system by finding γ_o,γ_2, and α_o. Normally, a γ slightly greater than γ_o is chosen, and then Matlab can be used to generate the H_∞ central controller as a start point. This controller is then transferred to a Fortran input file for use by DFP. Of note is that the problem is easier to solve at γ close to γ_2 when using "overbound" start points, because the start point ∞-norm is usually far less than the γ that generated it. Near γ_o, the slack in the $\|T_{ed}\| \leq \gamma$ portion of the problem is getting much tighter (in fact going to zero). This means that the start point becomes increasingly critical as $\gamma \rightarrow \gamma_o$. At each γ level, the μ that is initially set is a guess that takes into account how close the starting point is to the minimum entropy solution and how much μ can be decreased from the starting point and still get numerical convergence. Starting with the H_∞ central solution, the first DFP run would probably use $.5 \leq \mu \leq .99$. The controller output from that run is then used in a subsequent DFP run at a lower μ. The amount that μ can be decreased between runs seems to depend largely on the closeness to γ_o. Near γ_o, μ might be decremented as 0.9, 0.7, 0.5, 0.4, 0.3, 0.2, 0.1, 0.01, whereas near γ_2, μ might be decremented as 0.5, 0.1, 0.01, 0.001. This is, of course, problem dependent, and one must keep in mind that the problem may be changing drastically with changes in μ. From the problems that were done in

connection with this thesis, a μ of about 0.001 is adequate for convergence to the mixed solution at a given γ level. This gives $\|T_{ed}\|_\infty = \gamma$ to about four decimal places and $\|T_{zw}\|_2$ unchanging to about 7 decimal places. An advantage to starting the γ sweep near γ_o and moving toward γ_2 is that subsequent γ levels can be started using the converged output controller from the previous γ level ($\|T_{ed}\|_\infty \leq \gamma$ and K stabilizing is automatically satisfied). Thus, the H_∞ central controller need not be generated for each γ level. A procedural flowchart is given in Figure 3.2.

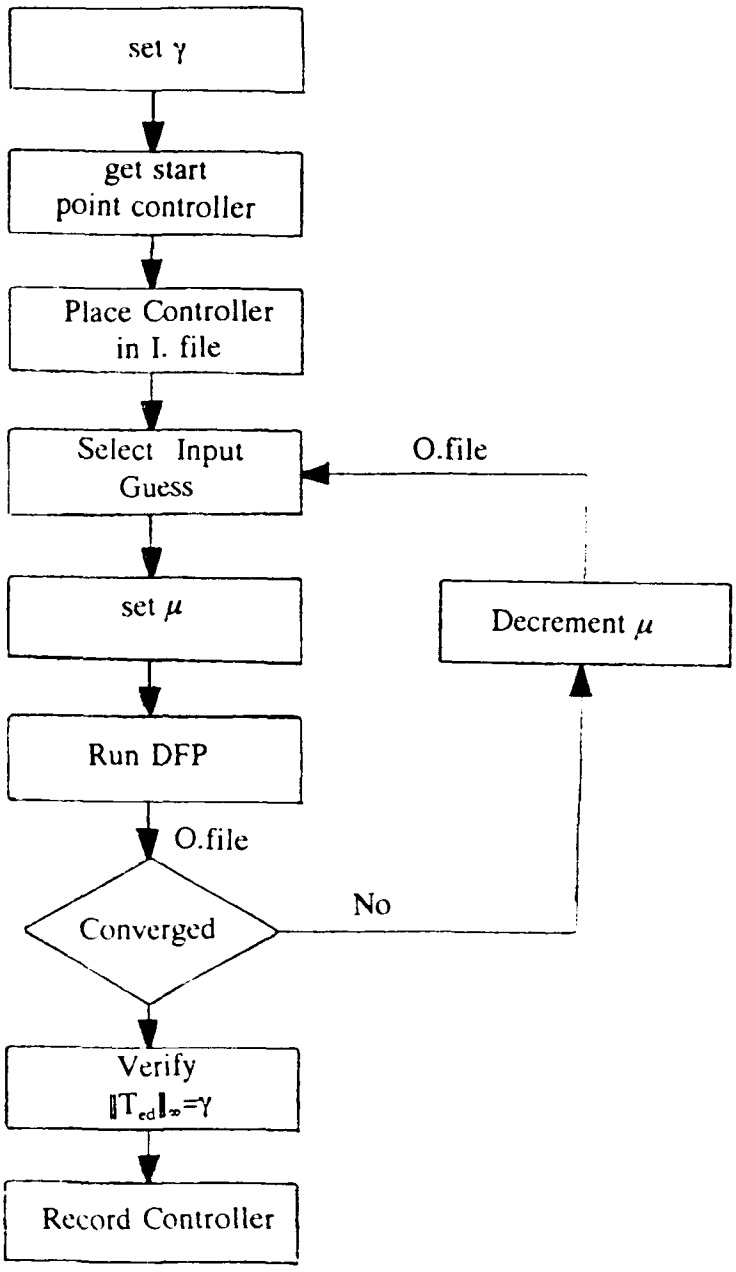

Figure 3.2 Procedural Flowchart

3.3 Set-up

For a given physical system, the block diagram for the system is manipulated into the state space form:

$$\dot{x} = Ax + B_d d + B_w w + B_u u \tag{3.6}$$

$$e = C_e x + D_{ed} d + D_{ew} w + D_{eu} u \tag{3.7}$$

$$z = C_z x + D_{zd} d + D_{zw} w + D_{zu} u \tag{3.8}$$

$$y = C_y x + D_{yd} d + D_{yw} w + D_{yu} u \tag{3.9}$$

There are several tuning parameters available for the designer to control the optimization. The P matrix elements B_d, B_w, C_e, C_z, D_{yd}, D_{yw}, D_{eu}, and D_{zu} are selectable and have the following interpretation:

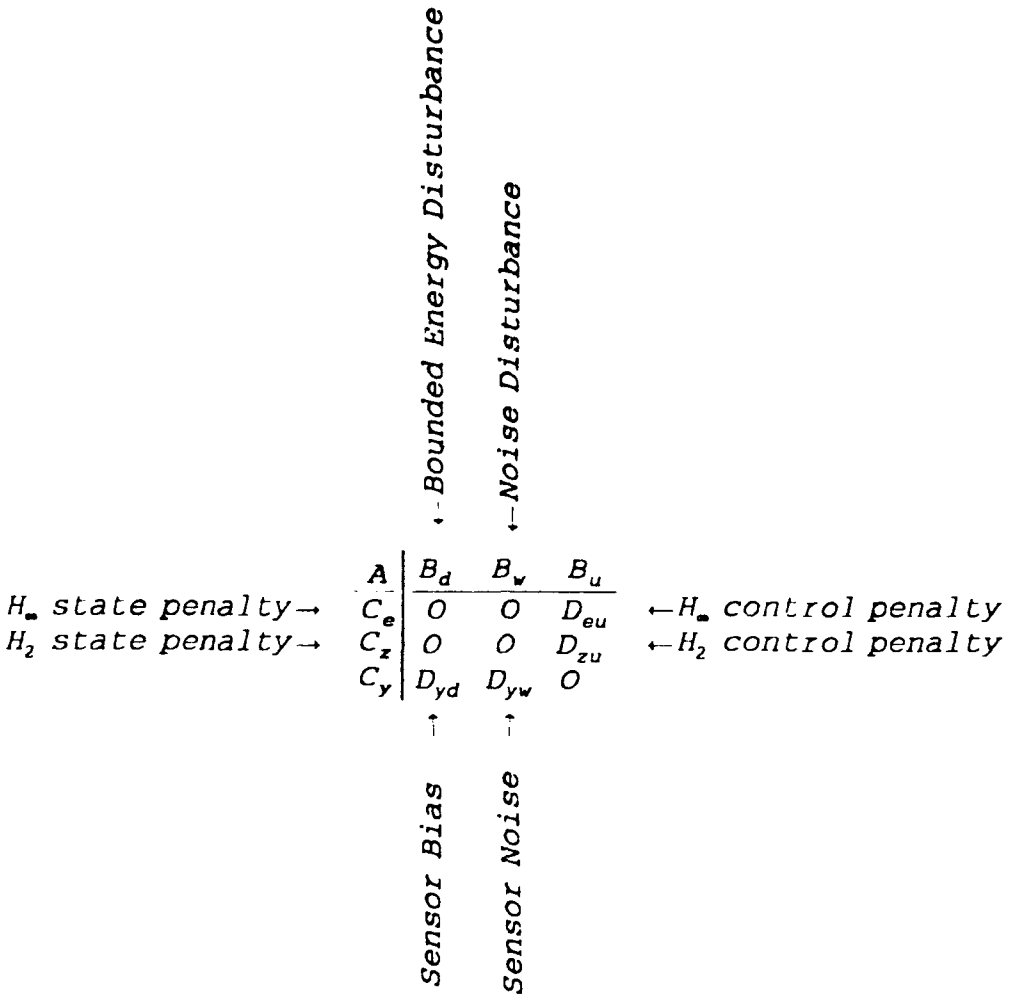

From here, an input file is created (see Appendix A for an example). The DFP program has all real numbers in DOUBLE PRECISION format. For this thesis, all DFP runs were made with the following parameters:

Q_2 positive definiteness boundary = -10^{-20}

Q_∞ positive definiteness boundary = -10^{-20}

X positive definiteness boundary = -10^{-10}

Y positive definiteness boundary = -10^{-10}

$[\tilde{A} + \gamma_{-2} Q_\infty C_e^T C_e]$ stability boundary = $+10^{-8}$

Convergence Criteria ε (Checkstop) = $+10^{-8}$

Chapter IV. One Exogenous Input One Exogenous Output

4.1 Problem Synthesis

This system has one exogenous input and one exogenous output (1I1O). In standard form, it is represented as in Figure 4.1:

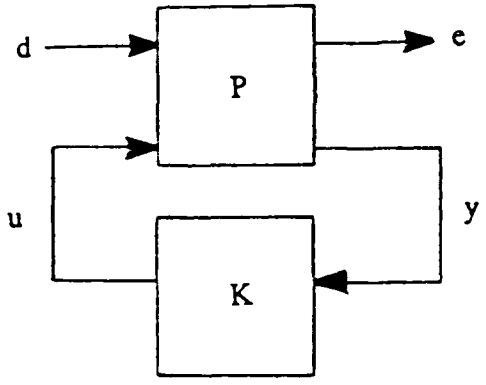

$$P = \left[\begin{array}{c|cc} A & B_d & B_u \\ \hline C_e & O & D_{eu} \\ C_y & D_{yd} & O \end{array}\right]$$

Figure 4.1 1I1O Standard Form

Thus, the mixed problem is

$$\inf_{K \text{ stabilizing}} \|T_{ed}\|_2 \qquad \text{subject to } \|T_{ed}\|_\infty \le \gamma$$

so that we are expecting both bounded energy inputs and noise inputs to be contained in d and we are looking at performance and robustness with respect to the same transfer function. In other words, performance with a guaranteed level of robustness, with respect to the same transfer function.

This is equivalent to

$$\inf_{K \text{ stabilizing}} \|T_{zw}\|_2 \qquad \text{subject to } \|T_{ed}\|_\infty \le \gamma$$

with $T_{ed} = T_{zw}$. An associated block diagram for such a system is shown in Figure 4.2.

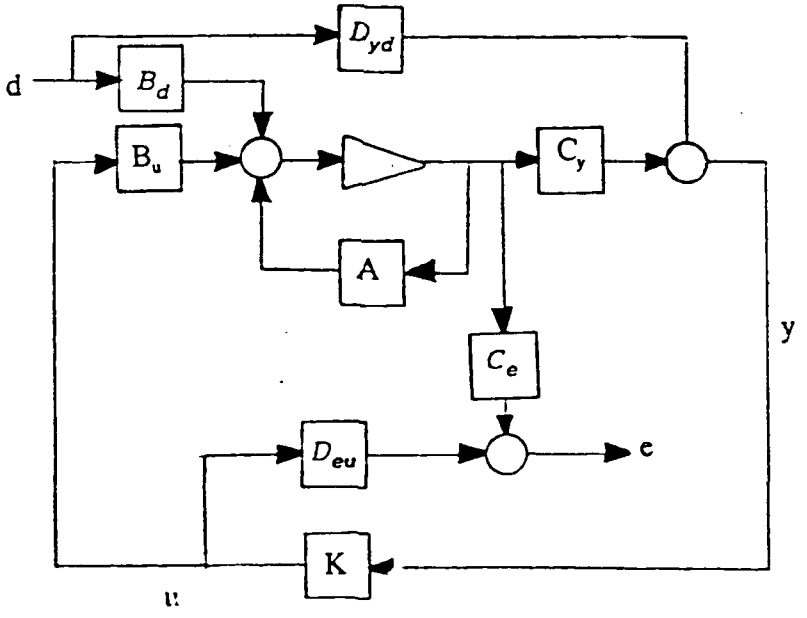

Figure 4.2 System Block Diagram

4.2 Background

Prior to the Mixed Solution, the best solution to this problem was the Minimum Entropy or H_∞ central solution. In this chapter, the Mixed Solution will be compared with an H_∞ central solution for an example system. It has been shown [6:12] that as $\gamma \rightarrow \infty$, the Minimum Entropy (ME) and the H_2 problem are equivalent. For γ less than ∞, $\|T_{ed}\|_\infty$ with the ME controller is less than γ and $\|T_{ed}\|_2$ with the ME controller is an upper bound on the minimum $\|T_{ed}\|_2$. This problem has an analytic solution. Changing the block diagram to that in Figure 4.3, K is the lower linear fractional transformation of J and Q, where

$$J = \left[\begin{array}{c|cc} A_j & \tilde{K}_f & K_{f1} \\ \hline -\tilde{K}_c & O & S_u^{-1} \\ K_{c1} & S_y & O \end{array}\right] = \begin{bmatrix} J_{uy} & J_{ui} \\ J_{oy} & J_{oi} \end{bmatrix}$$

J is found by solving a pair of algebraic Ricatti equations (with both solutions positive semidefinite). The only constraint on Q is that it be stable and that $\|Q\|_\infty < \gamma$. Thus, a K such that $\|T_{ed}\| \leq \gamma$ is not unique. However, in [6:19-22] it is shown that the ME controller is just J with Q=0, and hence the name H_∞ central. The ME controller then is

$$K = \left[\begin{array}{c|c} A_J & \bar{K}_f \\ \hline -\bar{K}_c & O \end{array} \right]$$

As noted in Chapter 2, this K is the same as the Mixed Solution with $\mu = 1$. Of key importance is that the ME solution is really only applicable to 1I1O systems.

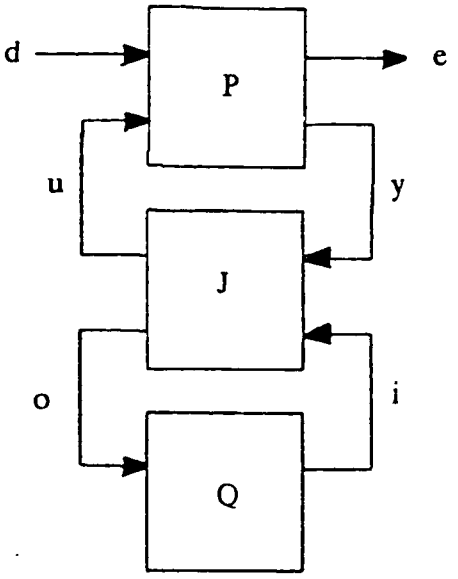

Figure 4.3 Extended Standard Form

4.3 Description

The system chosen was the same as in [1]. It is a third order, unstable, minimum phase system, with

$$\lambda_1, \lambda_2 = -.6812 \pm j\ 1.182$$
$$\lambda_3 = +.9549$$

zeros at -1.1990, $-.0490$

The open loop singular value (SV) plot is shown in Figure 4.4. Note the lightly damped zero. The state space matrices are:

$$A = \begin{bmatrix} -.3908 & -.4565 & 1.266 \\ 1.445 & -1.049 & 1.208 \\ -.1288 & .6744 & 1.032 \end{bmatrix}$$

$$B_d = \begin{bmatrix} .0488 \\ .3608 \\ .3564 \end{bmatrix} \quad B_u = \begin{bmatrix} -.4275 \\ -.4470 \\ -.9172 \end{bmatrix}$$

$$C_e = [\,.9420 \quad .0144 \quad .1187\,]$$

$$C_y = [\,-1.557 \quad -1.943 \quad -.0914\,]$$

$$D_{yd} = [\,.5185\,]$$

$$D_{eu} = [\,1.3575\,]$$

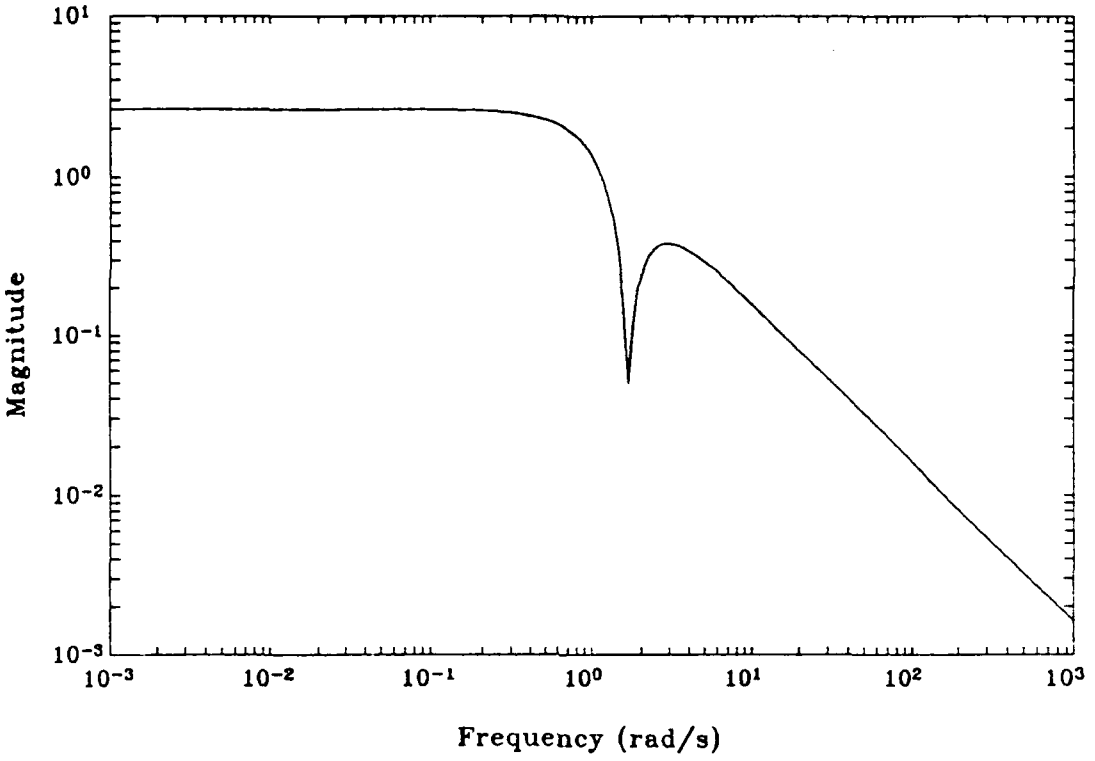

Figure 4.4 σ-Plot of the Open Loop System

Looking at the closed loop system using the optimal H_∞ controller, it can be seen in Figure 4.5 that an infinite bandwidth system results with $\gamma_o = 2.1426$. As shown in Figure 4.6, the controller also has infinite bandwidth. Closing the loop with the H_{2opt} controller results in a higher ∞-norm and a more typical finite bandwidth singular value plot (Figure 4.5). This controller results in $\gamma_2 = 4.163$ and $\alpha_o = 3.248$. Figure 4.6 shows that this controller has finite bandwidth. Of note is that both controllers have a spike corresponding to the lightly damped zero in the plant.

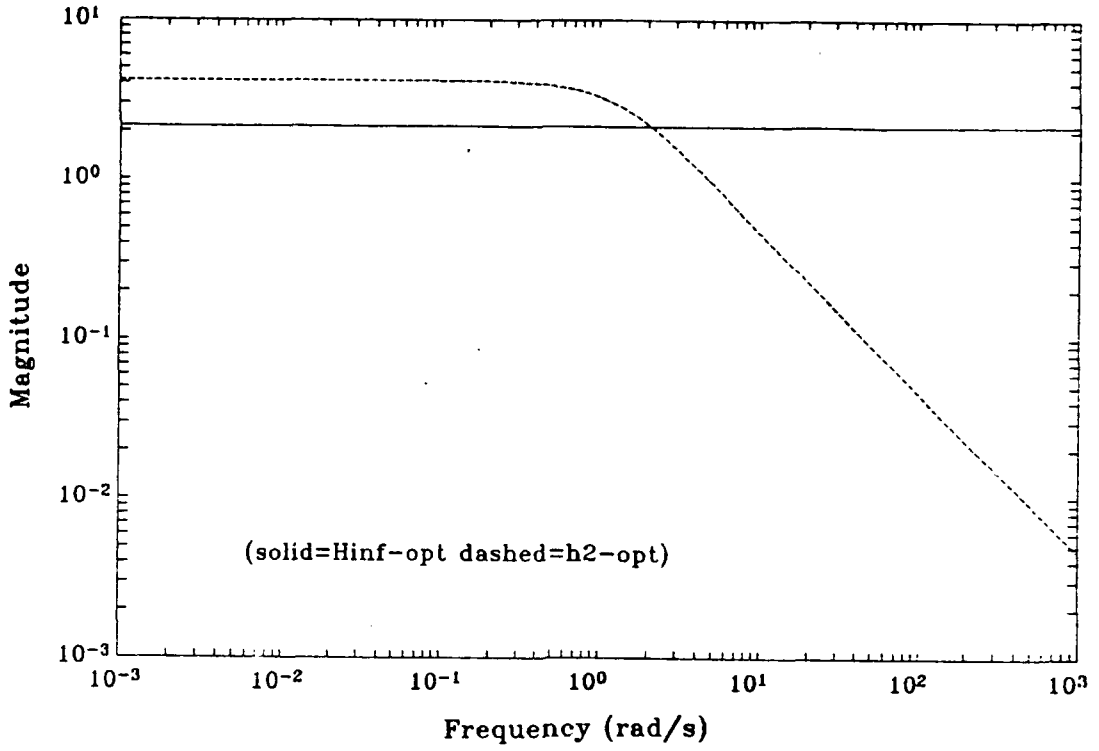

Figure 4.5 σ-Plot of the H_2 & H_∞ Optimal T_{ed}

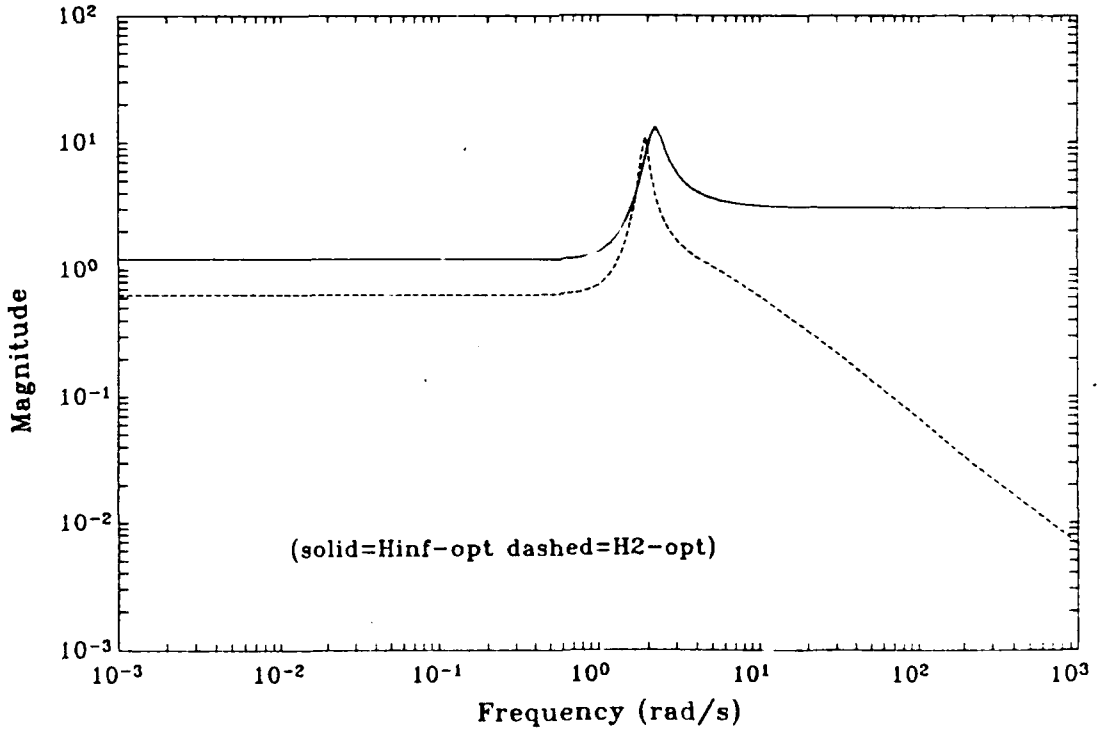

Figure 4.6 σ-Plot of H_2 & H_∞ Optimal Controllers

4.4 Results

The Mixed Solution for this system was determined using the procedure outlined previously. As shown in Figure 4.7, the Mixed Solution is clearly better than the H_∞ central solution. The maximum difference between the two solutions is about 5 percent at a γ_{mix} of about 2.5. As Figures 4.7 and 4.8 show, the two solutions converge as $\gamma \to \gamma_2$ or $\gamma \to \infty$. Table 4.1 shows the comparison for selected γ_{mix} levels. Note that care must be taken in such a table because $\gamma_{mix} = \|T_{ed}\|_\infty$ but $\|T_{ed}\|_\infty \leq \gamma_{H\ CENTRAL}$ so that for a fair comparison either γ_{mix} or $\gamma_{H\ CENTRAL}$ should be adjusted such that $\|T_{ed}\|_\infty$ is the same.

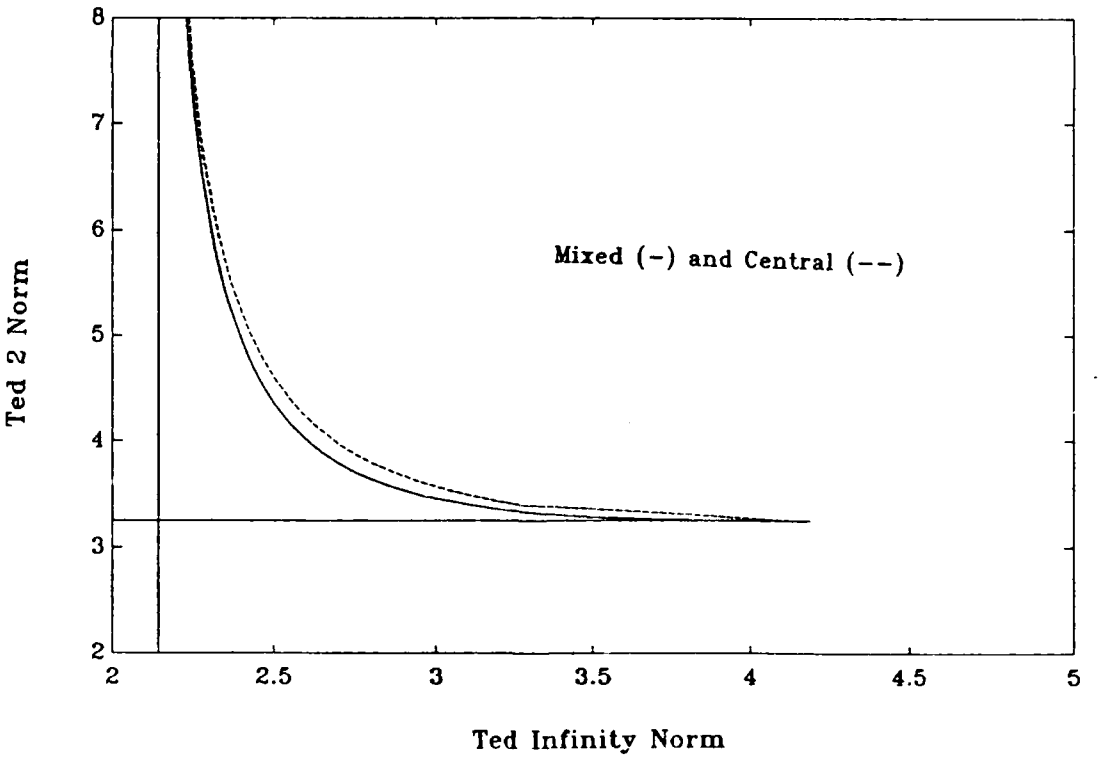

Figure 4.7 Comparison of Mixed and Central Controllers

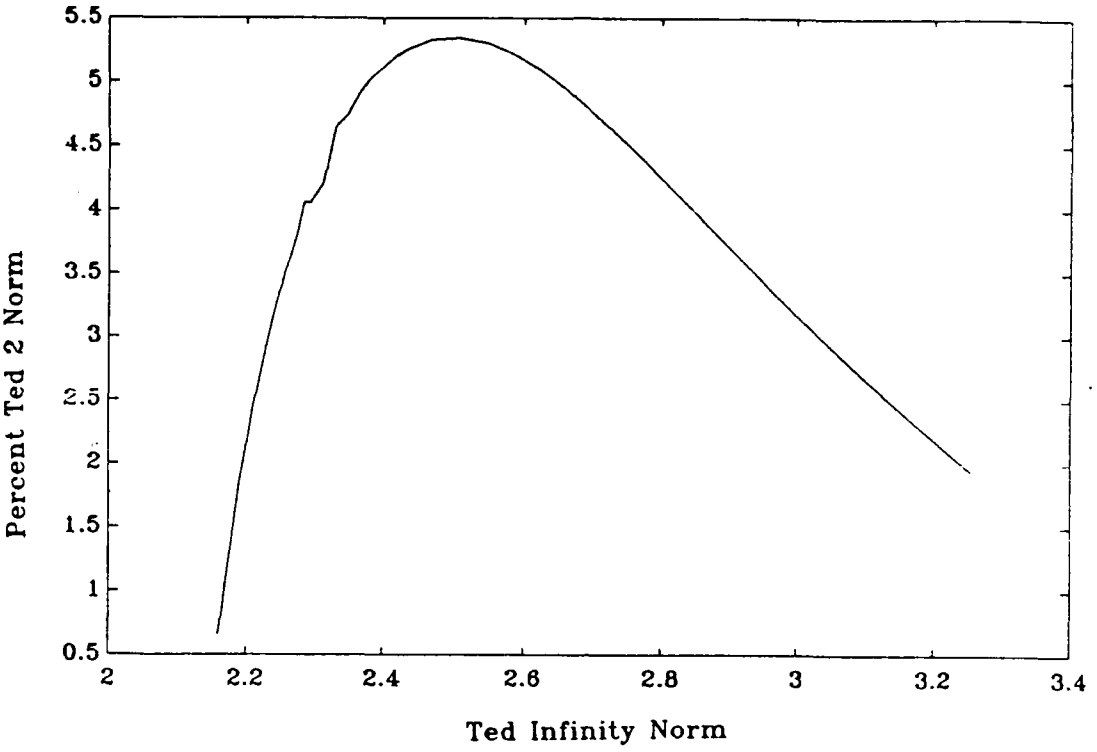

Figure 4.8 Mixed and Central 2-Norm Difference

Table 4.1. Comparison of Mixed vs Central

Mixed			H_∞ central		
γ_{mix}	$\|T_{ed}\|_\infty$	$\|T_{ed}\|_2$	γ_{HC}	$\|T_{ed}\|_\infty$	$\|T_{ed}\|_2$
2.15	2.15	27.6012	2.150	2.15	27.601
2.5	2.5	4.3536	2.540	2.5	4.5993
2.8	2.8	3.6345	2.9608	2.8	3.7956
3.7	3.7	3.2594	5.807	3.7	3.2765
4.163	4.163	3.248	∞	4.163	3.248

Complete numerical data for the above curves can be found in Appendix B.

Figure 4.9 shows the closed-loop Mixed Solution results

for γ_{mix} = 2.15, 2.5, 2.8, and 3.7 as well as the $H_{\infty opt}$ and H_{2opt} curves. In Figure 4.9 the arrow shows decreasing γ. The progression from H_{2opt} to $H_{\infty opt}$ with decreasing γ is clearly evident. Figure 4.10 shows the closed-loop H_∞ central solution results following the same trend from H_{2opt} to $H_{\infty opt}$. Note that at H_{2opt}, which corresponds to $\gamma = \infty$, the bandwidth is about 1 rad/s, while at γ = 2.15 the bandwidth is about 300 rad/s. The bandwidth goes to infinity with just a small change to γ = 2.1426, illustrating the highly non-linear nature of the problem.

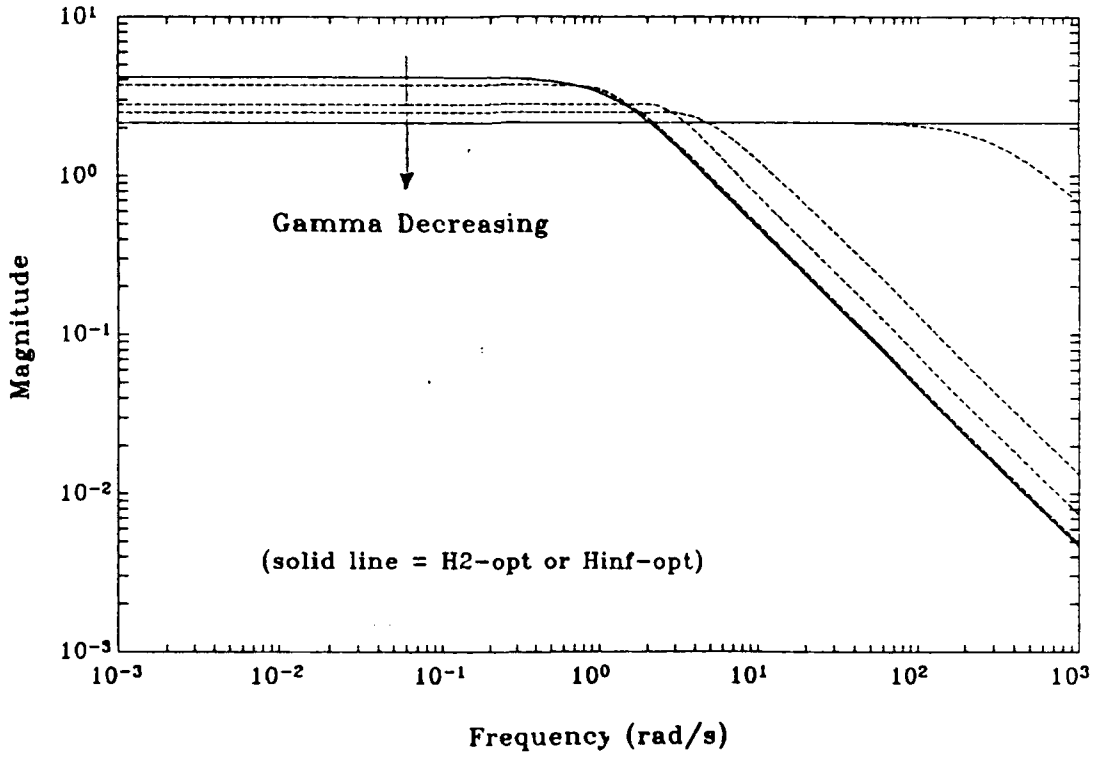

Figure 4.9 σ-Plot of Mixed Solution T_{ed}

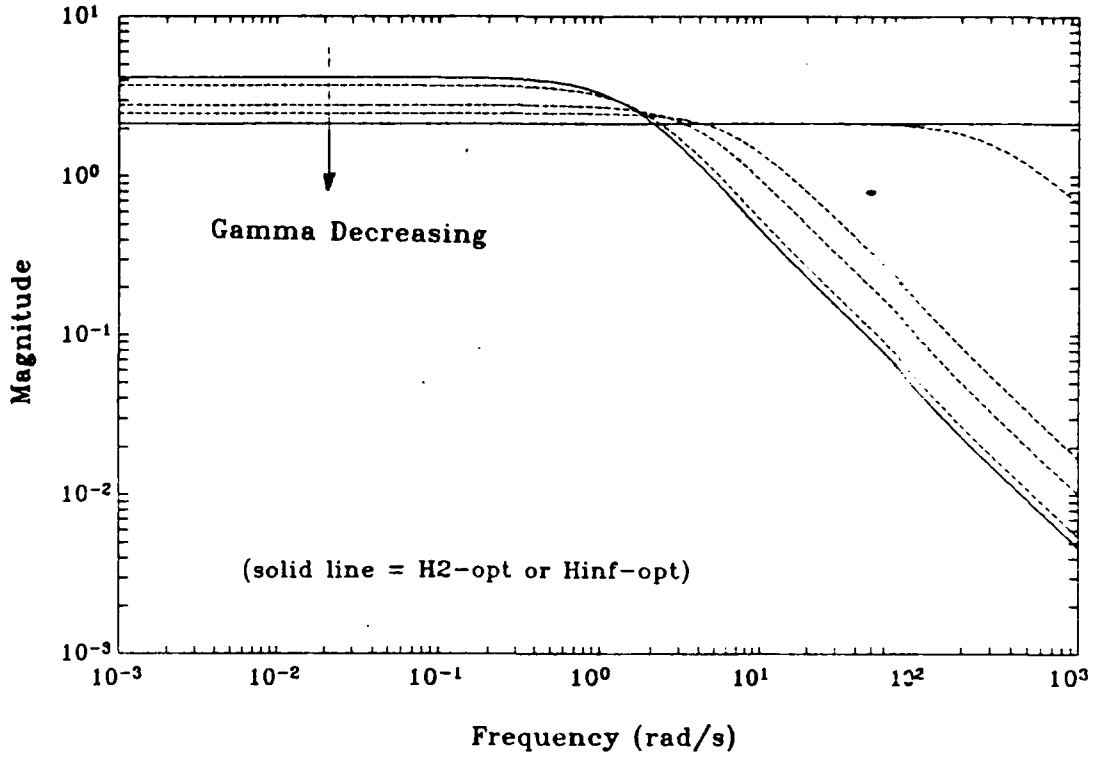

Figure 4.10 σ-Plot of H_∞ Central Solution T_{ed}

In Figure 4.11, the Mixed Solution controllers are shown (solid line shows $H_{\infty opt}$ and H_{2opt}) for the same γ levels as before. Again, with the arrow in the figure showing decreasing γ levels, the progression from H_{2opt} to $H_{\infty opt}$ is clearly evident. Figure 4.12 shows very similar results for the H_∞ central controller.

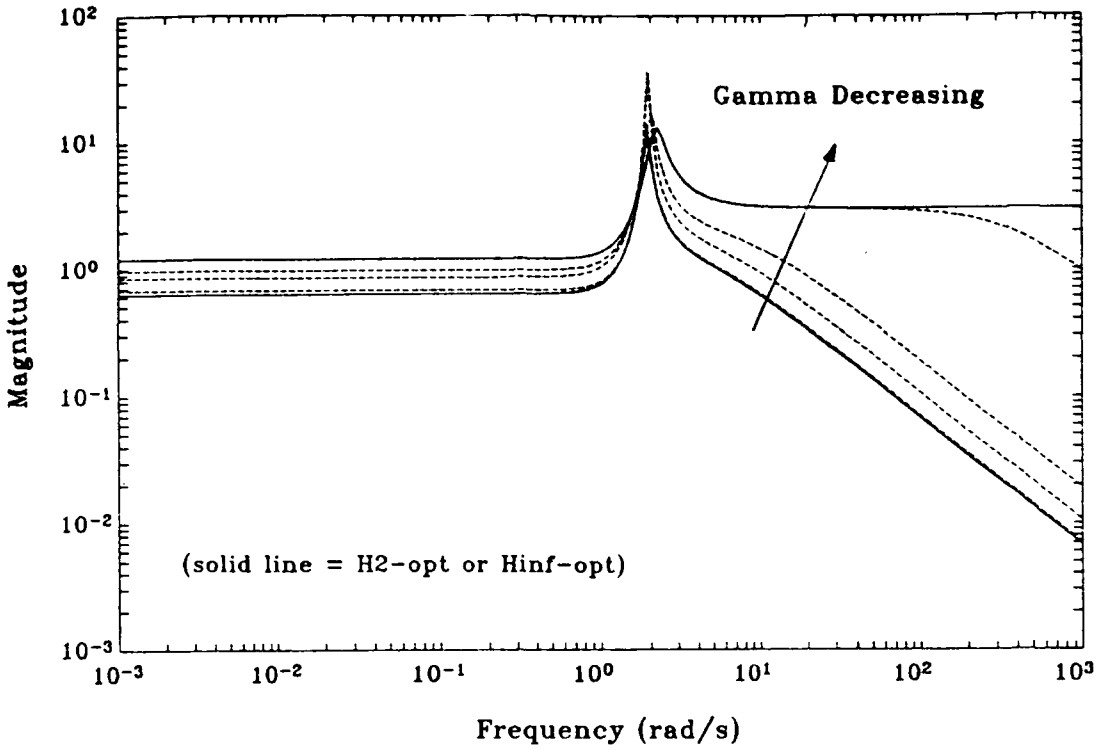

Figure 4.11 σ-Plot of the Mixed Controllers

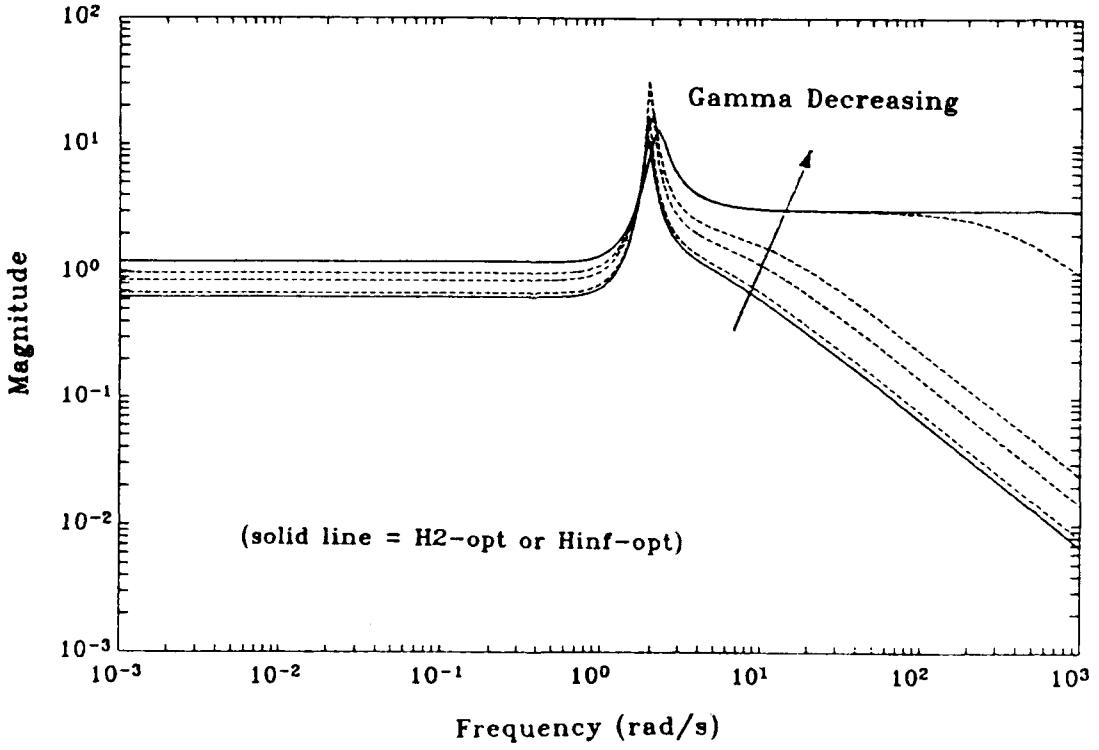

Figure 4.12 σ-Plot of the Central Controllers

Comparing the Mixed Solution and H_∞ central solution at specific $\|T_{ed}\|_\infty$ levels reveals some of the differences between the two solutions. As shown in Figures 4.13, 4.14, 4.15, and 4.16 there is virtually no difference in the controllers below 1 rad/s. It is at the higher frequencies that the differences become apparent. The roll-off appears to be similar at high frequencies, but the Mixed Solution roll-off appears offset downward. The amount of off-set is greatest in the $\|T_{ed}\|_\infty$ = 2.5 to 2.8 range, which corresponds to the area of greatest $\|T_{ed}\|_2$ difference between the two solutions. The solutions become very similar at γ near γ_2 and γ near γ_o, as expected.

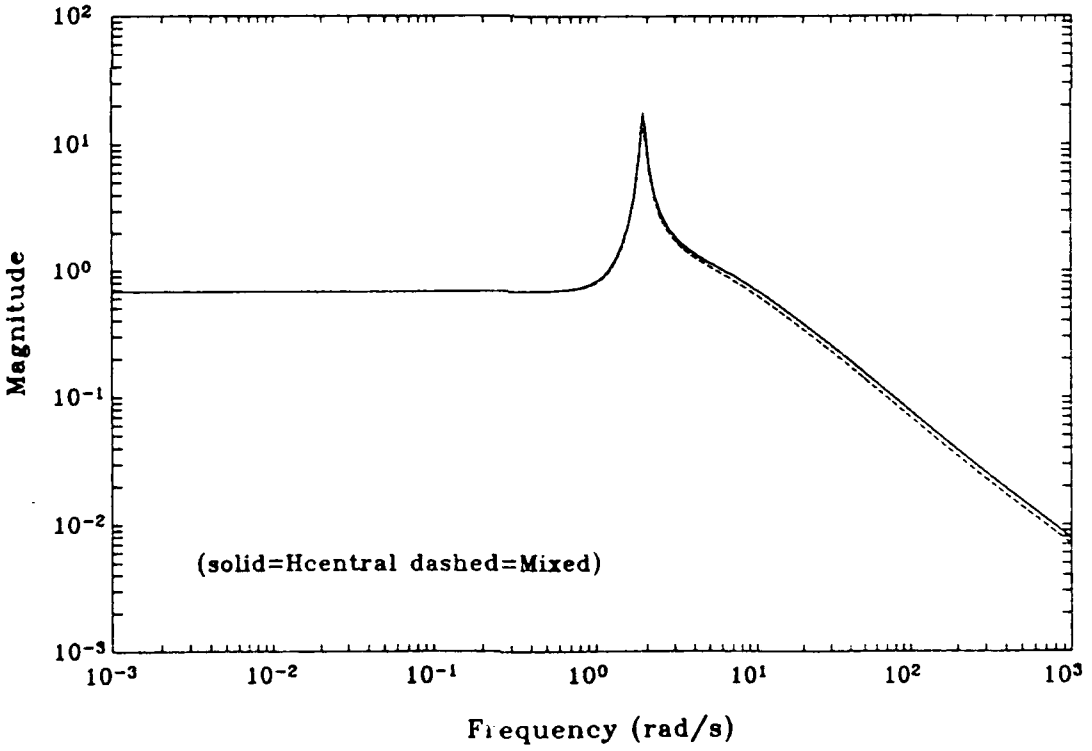

Figure 4.13 σ-Plot of Controllers (∞-norm = 3.7)

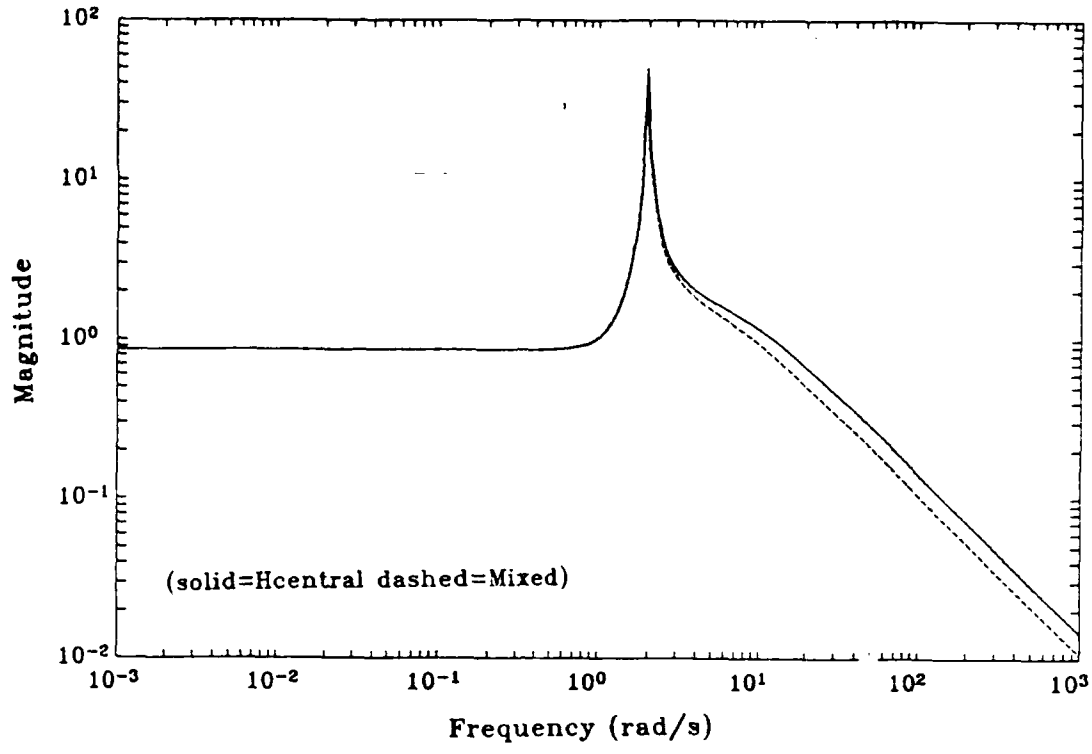

Figure 4.14 σ-Plot of Controllers (∞-norm = 2.8)

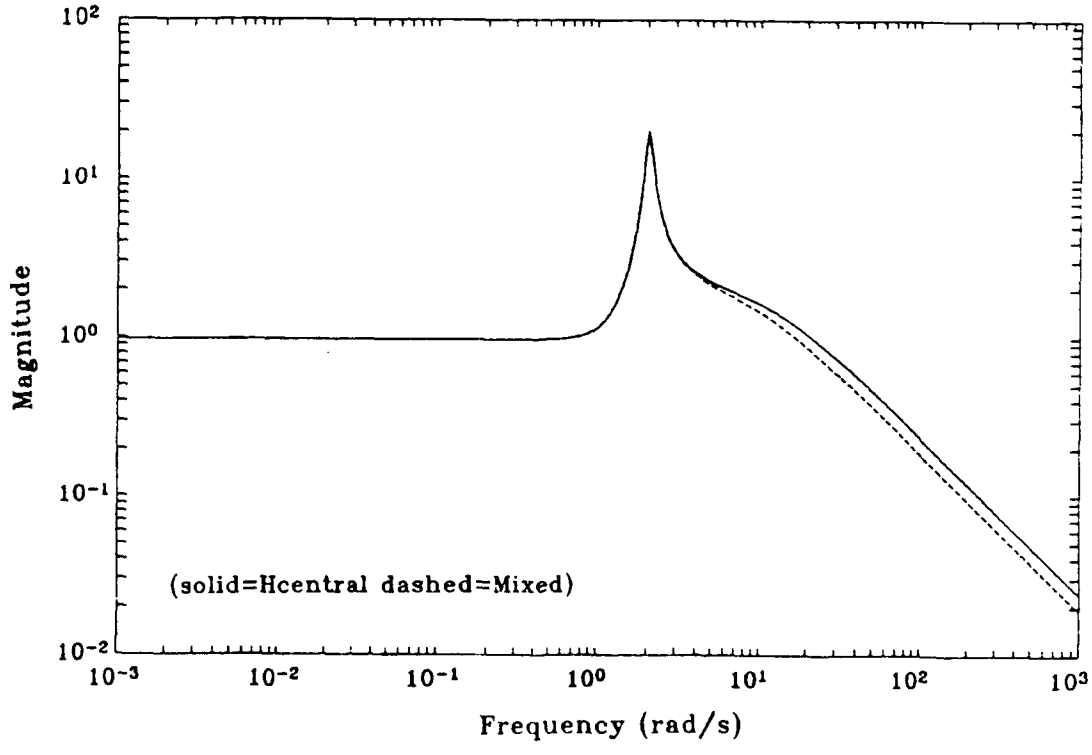

Figure 4.15 σ-Plot of Controllers (∞-norm = 2.5)

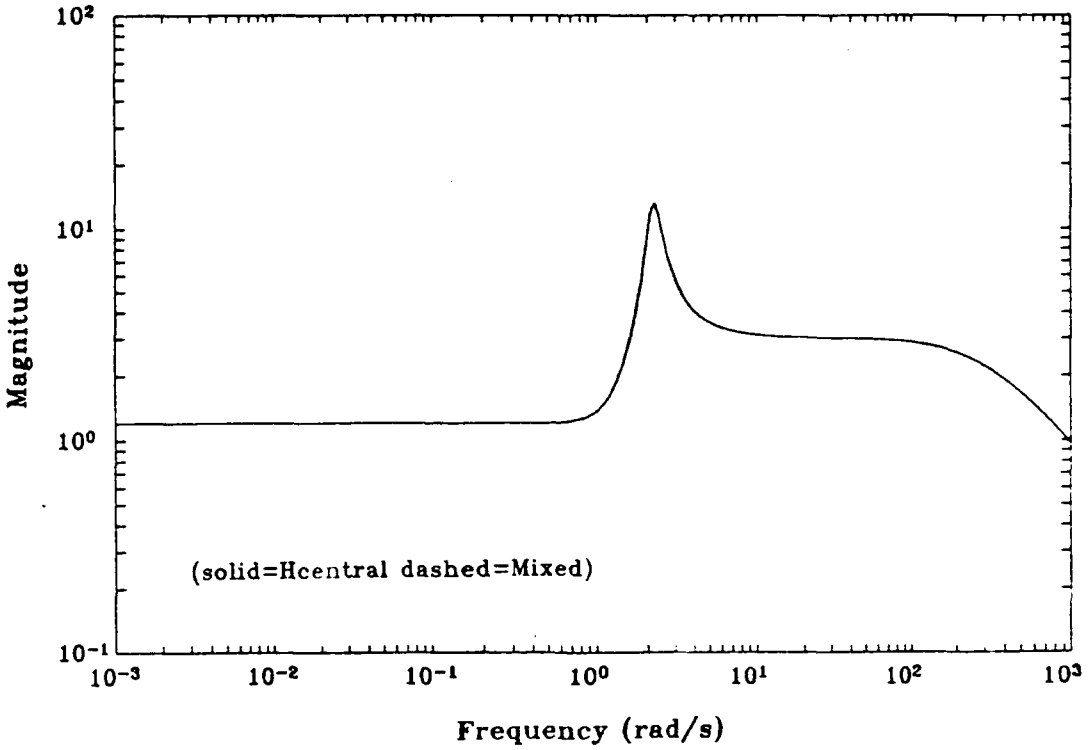

Figure 4.16 σ-Plot of Controllers (∞-norm = 2.15)

Looking at the closed loop comparisons in Figures 4.17, 4.18, 4.19, and 4.20, we see a very interesting phenomena. At low frequency, the curves are flat (at the $\|T_{ed}\|_\infty$ value), and then a roll-off begins near 1 rad/s. At this roll-off, however, the Mixed Solution appears to make a sharper corner than the H_∞ central solution and its singular value plot then passes under the H_∞ central curve. This characteristic is especially evident in Figures 4.18 and 4.19. Thus, the mixed solution has a lower 2-norm because it is trading low frequency gain for high frequency gain to lower the overall area under the curve. The Mixed Solution is able to do this because it can make a sharper corner to the roll-off. In

fact, in [4], it is conjectured that the optimal order controller would have a discontinuous corner. This would take an infinite order controller.

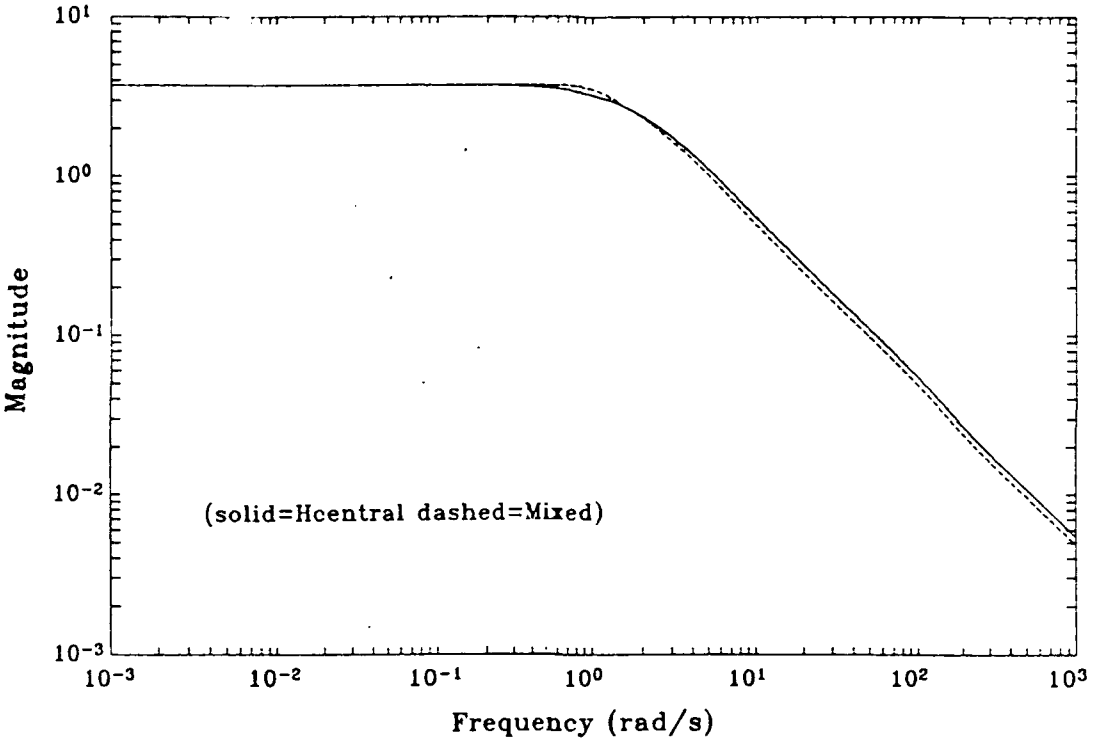

Figure 4.17 σ-Plot of T_{ed} (∞-norm = 3.7)

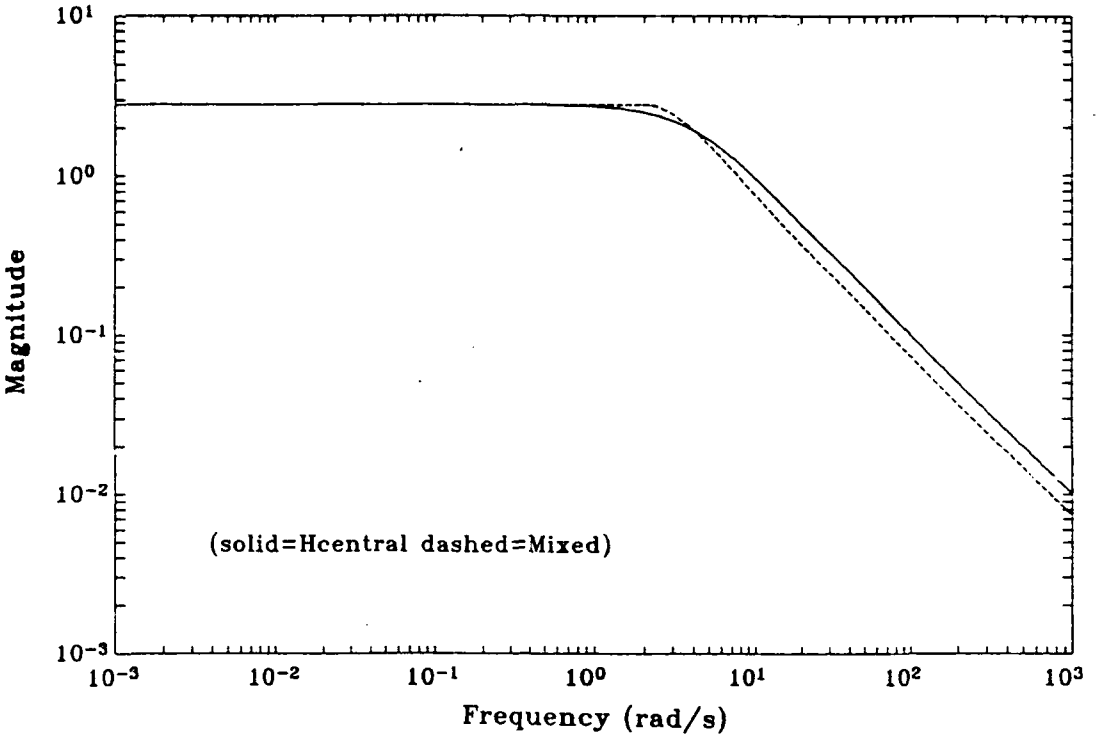

Figure 4.18 σ-Plot of T_{ed} (∞-norm = 2.8)

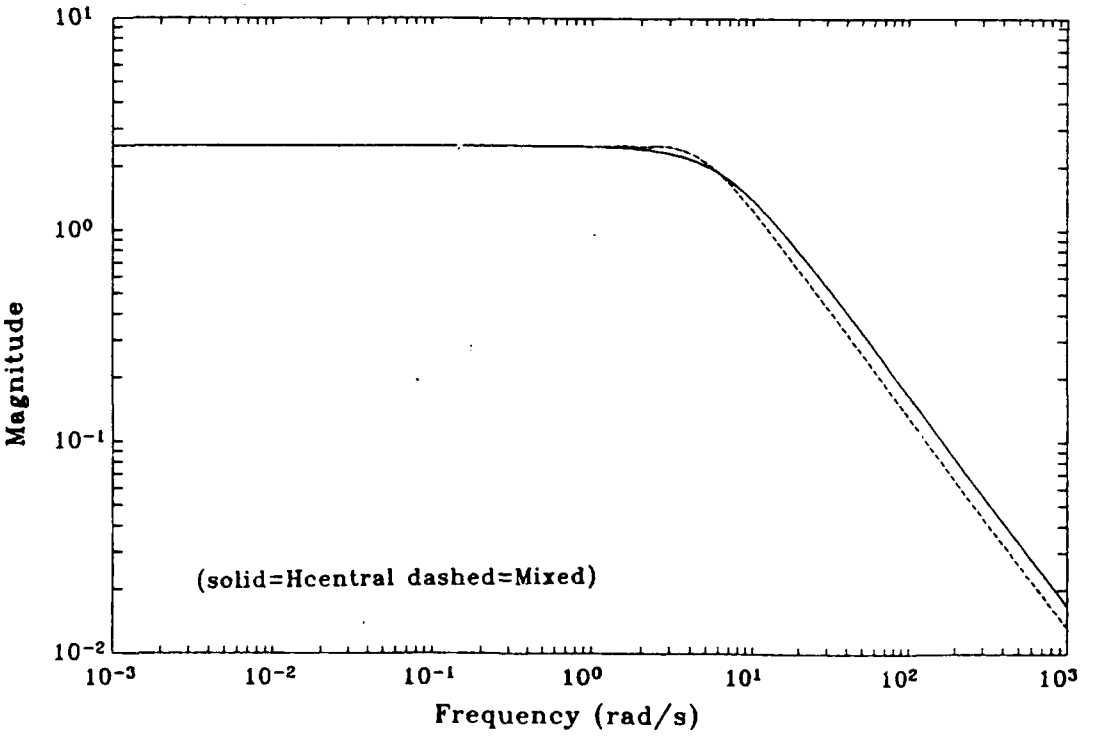

Figure 4.19 σ-Plot of T_{ed} (∞-norm = 2.5)

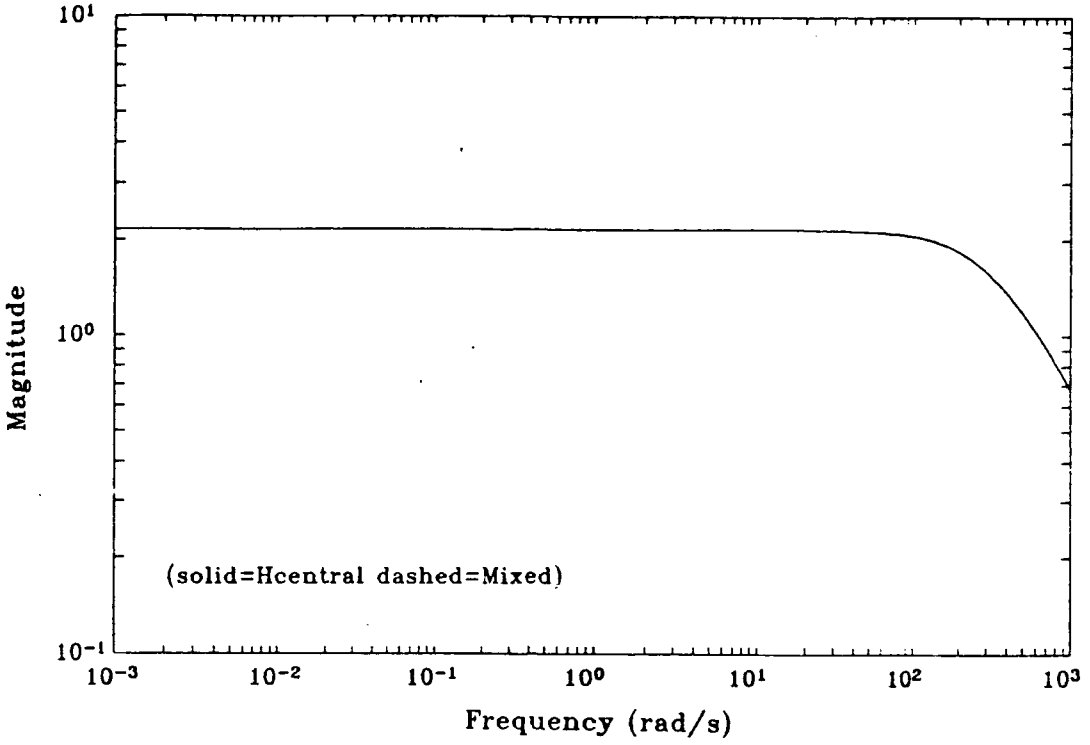

Figure 4.20 σ-Plot of T_{ed} (∞-norm = 2.15)

Thus for the 1I1O system the Mixed Solution is superior to the H_∞ central solution. As expected, the two solutions converge at γ_o and γ_2. The difference between the two solutions seems to manifest itself as a sharper corner to the roll-off in the T_{ed} σ-plot. This difference is greatest for γ's roughly mid-way between γ_o and γ_2. The next level of problem is the 1I2O system that will be covered in Chapter 5.

Chapter V. One Exogenous Input Two Exogenous Outputs

5.1 Problem Synthesis

This system has one exogenous input and two exogenous outputs (1I2O). In standard form it is represented as seen in Figure 5.1:

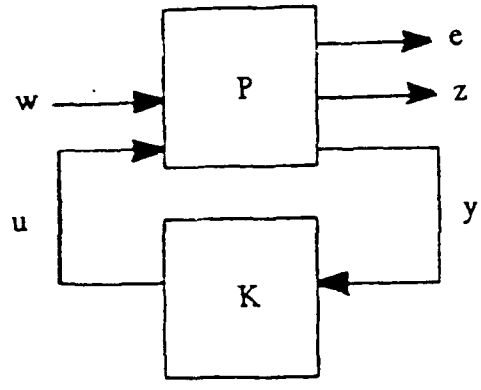

$$P = \left[\begin{array}{c|cc} A & B_w & B_u \\ \hline C_e & O & D_{eu} \\ C_z & O & D_{zu} \\ C_y & D_{yw} & O \end{array}\right]$$

Figure 5.1 1I2O Standard Form

Thus, the mixed problem is

$$\inf_{K \text{ stabilizing}} \|T_{zw}\|_2 \quad \text{subject to } \|T_{ew}\|_\infty \le \gamma$$

so that we are modelling both bounded energy inputs and noise inputs in w while evaluating the performance and robustness with respect to separate outputs. A practical

motivation for such a problem might be an active control surface on an airplane; the motion of the airplane would respond to actuator noise (or perhaps stabilizing high frequency commands) as well as typical step flight path commands coming into the control surface. Then T_{zw} and T_{ew} might represent high and low frequency models, respectively.

5.2 Background

The Mixed Solution has full capability to handle a wide range of different models resulting in a 1I20 system. However, prior to the Mixed Solution the only solution to this problem was Bernstein and Haddad's (B & H) approach forwarded in [5]. This approach uses an overbound technique and is somewhat restrictive, as will become apparent. The Mixed Solution will be compared with a B & H solution on an example system shown in [5]. The general B & H block diagram is shown in Figure 5.2.

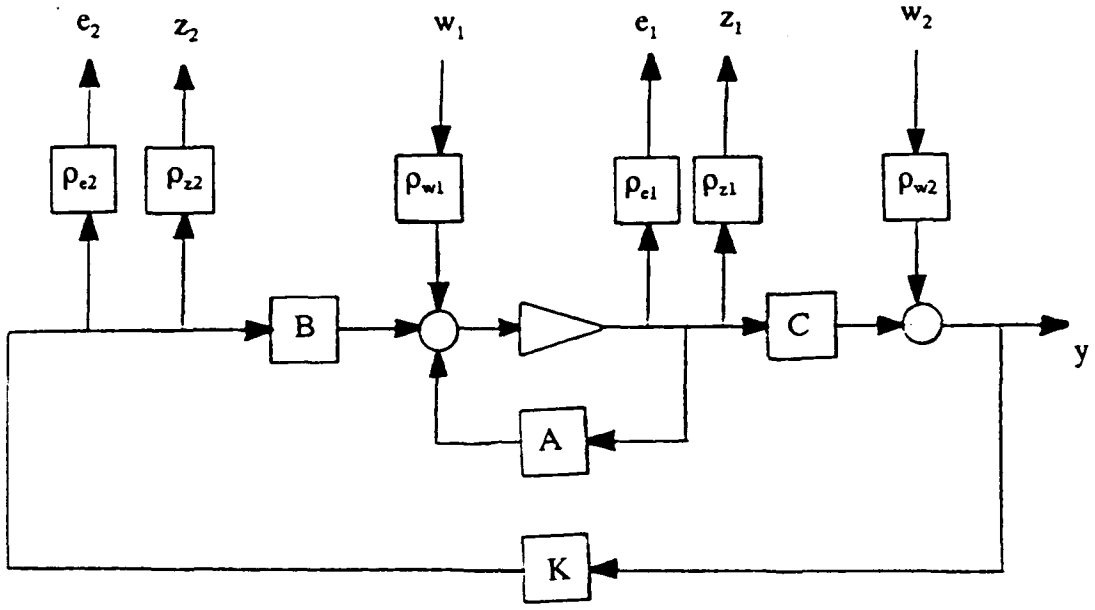

Figure 5.2 System Block Diagram

Briefly reviewing the B & H approach, the equivalent B & H state space representation is

$$P=\left[\begin{array}{c|cc} A & D_1 & B \\ \hline E_{1\infty} & O & E_{2\infty} \\ E_1 & O & E_2 \\ C & D_2 & O \end{array}\right]$$

and the following coupled set of Ricatti equation must be solved:

$$O = AQ + QA^T + Q(\gamma^{-2}R_{1\infty} - \Sigma)Q + V_1 \tag{5.1}$$

$$O = (A + \gamma^{-2}[Q + \hat{Q}]R_{1\infty})^T P + P(A + \gamma^{-2}[Q + \hat{Q}]R_{1\infty}) - S^T P \Sigma P S + R_1 \tag{5.2}$$

$$O = (A - \Sigma P + \gamma^{-2} Q R_{1\infty})\hat{Q} + \hat{Q}(A - \Sigma P + \gamma^{-2} Q R_{1\infty})^T + \hat{Q}(\gamma^{-2}(R_{1\infty} + \beta^2 S^T P \Sigma P S))\hat{Q} + Q\hat{\Sigma}Q \tag{5.3}$$

where

$$V_1 = D_1 D_1^T$$
$$R_1 = E_1^T E_1$$
$$R_2 = E_2^T E_2$$
$$R_{1\infty} = E_{1\infty}^T E_{1\infty}$$
$$\Sigma = B(E_2^T E_2)B^T$$
$$\hat{\Sigma} = C^T(D_2 D_2^T)C$$
$$E_{2\infty} = \beta E_2$$
$$S = (I + \beta^2 \gamma^{-2} \hat{Q} P)^{-1}$$

Note that the H_∞ control penalty $E_{2\infty}$ must be a scalar multiple of the H_2 control penalty. The general B & H equations 5.1, 5.2, and 5.3 are not analytically solvable, and thus far no one has numerically solved them either. However, with $\beta = 0$ they are solvable by Homotopy Techniques. This is the case where there is no H_∞ control penalty, and in the example problem presented in [5] this is what was chosen. The Ricatti Equations then become:

$$O = AQ + QA^T + Q(\gamma^{-2}R_{1\infty} - \Sigma)Q + V_1 \tag{5.4}$$

$$O = (A + \gamma^{-2}[Q + \hat{Q}]R_{1\infty}^T P + P(A + \gamma^{-2}[Q + \hat{Q}]R_{1\infty}) - P\Sigma P + R_1 \tag{5.5}$$

$$O = (A - \Sigma P + \gamma^{-2}QR_{1\infty})\hat{Q} + \hat{Q}(A - \Sigma P + \gamma^{-2}QR_{1\infty})^T + \hat{Q}(\gamma^{-2}R_{1\infty})\hat{Q} + Q\Sigma Q \tag{5.6}$$

where

$$B_c = QC^T(R_2)^{-1}$$
$$C_c = -(R_2)^{-1}B^T P$$
$$A_c = A + BC_c - B_c C + \gamma^{-2}QR_{1\infty}$$

Eqn 5.4 is uncoupled and may be solved immediately. A direct Homotopy approach will solve Equations 5.5 and 5.6 for $\gamma^* < \gamma < \infty$ where $\gamma_o < \gamma^* < \gamma_2$, but γ^* may be substantially larger than γ_o. Therefore, a full $\|T_{zw}\|_2$ vs $\|T_{ew}\|_\infty$ plot cannot be generated. A direct Homotopy algorithm was coded in Matlab M.file form (BH.M in Appendix A), but it was not possible to get γ^* very low for any example tried.

A different algorithm, forwarded in [3], was subsequently coded up (BLACK.M in Appendix A) and found to be much better. The Ricatti equations for this algorithm are:

$$O = A^T P_o + P_o A - P_o \Sigma P_o + R_1 \tag{5.7}$$

$$O = (A - \Sigma P)\,\hat{Q}_o + \hat{Q}_o\,(A - \Sigma P)^T + Q\Sigma Q \tag{5.8}$$

$$O = AQ + QA^T + Q(\gamma^{-2} R_{1\infty} - \Sigma)\,Q + V_1 \tag{5.9}$$

$$O = (A + \gamma^{-2}\,[Q + \hat{Q}]\,R_{1\infty})^T P + P\,(A + \gamma^{-2}\,[Q + \hat{Q}]\,R_{1\infty}) - P\Sigma P + R_1 \tag{5.10}$$

$$O = (A - \Sigma P + \gamma^{-2}\,(Q + \frac{\hat{Q}_K}{2})\,R_{1\infty})\,\hat{Q}_{K+1} + \hat{Q}_{K+1}\,(A - \Sigma P + \gamma^{-2}\,(Q + \frac{\hat{Q}_K}{2} R_{1\infty}) + Q\Sigma Q \tag{5.11}$$

The flowchart diagram for this algorithm is shown in Figure 5.3. Of note is that the only input required in this algorithm is γ. The algorithm generates its own start point, so "solution cascading" going from a higher to a lower γ is not required. This algorithm was used to generate all B & H solutions in this chapter.

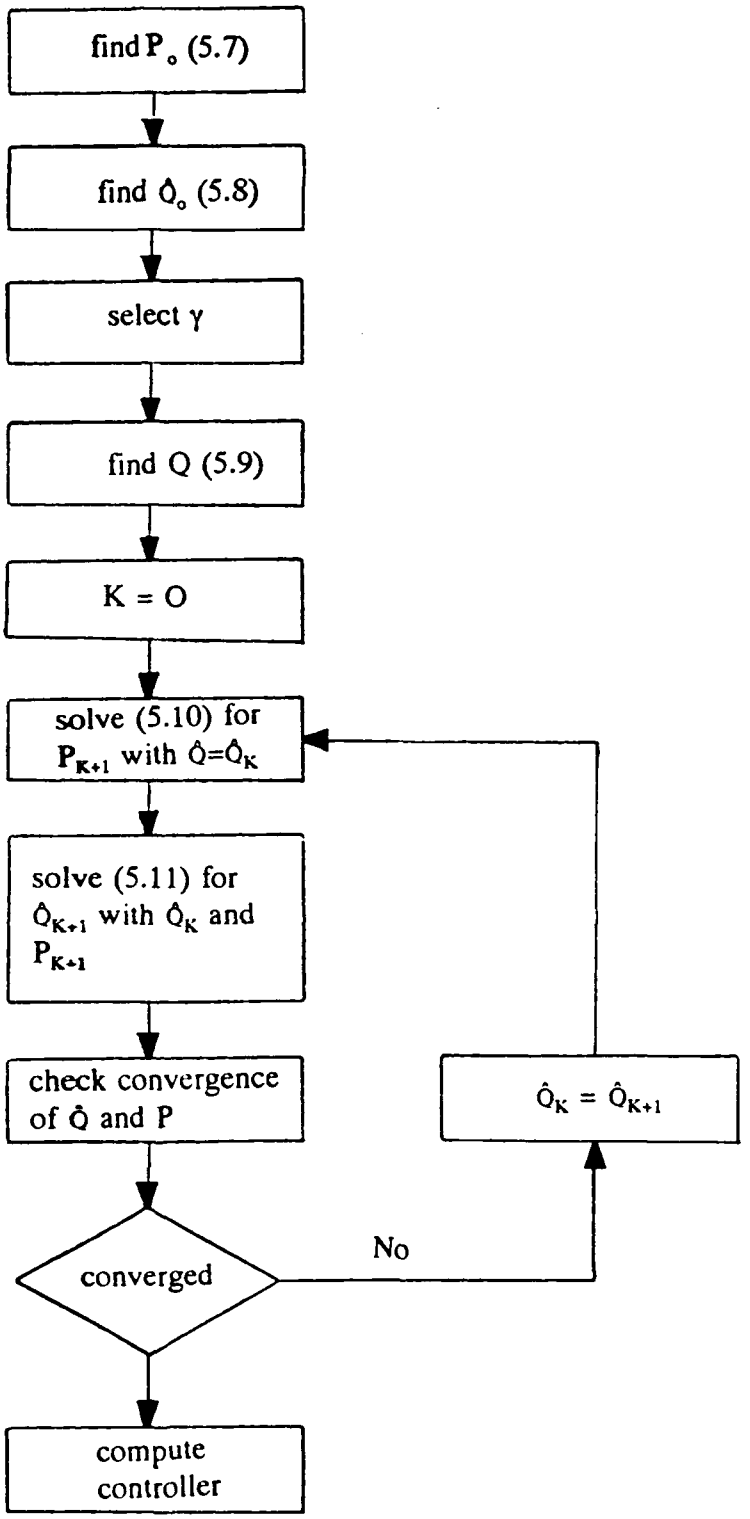

Figure 5.3 Black Algorithm

5.3 The Dual

For completeness, the dual of this problem must be covered. This problem, as represented in Figure 5.4, was first forwarded in [7]. It was subsequently shown in [2] to be the dual of the BH problem.

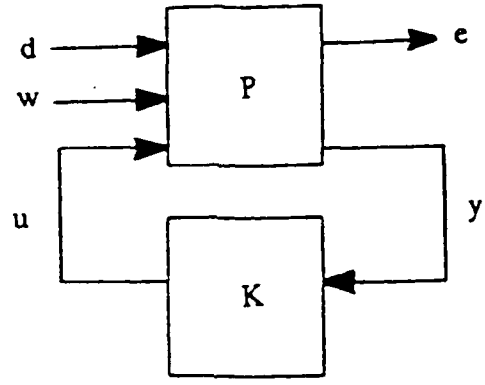

Figure 5.4 Dual Standard Form

This problem is formulated as

$$\inf_{K \text{ stabilizing}} \|T_{ew}\|_2 \qquad \text{subject to } \|T_{ed}\|_\infty \le \gamma$$

so that we are modelling bounded energy inputs in d and noise inputs in w, with all outputs modelled in e.

The mixed state space representation is

$$P = \left[\begin{array}{c|ccc} A & B_d & B_w & B_u \\ \hline C_e & O & O & D_{eu} \\ C_y & D_{yd} & D_{yw} & O \end{array}\right]$$

while the equivalent B & H state space is

$$P=\left[\begin{array}{c|ccc} A & D_{1\infty} & D_1 & B \\ \hline E_1 & O & O & E_2 \\ C & D_{2\infty} & D_2 & O \end{array}\right]$$

Similar to the original B & H problem, $D_{2\infty}$ must be set to zero to obtain the following set of Ricatti equations:

$$O=A^T Q+QA+Q(\gamma^{-2}V_{1\infty}-\Sigma)Q+R_1 \tag{5.12}$$

$$O=(A+\gamma^{-2}V_{1\infty}[Q+\hat{Q}])P+P(A+\gamma^{-2}V_{1\infty}[Q+\hat{Q}])^T + P\Sigma P+V_1 \tag{5.13}$$

$$O=(A-P\Sigma+\gamma^{-2}V_{1\infty}Q)^T\hat{Q}+\hat{Q}(A-P\Sigma+\gamma^{-2}V_{1\infty}Q) + \hat{Q}(\gamma^{-2}V_{1\infty})\hat{Q}+Q\Sigma Q \tag{5.14}$$

where all definitions are the same as before, but with the addition of $D_{1\infty}$, $D_{2\infty}$, and $V_{1\infty}$ ($V_{1\infty} = D_{1\infty} D_{1\infty}^T$). A direct Homotopy algorithm in Matlab M.file form (BHD.M in Appendix A) was coded, but no comparisons with the Mixed Solution were done for this dual problem.

5.4 Description

The system chosen was the same as in [5]. It is an eighth order, neutrally stable, non-minimum phase system, with:

$\lambda_1, \lambda_2 = -.037 \pm j\ 1.85$
$\lambda_3, \lambda_4 = -.028 \pm j\ 1.41$
$\lambda_5, \lambda_6 = -.015 \pm j\ 7.65$
$\lambda_7, \lambda_8 = 0, 0$
zero at 1.0

In [5], it is said that this represents a physical system which has coupled rotating disks with noncolocated sensors and actuators.

The open loop singular value plot is shown in Figure 5.5. Of special note is the response between 0.5 and 3 rad/s, with three ripple-like spikes at 0.7, 1.5, and 1.9 rad/s. As will be seen, the controller is most active controlling these spikes. The state space matrices are:

$$A = \begin{bmatrix} -.161 & 1 & 0 & 0 & 0 & 0 & 0 & 0 \\ -6.004 & 0 & 1 & 0 & 0 & 0 & 0 & 0 \\ -.5822 & 0 & 0 & 1 & 0 & 0 & 0 & 0 \\ -9.9835 & 0 & 0 & 0 & 1 & 0 & 0 & 0 \\ -.4073 & 0 & 0 & 0 & 0 & 1 & 0 & 0 \\ -3.982 & 0 & 0 & 0 & 0 & 0 & 1 & 0 \\ 0 & 0 & 0 & 0 & 0 & 0 & 0 & 1 \\ 0 & 0 & 0 & 0 & 0 & 0 & 0 & 0 \end{bmatrix}$$

$$C_e = E_{1\bullet} = \begin{bmatrix} 0 & 0 & 0 & 0 & .00055 & .011 & .00132 & .018 \\ 0 & 0 & 0 & 0 & 0 & 0 & 0 & 0 \end{bmatrix}$$

$$C_z = E_1 = \begin{bmatrix} 0 & 0 & 0 & 0 & .00055 & .011 & .00132 & .018 \\ 0 & 0 & 0 & 0 & 0 & 0 & 0 & 0 \end{bmatrix}$$

$$C_y = C = [1\ 0\ 0\ 0\ 0\ 0\ 0\ 0]$$

$$D_{y\bullet} = D_2 = [0\ 1]$$

$$D_{zu} = E_2 = \begin{bmatrix} 0 \\ 1 \end{bmatrix}$$

$$D_{eu} = E_{2\infty} = \begin{bmatrix} 0 \\ 0 \end{bmatrix}$$

$$B_w = D_1 = \begin{bmatrix} 0 & 0 \\ 0 & 0 \\ .0064 & 0 \\ .00235 & 0 \\ .0713 & 0 \\ 1.0002 & 0 \\ .1045 & 0 \\ .9955 & 0 \end{bmatrix} \qquad B_u = B = \begin{bmatrix} 0 \\ 0 \\ .0064 \\ .00235 \\ .0713 \\ 1.0002 \\ .1045 \\ .9955 \end{bmatrix}$$

Looking at the form of the above matrices we see that an equivalent block diagram would be like that in Figure 5.6. The w_1 disturbance is coming into the plant added to u. The disturbance w_2 is coming into the output y. Finally, the outputs e_1 and z_1 are being collected (through the weighting matrix ρ_{ez}) directly from the plant states. Thus the plant output y is uncoupled from the "unmeasured" e_1 and z_1 outputs that have ∞-norm and 2-norm significance, respectively. Note the absence of e_2 to place a penalty on control effort expended on the ∞-norm side of the problem.

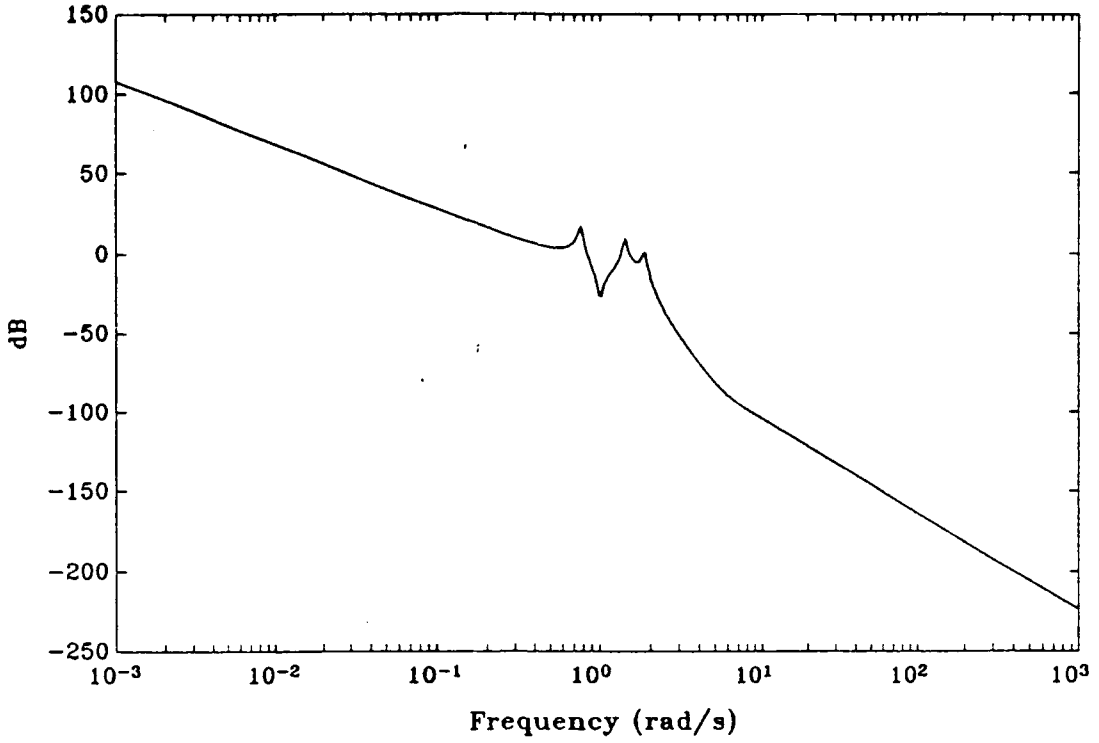

Figure 5.5 σ-Plot of the Open Loop System

Because the H_∞ control penalty is zero, the H_∞ optimal controller is difficult to calculate for this problem. In [3], a γ_o of 0.12 was found for this problem using bisection techniques. Closing the loop with the H_{2opt} controller gives a T_{zw} with the characteristics shown in Figure 5.7. This controller results in $\alpha_o = 0.37856$. Note that this controller (Figure 5.8) has three distinct dips corresponding to the 0.7, 1.5, and 1.9 rad/s ripples in the upper T_{zw} σ-plot. Figure 5.9 shows T_{ew} with this H_{2opt} controller. Here, $\gamma_2 = \|T_{ew}\|_\infty = 1.3923$. Because e_1 and z_1 share the same weighting matrix (ρ_{ez} in Figure 5.5), the lower T_{zw} σ-plot is very similar to the T_{ew} σ-plot with the same spikes and dips.

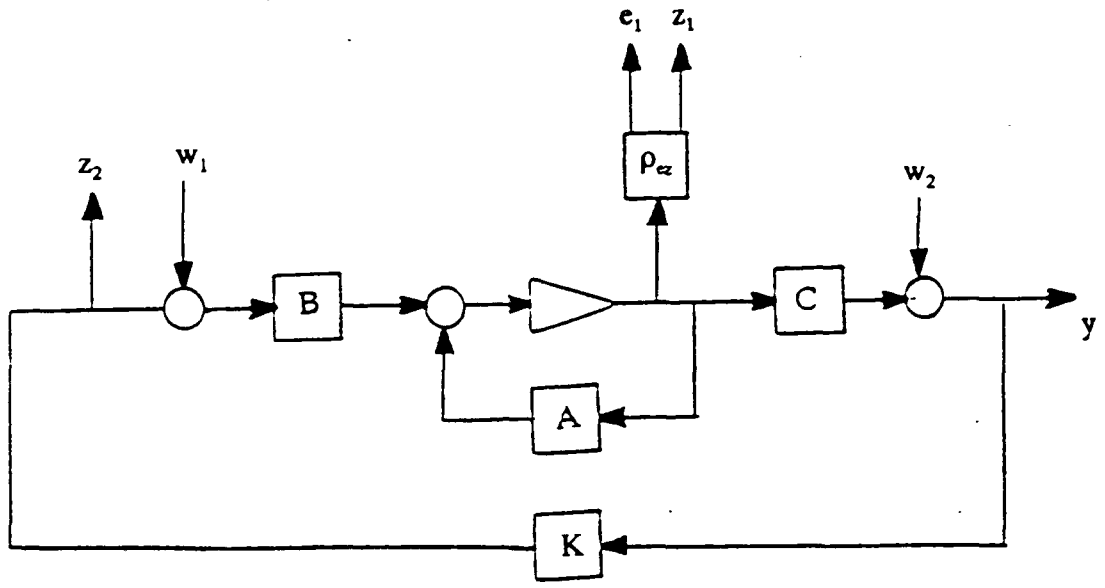

Figure 5.6 Equivalent Block Diagram

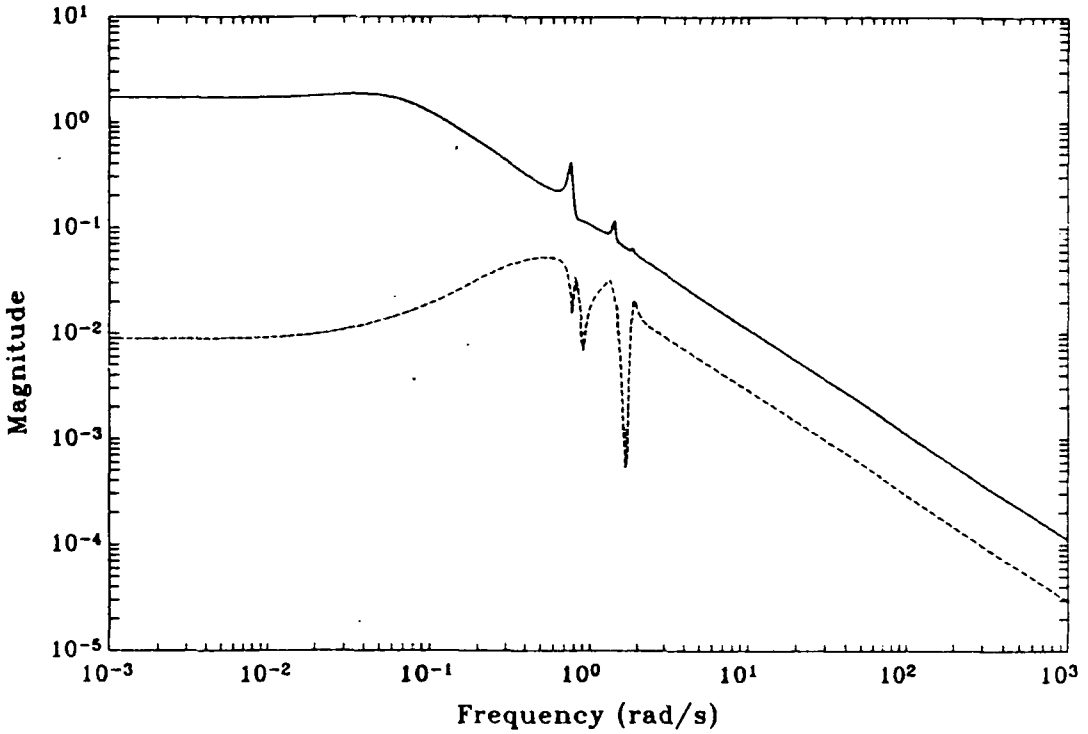

Figure 5.7 σ-Plot of the H_{2opt} T_{zw}

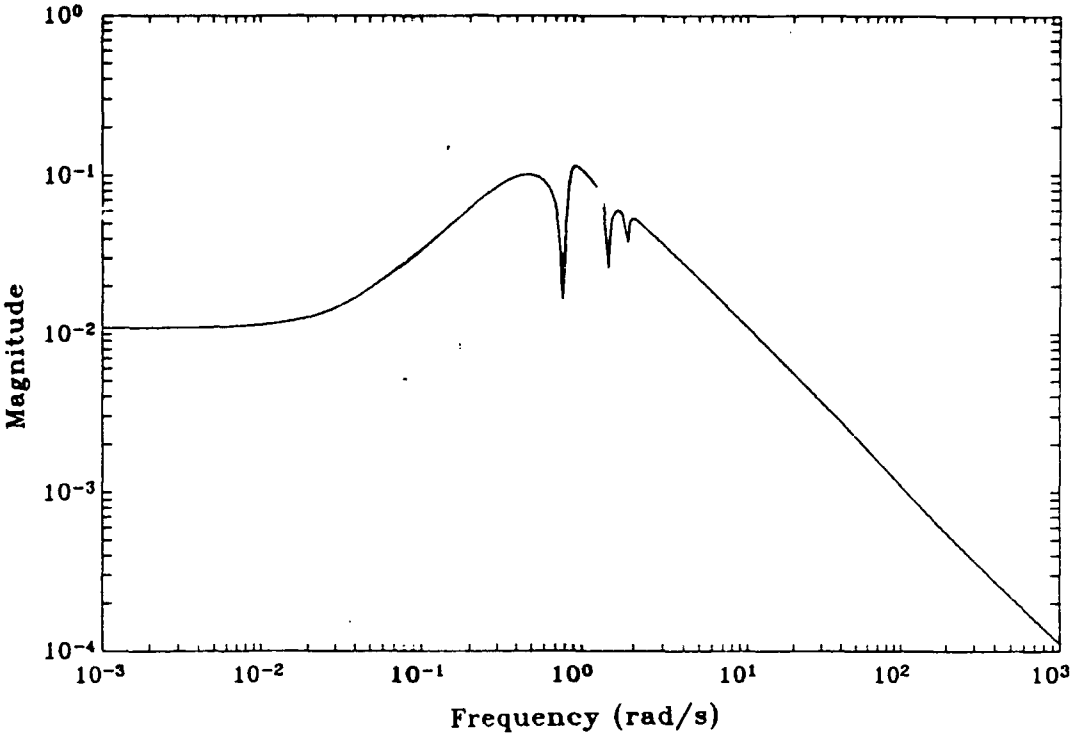

Figure 5.8 σ-Plot of the H_{2opt} Controller

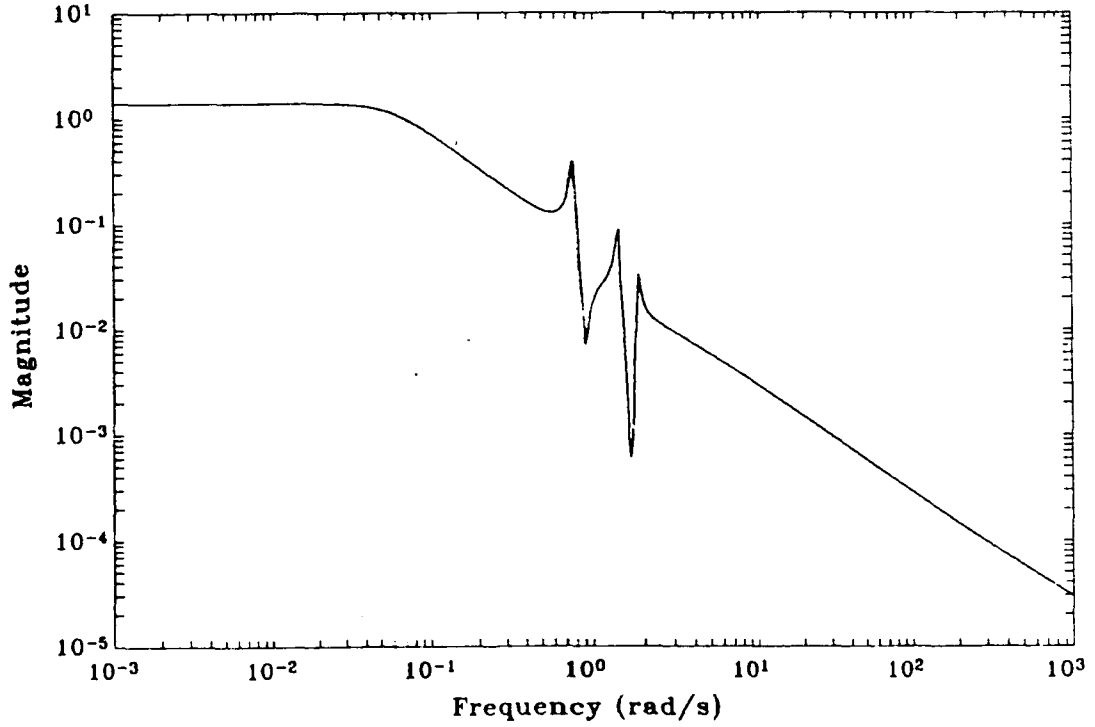

Figure 5.9 σ-Plot of the T_{ew} with T_{zw} H_{2opt} Controller

Since the H_∞ central controller is difficult to generate for this problem, the B & H results served as a starting point for the Mixed Solution. This worked very well as long as γ_{mix} was significantly greater than $\|T_{ew}\|_{\infty BH}$. The Mixed Solution would reliably start with $\mu = 0.01$ in this case. The problem is that when the B & H problem cannot be solved at a γ near γ_o, the Mixed Solution has no start point. The practical limit of about $\gamma = 0.27$ was found, below which the B & H solution wouldn't work to start the Mixed Solution.

5.5 Results

The Mixed Solution is clearly better than the B & H solution as shown in Figure 5.10. As γ_o is approached, the difference between the two solutions becomes large, while as γ_2 is approached, the two converge to the same answer. Table 5.1 shows the comparison for selected γ_{mix} levels. Once again, care must be taken in such a table because $\|T_{ew}\|_\infty \leq \gamma_{BH}$ while $\|T_{ew}\|_\infty = \gamma_{mix}$, so either γ_{BH} or γ_{mix} must be adjusted such that $\|T_{ew}\|_\infty$ is the same.

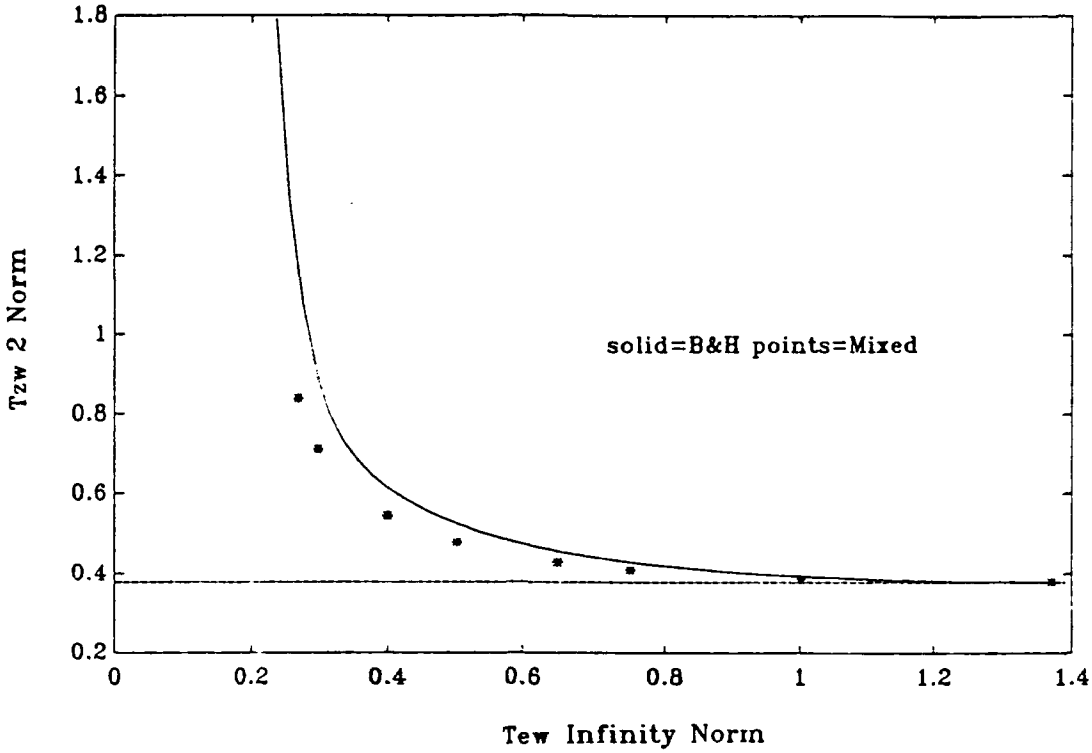

Figure 5.10 Comparison of Mixed and B & H Controllers

Table 5.1 Comparison of Mixed vs B & H

Mixed			B & H		
γ_{mix}	$\|T_{ew}\|_\infty$	$\|T_{zw}\|_2$	γ_{BH}	$\|T_{ew}\|_\infty$	$\|T_{zw}\|_2$
.27	.27	.8382	.2750	.27	1.1531
.40	.40	.5444	.4133	.40	.61521
.65	.65	.4281	.7046	.65	.4554
.75	.75	.4097	.8412	.75	.4288
1.00	1.00	.3865	1.329	1.00	.3931
1.37	1.37	.3786	6.81	1.37	.3786
1.3923	1.3923	.3786	∞	1.3923	.3786

Complete numerical data for the B & H curve can be found in Appendix B.

Figure 5.11 shows the closed-loop Mixed Solution T_{ew}

results for γ_{mix} = 0.27, 0.40, 0.65, 0.75, 1.00, and 1.37 as well as the H_{2opt} T_{ew} curve. In the figure, the arrow shows decreasing γ. The progression away from H_{2opt} is readily apparent. Note that as γ progresses to lower values, the major change in T_{ew} is at low frequency (below 0.8 rad/s), and above 1.5 rad/s no change is discernable. In Figure 5.12, the closed-loop Mixed Solution T_{zw} results for the same γ levels are shown. Again the smooth progression away from H_{2opt} is evident. Note how low frequency energy is being pushed out to higher frequencies as γ is decreased. In Figure 5.13, the Mixed Solution controllers are shown for the same γ levels. Of note here is that the Mixed controller has only two dips in the γ = 1.00, 0.75, and 0.65 cases; the 1.9 rad/s dip disappears.

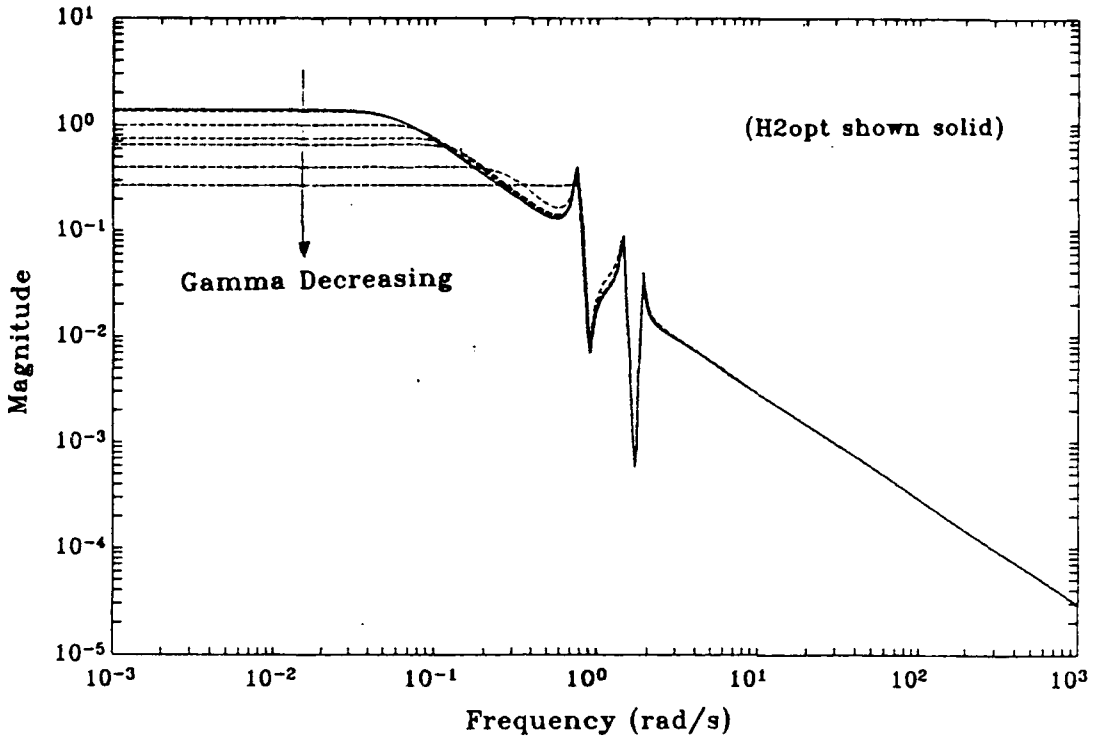

Figure 5.11 σ-Plot of the Mixed T_{ew}

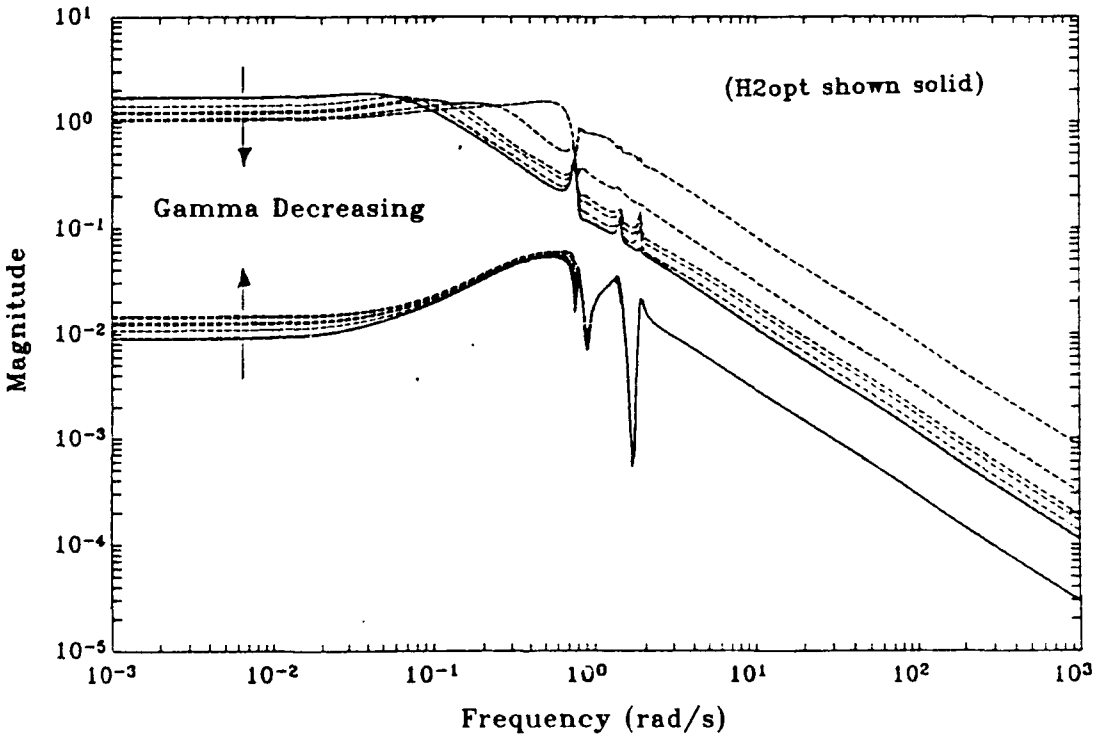

Figure 5.12 σ-Plot of the Mixed T_{zw}

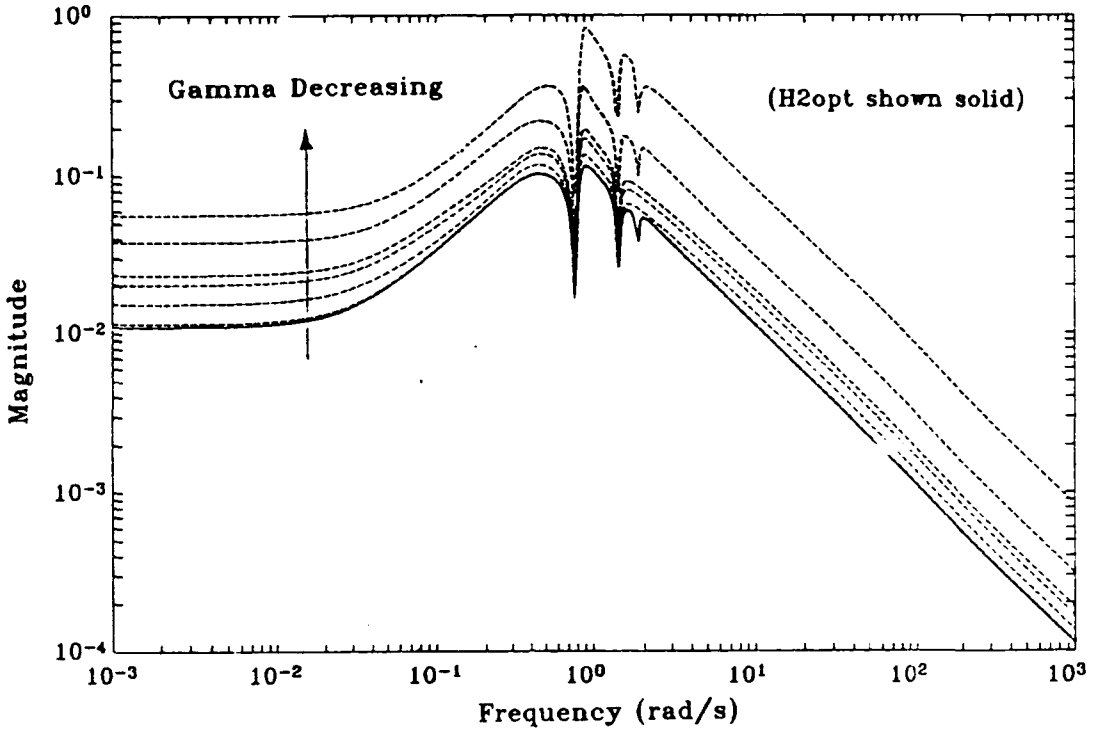

Figure 5.13 σ-Plot of the Mixed Controllers

Figures 5.14 and 5.15 show the closed-loop B & H solution T_{ew} and T_{zw} results for the same γ levels. These curves show the same progression away from H_{2opt} with decreasing γ, and show similar trend characteristics as compared with the Mixed results. Figure 5.16 shows the B & H controllers for these same γ levels. It is very interesting that the B & H controllers always possess three dips, very similar to the H_{2opt}, controller while the Mixed controller, transitions to and from a three dip controller depending on the γ.

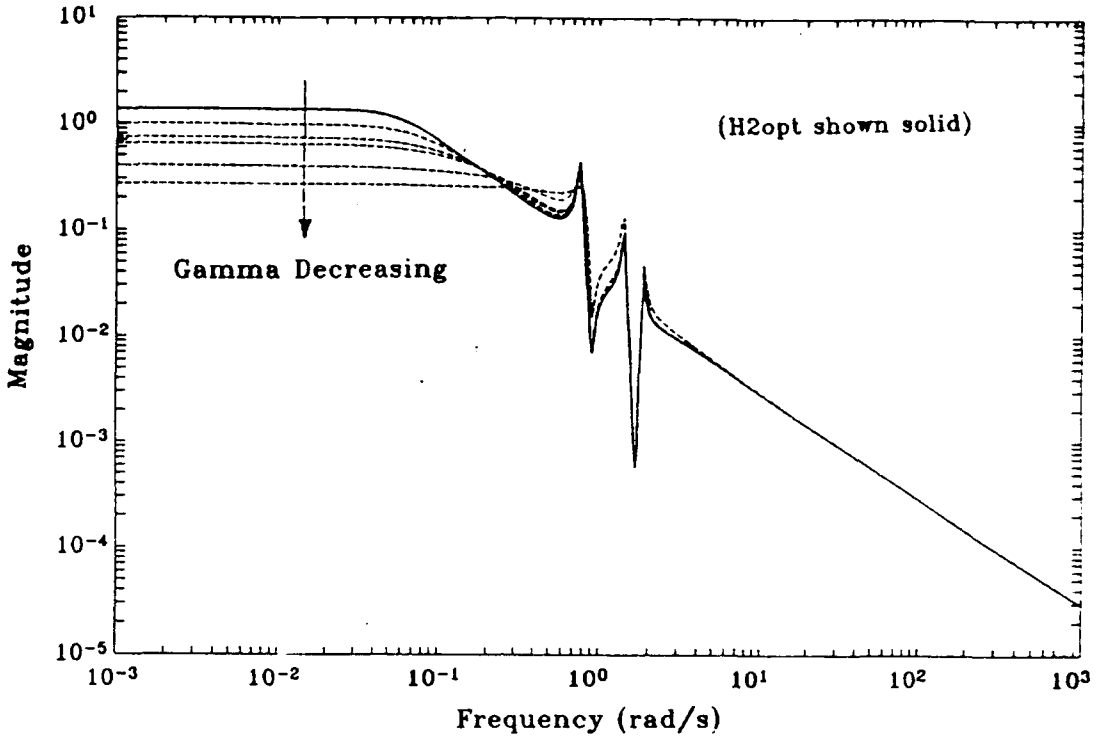

Figure 5.14 σ-Plot of B & H T_{ew}

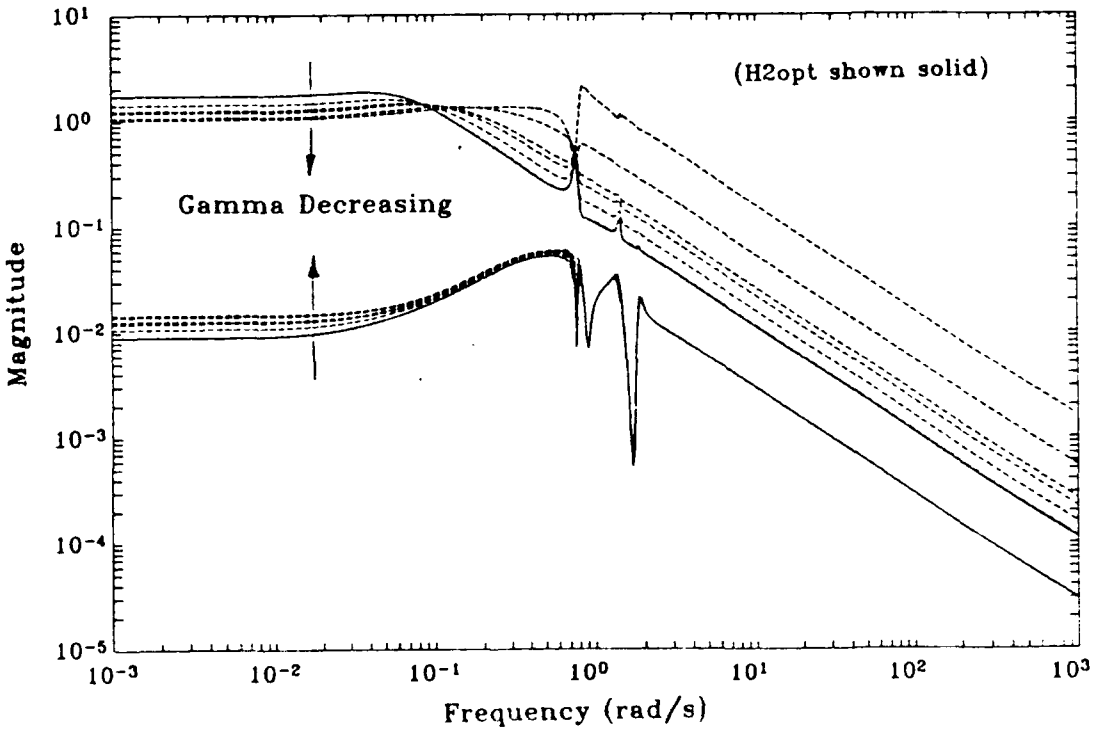

Figure 5.15 σ-Plot of B & H T_{zw}

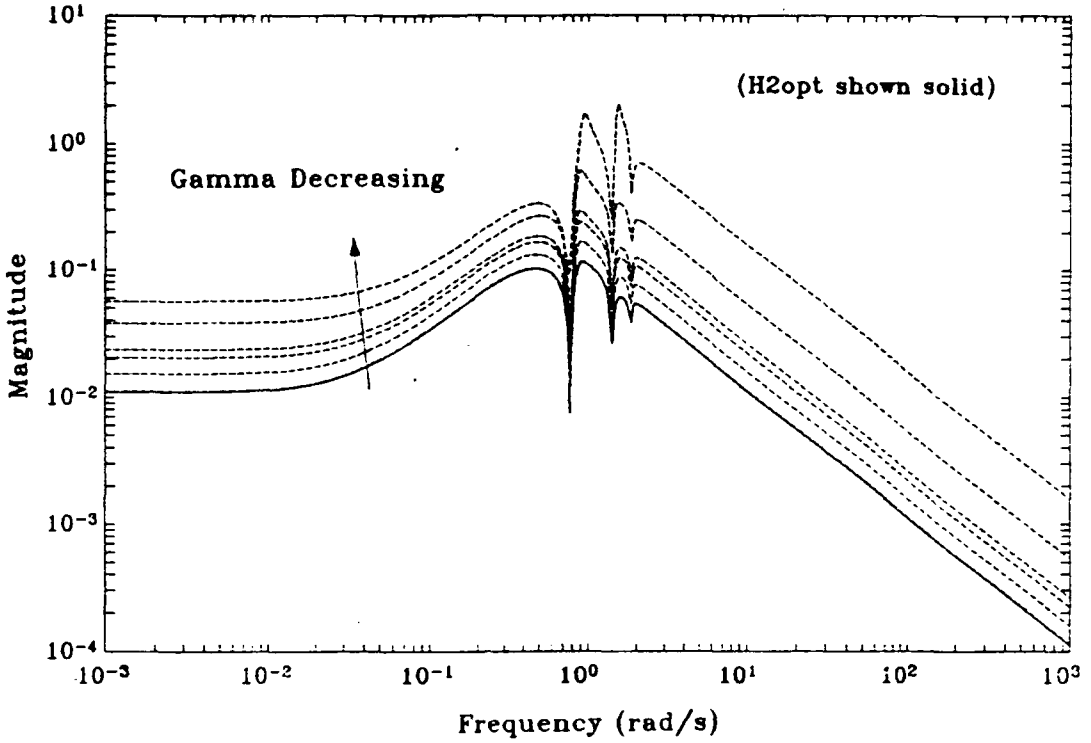

Figure 5.16 σ-Plot of B & H Controllers

Comparing the Mixed Solution and B & H solution at specific $\|T_{ew}\|_\infty$ levels reveals some of the differences between the two solutions. Starting with Figures 5.17 and 5.18, which show T_{ew} and T_{zw}, respectively, at $\|T_{ew}\|_\infty = 1.37$, we see the two solutions are very close. Although it can not be seen on these two plots, the Mixed T_{ew} has a slightly greater bandwidth than the B & H T_{ew}, while the Mixed T_{zw} has a slightly higher peak sigma value than the B & H T_{zw}. Both of these trends will continue as γ is decreased. The controllers shown in Figure 5.19 are almost identical and both show the three dip phenomenon. Moving down to $\|T_{ew}\|_\infty = 1.00$, Figure 5.20 shows how the Mixed T_{ew} has a larger

bandwidth than the B & H T_{ew}. As in Chapter 4, it will become increasingly apparent that as γ decreases, as the Mixed Solution is making a "sharper corner" to roll-off for the ∞-norm side of the problem. In this figure, also note the spike at 0.7 rad/s. As γ gets lower this spike will become increasingly important. Figure 5.21 shows that the Mixed Solution is reducing higher frequency response of T_{zw} by increasing lower frequency response (at the 0.08 rad/s hump). Note that the Mixed controller in Figure 5.22 has transitioned to a two dip controller, while the B & H controller still has an H_{2opt}-like three dip controller. Thus, the Mixed Solution is not dealing with the 1.9 rad/s T_{zw} ripple. In fact, the B & H controller always appears to be a scaled H_{2opt} controller. At $\|T_{ew}\|_\infty = 0.65$, Figure 5.23 shows the increasingly large T_{ew} spike at 0.7 rad/s. Note that above 0.7 rad/s both the B & H solution and the Mixed Solution are the same. Figure 5.24 shows the increasing divergence between the two solutions for T_{zw} between 0.03 and 10 rad/s. Figure 5.25 shows the controller comparison similar to the $\|T_{ew}\|_\infty = 1.00$ controller. For $\|T_{ew}\|_\infty = 0.4$ Figures 5.26 and 5.27 show T_{ew} and T_{zw} respectively. Note that for T_{ew} the 0.7 rad/s spike nearly reaches $\|T_{ew}\|_\infty$. Again note the sharpness of the roll-off corner. In the T_{zw} curve we see the Mixed Solutions pronounced ability to reduce the gain above 0.3 rad/s. This was achieved with only a small increase in the maximum T_{zw} gain. Figure 5.28 shows the

controller comparison for the $\|T_{ew}\|_\infty$ level. Interestingly, the Mixed controller has now transitioned back to three dips, probably to deal with the emerging 1.9 rad/s T_{ew} spike. At $\|T_{ew}\|_\infty = 0.27$, the lowest level, the problem is changing radically. In Figure 5.29, the T_{ew} 0.7 rad/s spike has joined with the Mixed T_{ew} curve at the roll-off point resulting in a very sharp roll-off corner. Meanwhile, the B & H roll-off corner is quite rounded. For the first time, higher frequency differences are apparent as well. This is shown better in Figure 5.30. The T_{zw} curve in Figure 5.31 tells us why the $\|T_{zw}\|_2$ are so different for these solutions at this $\|T_{ew}\|_\infty$ level; the B & H T_{zw} has a large gain step at 0.7 rad/s that the Mixed Solution just does not have. The B & H solution seems unable to trade-off this large spike for a slight increase in lower frequency gain. Figure 5.32 shows both controllers having the same three dip characteristic as H_{2opt}. Thus, we can conclude that the H_2 overbound used in the B & H solution becomes increasingly poor as γ is decreased. This is especially evidenced by the $\|T_{ew}\|_\infty$=.27 T_{zw} plot, where the Mixed Solution is making shrewd high/low gain trade-offs and the B & H solution is not.

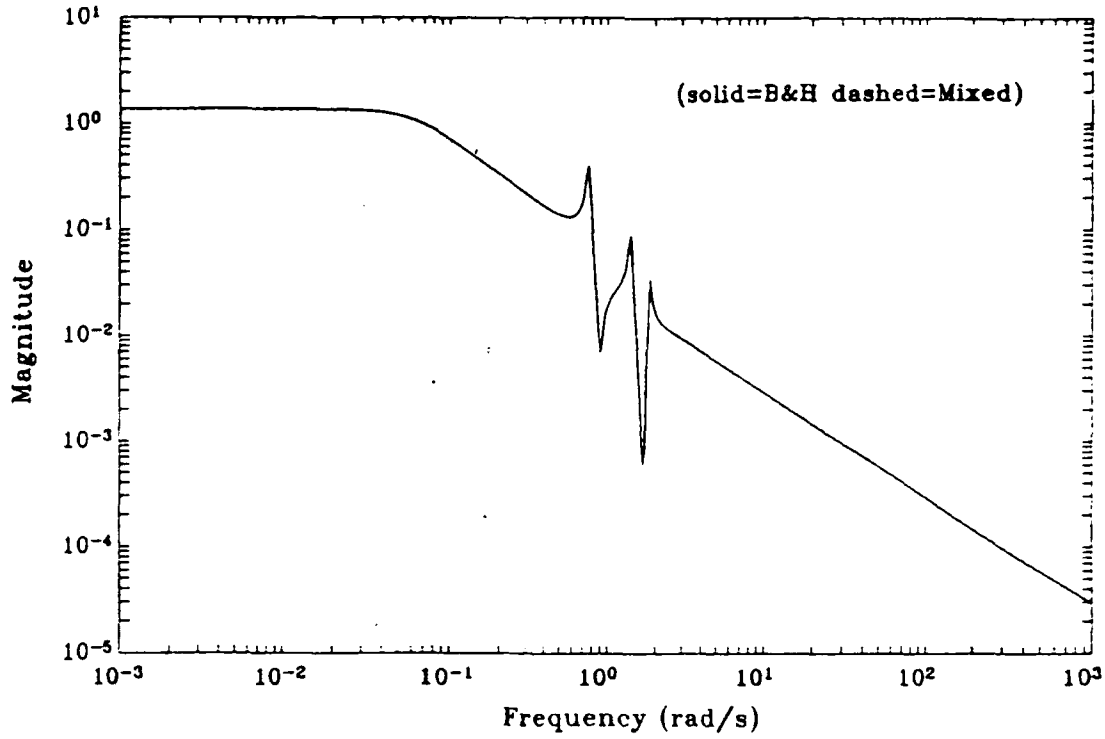

Figure 5.17 σ-Plot of the T_{ew} (∞-norm = 1.37)

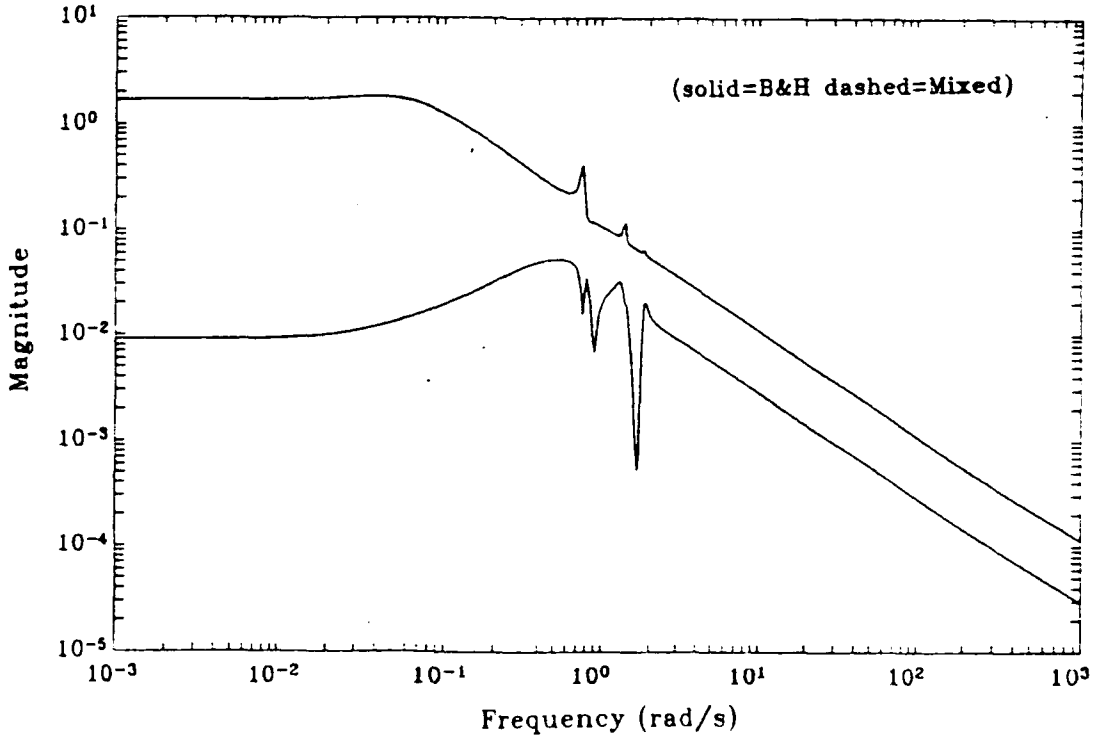

Figure 5.18 σ-Plot of the T_{zw} (∞-norm = 1.37)

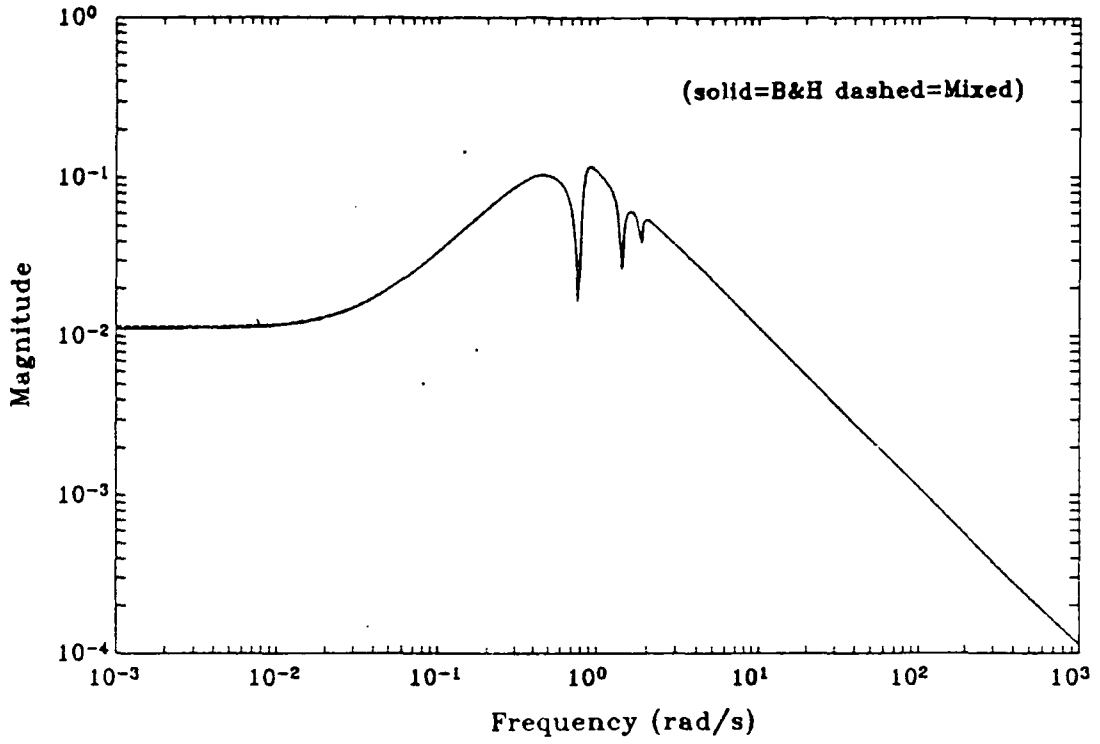

Figure 5.19 σ-Plot of Controllers (∞-norm = 1.37)

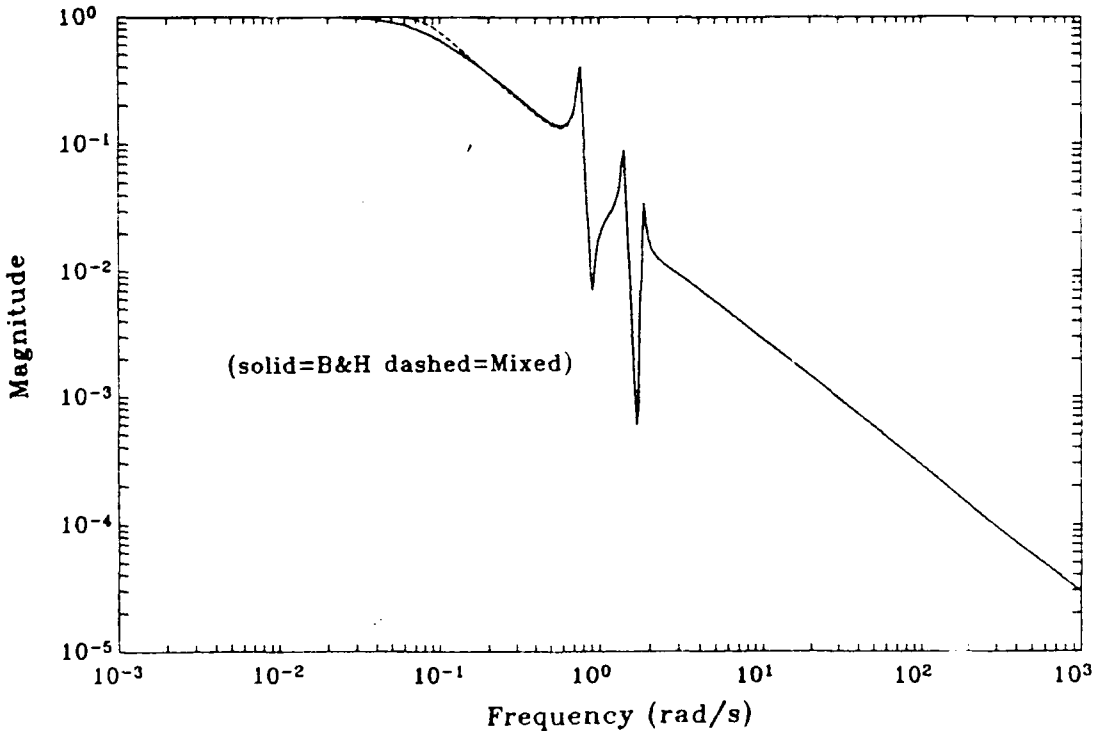

Figure 5.20 σ-Plot of T_{ew} (∞-norm = 1.0)

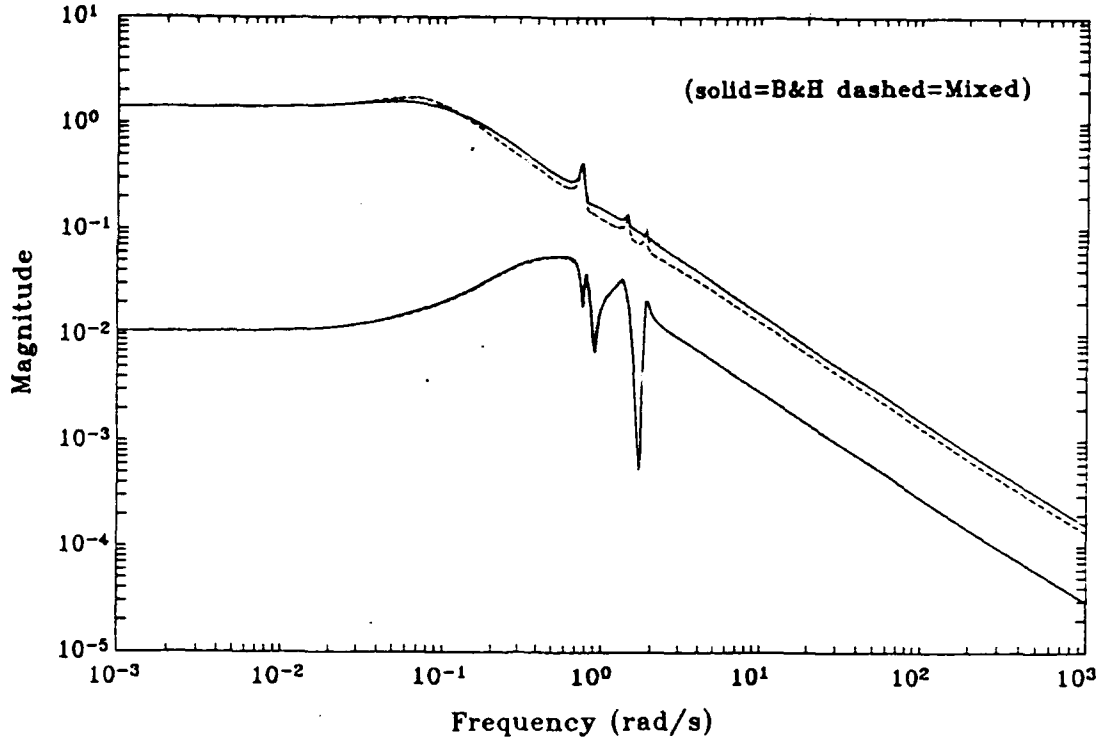

Figure 5.21 σ-Plot of T_{zw} (∞-norm = 1.0)

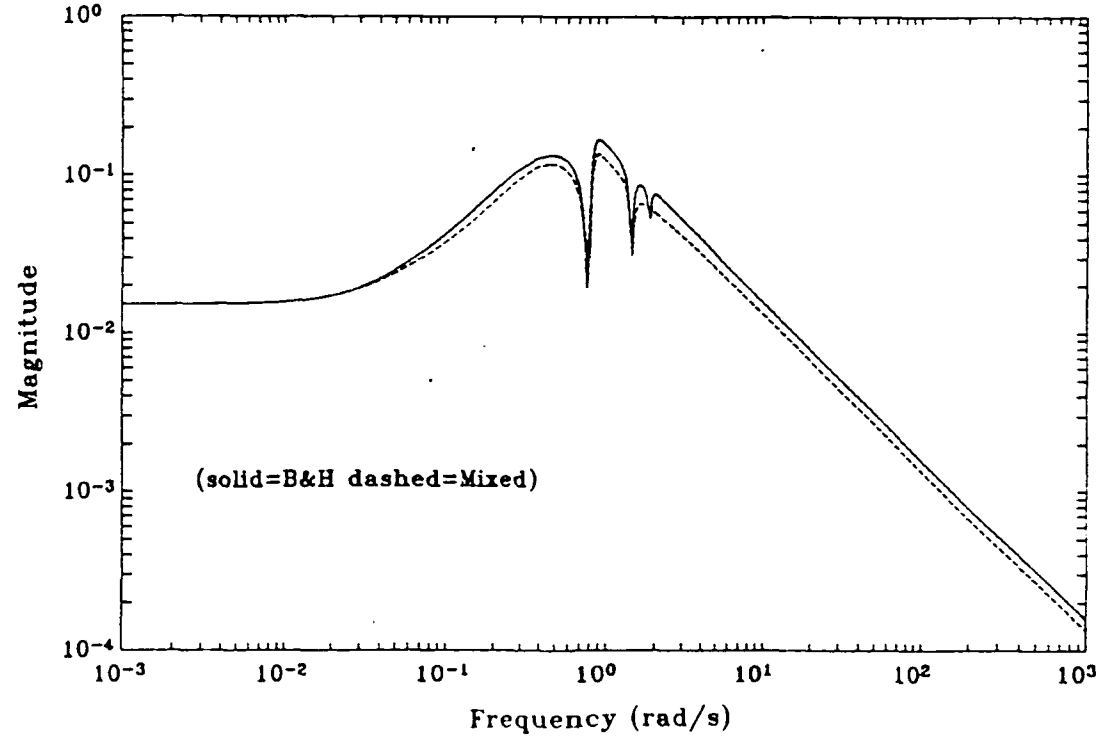

Figure 5.22 σ-Plot of Controllers (∞-norm = 1.0)

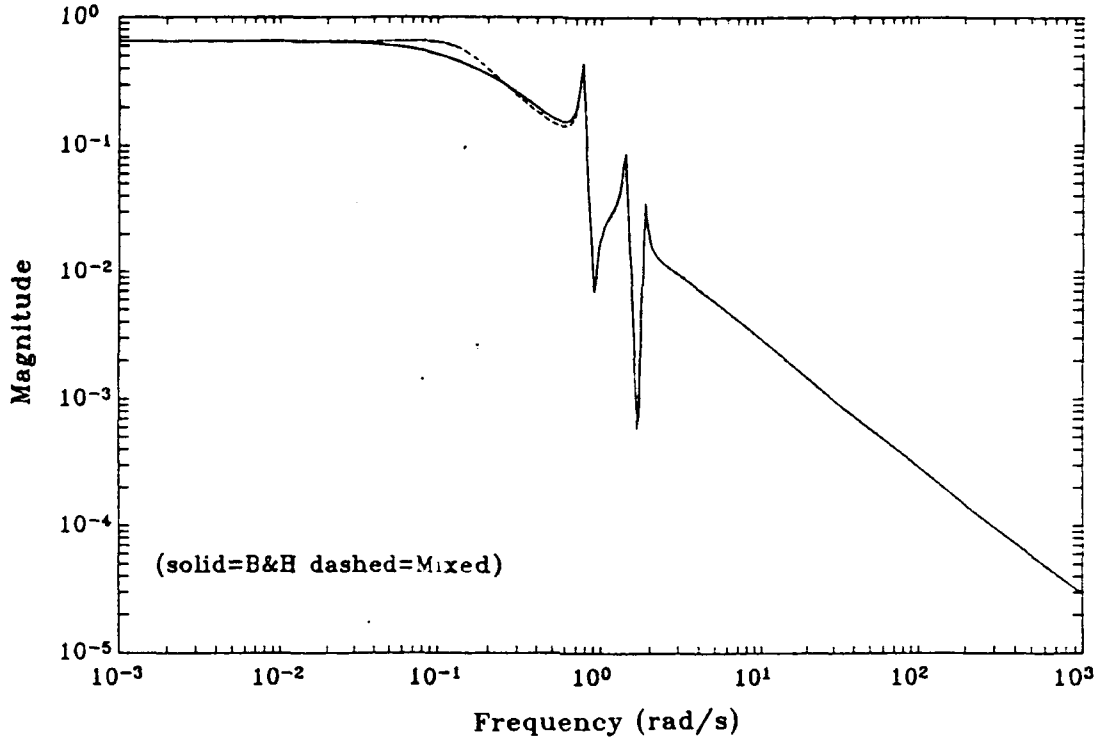

Figure 5.23 σ-Plot of T_{ew} (∞-norm = 0.65)

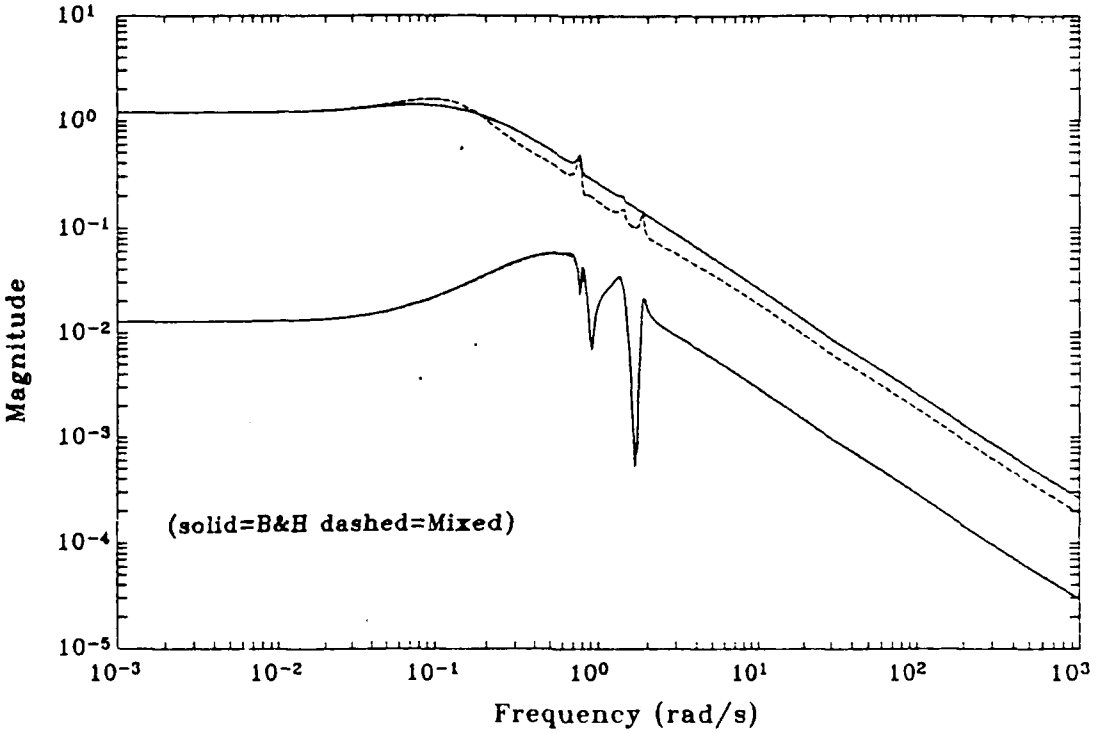

Figure 5.24 σ-Plot of T_{zw} (∞-norm = 0.65)

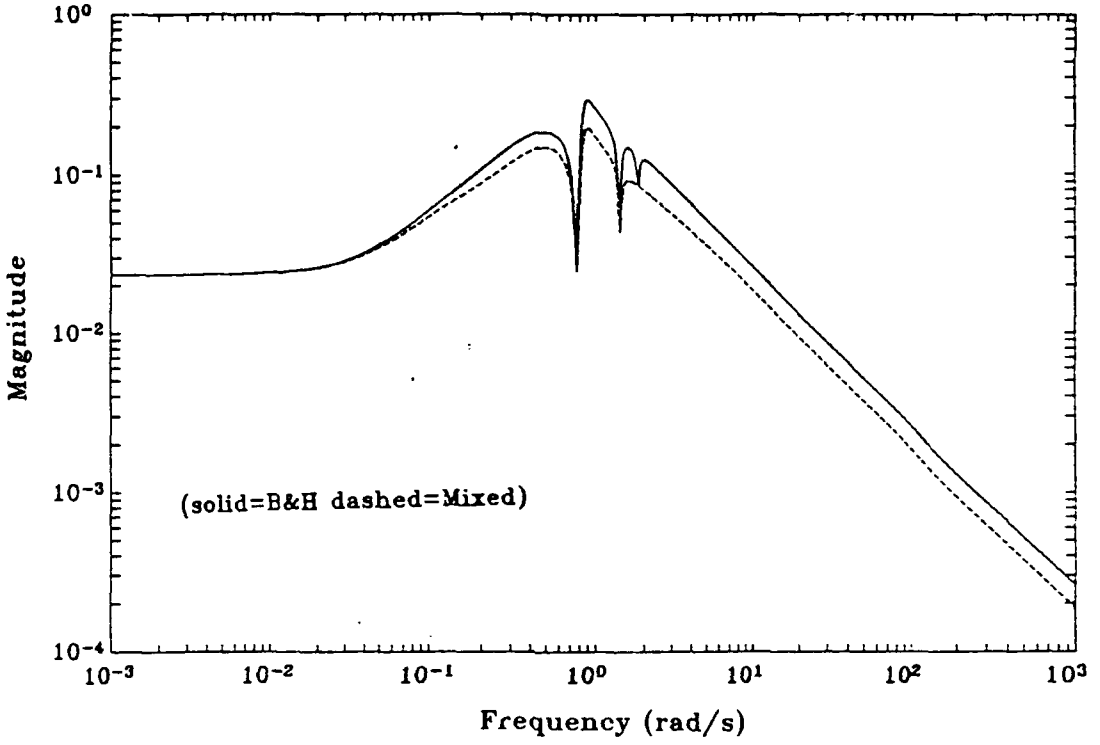

Figure 5.25 σ-Plot of Controllers (∞-norm = 0.65)

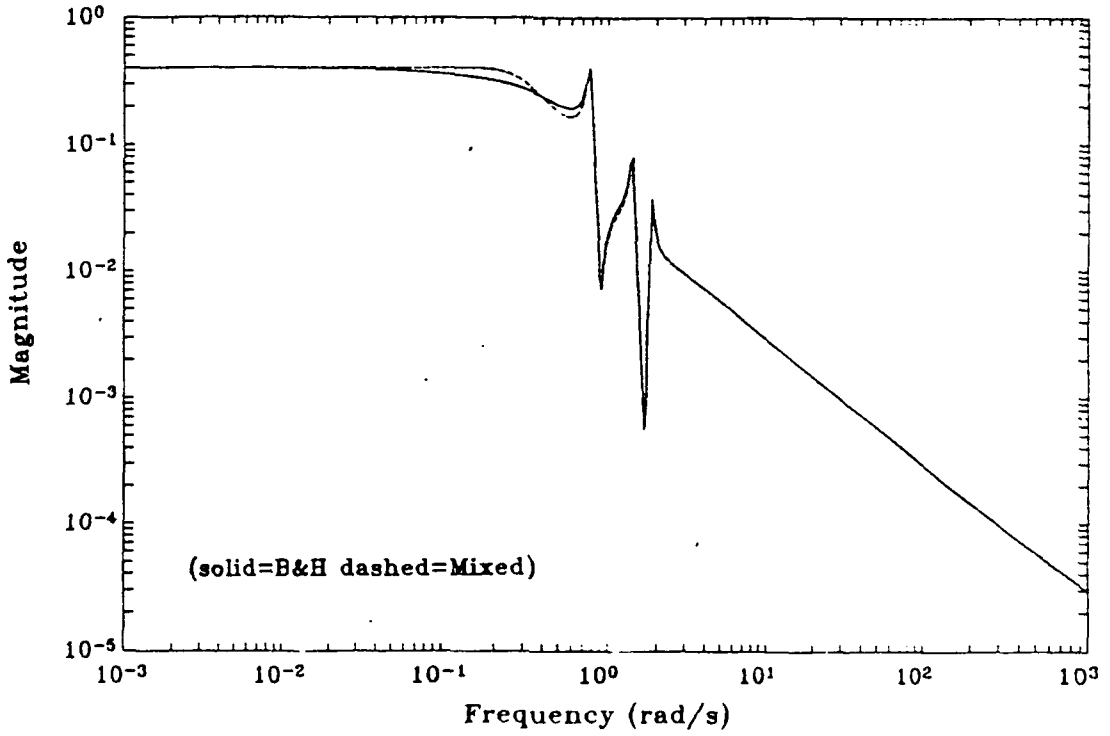

Figure 5.26 σ-Plot of T_{ew} (∞-norm = 0.40)

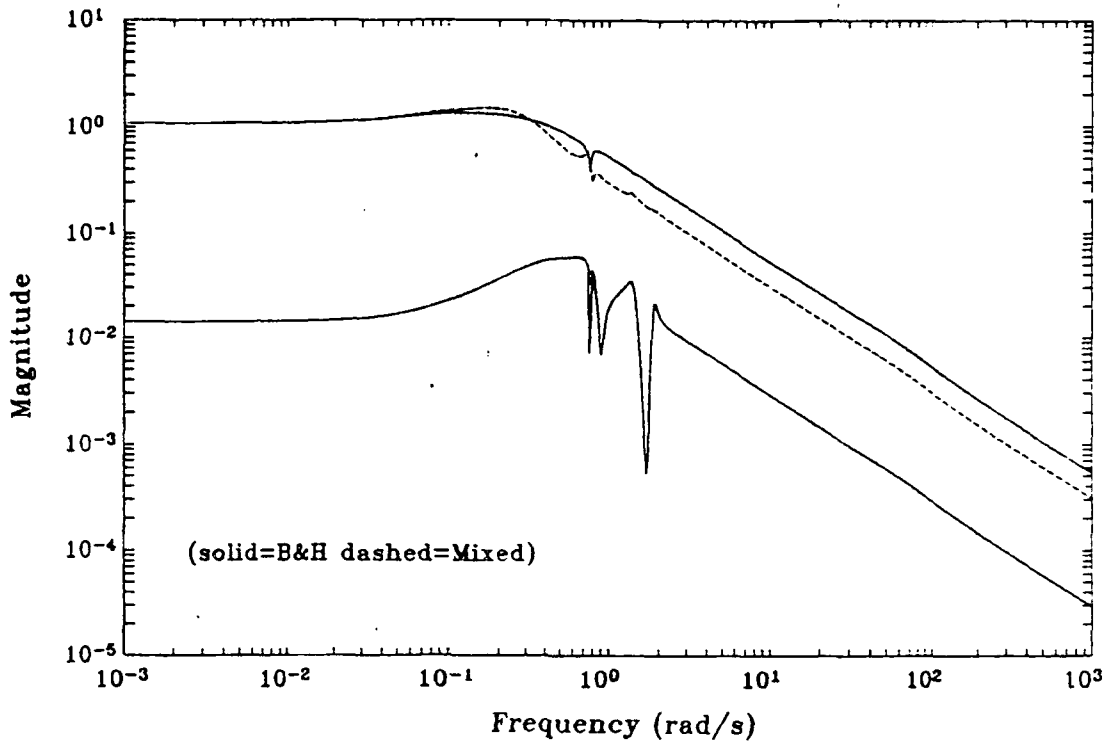

Figure 5.27 σ-Plot of T_{zw} (∞-norm = 0.40)

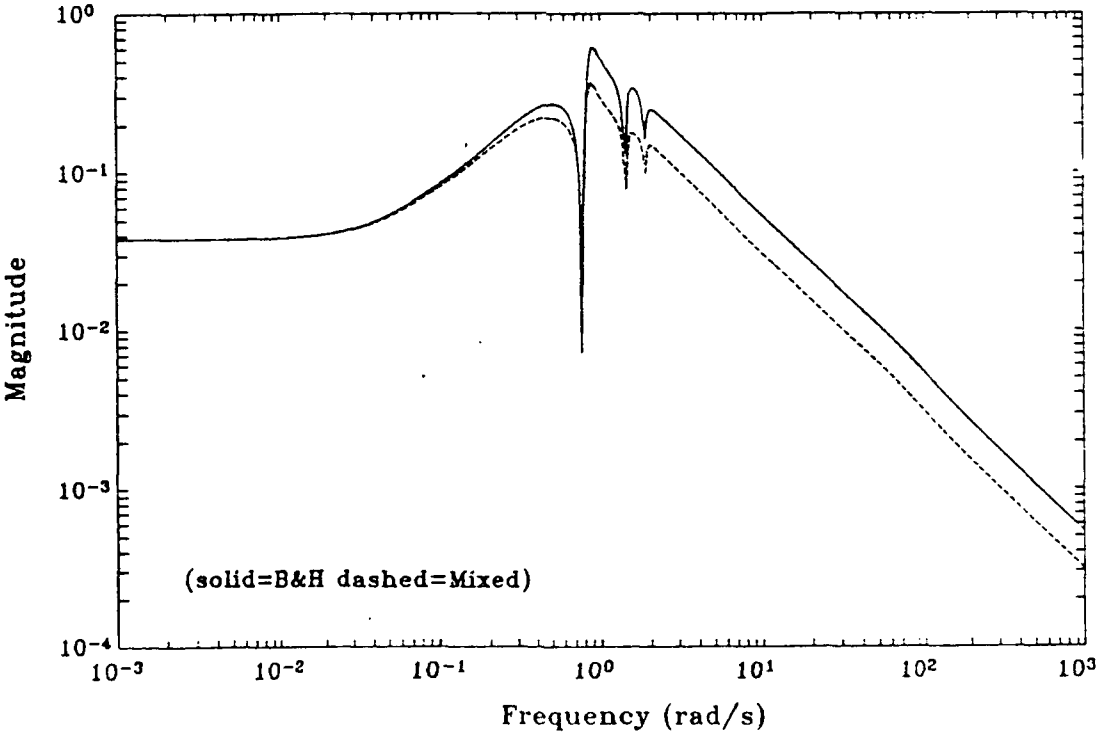

Figure 5.28 σ-Plot of Controllers (∞-norm = 0.40)

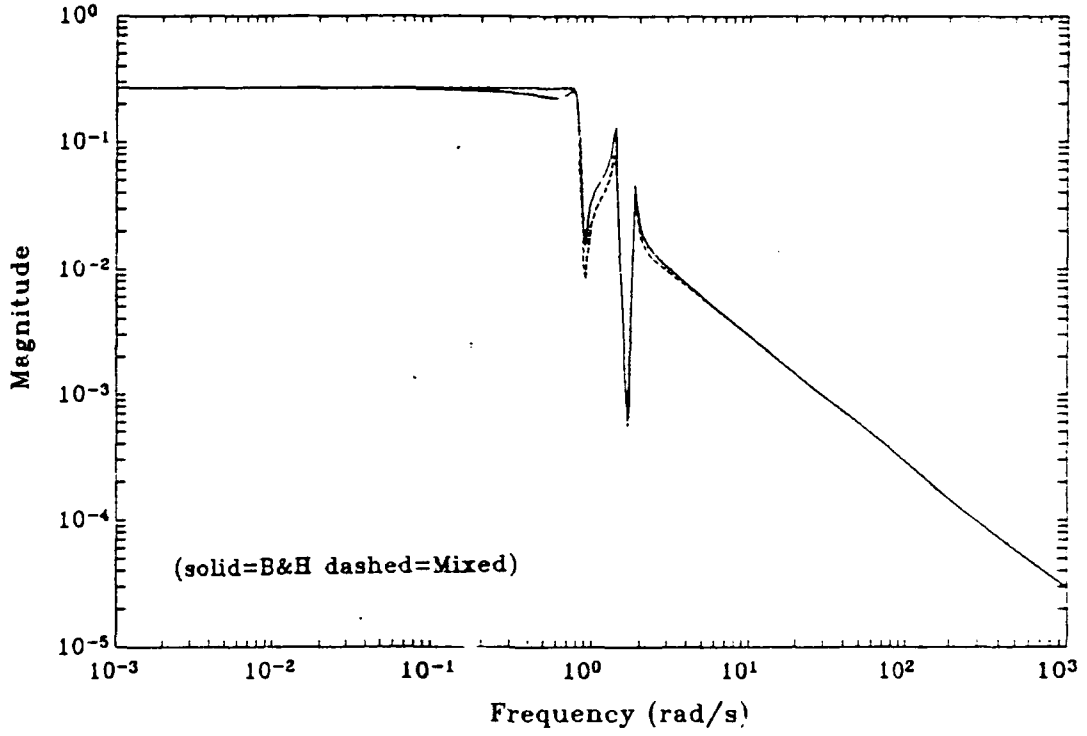

Figure 5.29 σ-Plot of T_{ew} (∞-norm = 0.27)

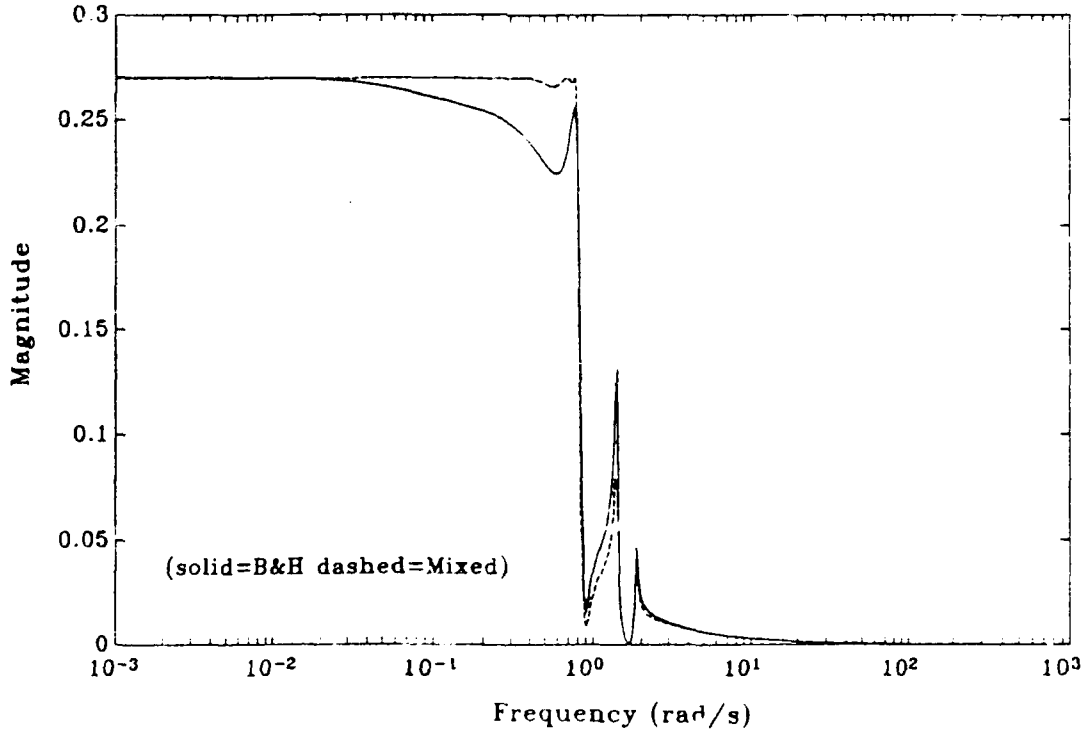

Figure 5.30 σ-Plot of T_{ew} (∞-norm = 0.27)

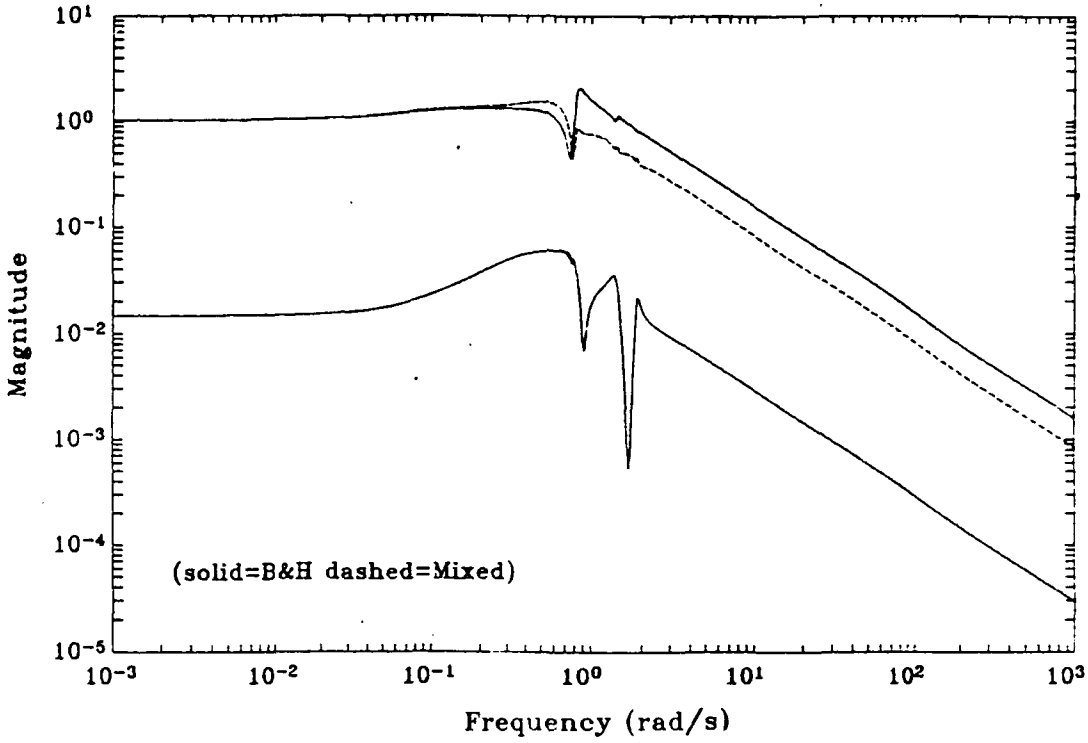

Figure 5.31 σ-Plot of T_{zw} (∞-norm = 0.27)

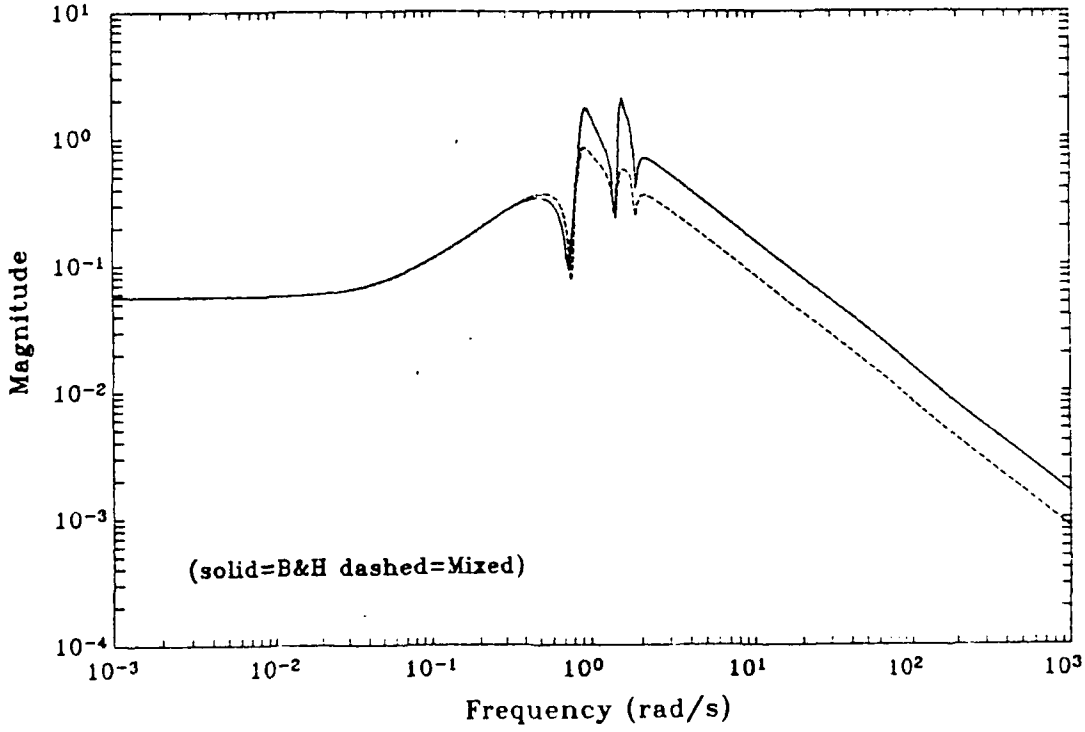

Figure 5.32 σ-Plot of Controllers (∞-norm = 0.27)

Chapter VI. Two Exogenous Inputs Two Exogenous Outputs

6.1 Problem Synthesis

This system has two exogenous inputs and two exogenous outputs (2I2O). In standard form, it is represented as in Figure 6.1.

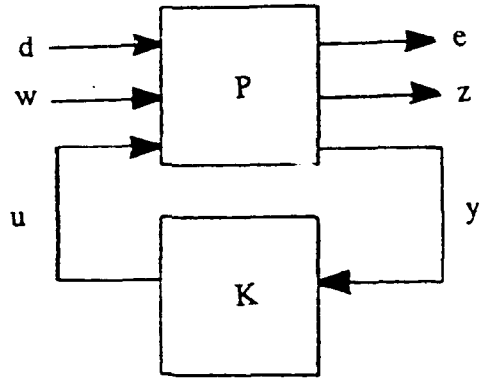

$$P=\left[\begin{array}{c|ccc} A & B_d & B_w & B_u \\ \hline C_e & 0 & D_{ew} & D_{eu} \\ C_z & D_{zd} & 0 & D_{zu} \\ C_y & D_{yd} & D_{yw} & 0 \end{array}\right]$$

Figure 6.1 2I2O Standard Form

Thus, the mixed problem is

$$\inf_{K \text{ stabilizing}} \|T_{zw}\|_2 \quad \text{subject to } \|T_{ed}\|_\infty \le \gamma$$

so that we are optimizing noise performance in the T_{zw} transfer function while we are concerned about robustness in

the T_{ed} transfer function. T_{ed}, for example, could be associated with command following error, while T_{zw} could be associated with plant response to noise.

6.2 Background

There are currently no other techniques to handle a 2I2O system. The Mixed Solution is the only real solution in this case. It is possible to generate an H_∞ central solution based only on T_{ed}, but this is not really mixed at all since T_{zw} is not considered in the problem. The only true comparisons in this case are with the $H_{\infty opt}$ and H_{2opt} solutions at each end of the trade-off.

6.3 Description

The B & H system in Chapter 5 can be readily extended to a 2I2O problem with a block diagram as in Figure 6.2. Manipulating the state space we have

$$\dot{x} = Ax + B\left(u + \rho_{d1}\, d_1 + \rho_{w1}\, W_1\right)$$
$$y = C_x + \rho_{d2}\, d_2 + \rho_{w2}\, w_2$$

$$e = \begin{bmatrix} e_1 \\ e_2 \end{bmatrix} = \begin{bmatrix} \rho_{e1} x \\ \rho_{e2} u \end{bmatrix}$$

$$z = \begin{bmatrix} z_1 \\ z_2 \end{bmatrix} = \begin{bmatrix} \rho_{z1} x \\ \rho_{z2} u \end{bmatrix}$$

or

$$P=\left[\begin{array}{c|ccccc} A & B\rho_{d1} & 0 & B\rho_{w1} & 0 & B \\ \hline \rho_{e1} & 0 & 0 & 0 & 0 & 0 \\ 0 & 0 & 0 & 0 & 0 & \rho_{e2} \\ \rho_{z1} & 0 & 0 & 0 & 0 & 0 \\ 0 & 0 & 0 & 0 & 0 & \rho z_2 \\ C & 0 & \rho_{d2} & 0 & \rho_{w2} & 0 \end{array}\right]$$

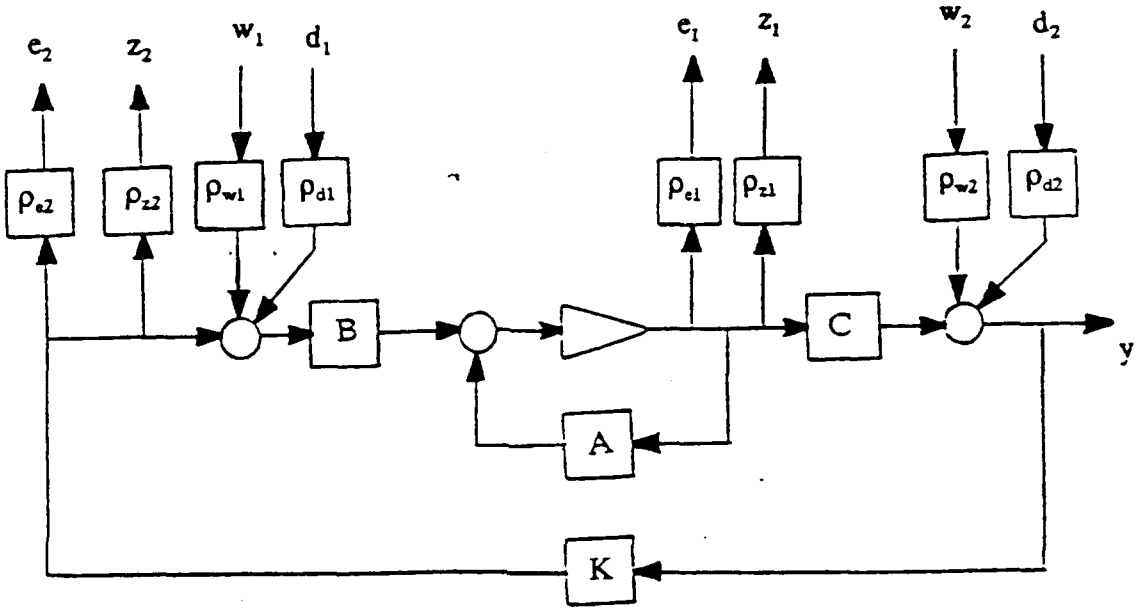

Figure 6.2 System Block Diagram

The A, B_w, B_u, C_e, C_z, C_y, D_{yw}, and D_{eu} matrices are as in Chapter 5, while

$$D_{eu}=\begin{bmatrix} 0 \\ .0001 \end{bmatrix}$$

$$B_d = B_w$$

$$D_{yd}=D_{yw}$$

Thus, we have disturbances entering the system at the plant input and output. Robustness is being measured with

respect to some plant states different than the measured states. Noise is also coming into the system at the plant input and output, with performance being measured with respect to some plant states different than the measured states. All of the ρ weighting matrices are non-zero in this example.

The $H_{\infty opt}$ and H_{2opt} controllers are as shown in Figure 6.3. Note the large gain increase in the $H_{\infty opt}$ controller above 1 rad/s in contrast to the H_{2opt}'s roll-off. These controllers result in $\gamma_o = 0.12015$, $\gamma_2 = 1.3923$, and $\alpha_o = 0.3786$. Figure 6.4 shows the resulting closed loop T_{zw} and T_{ed} with the H_{2opt} controller. Since this is the T_{zw}-H_{2opt} controller, $\|T_{zw}\|_2$ is minimized here, but T_{ed} is showing similar characteristics with this controller. Figure 6.5 shows the resulting closed loop T_{ed} and T_{zw} with the $H_{\infty opt}$ controller. Here we see the typical flat $\bar{\sigma}$ (T_{ed}) curve. Note that $\|T_{zw}\|_2$ is going to infinity.

6.4 Results

The $\|T_{ed}\|_\infty$ versus $\|T_{zw}\|_2$ trade-off is clearly shown in Figure 6.6. This data is also displayed in Table 6.1.

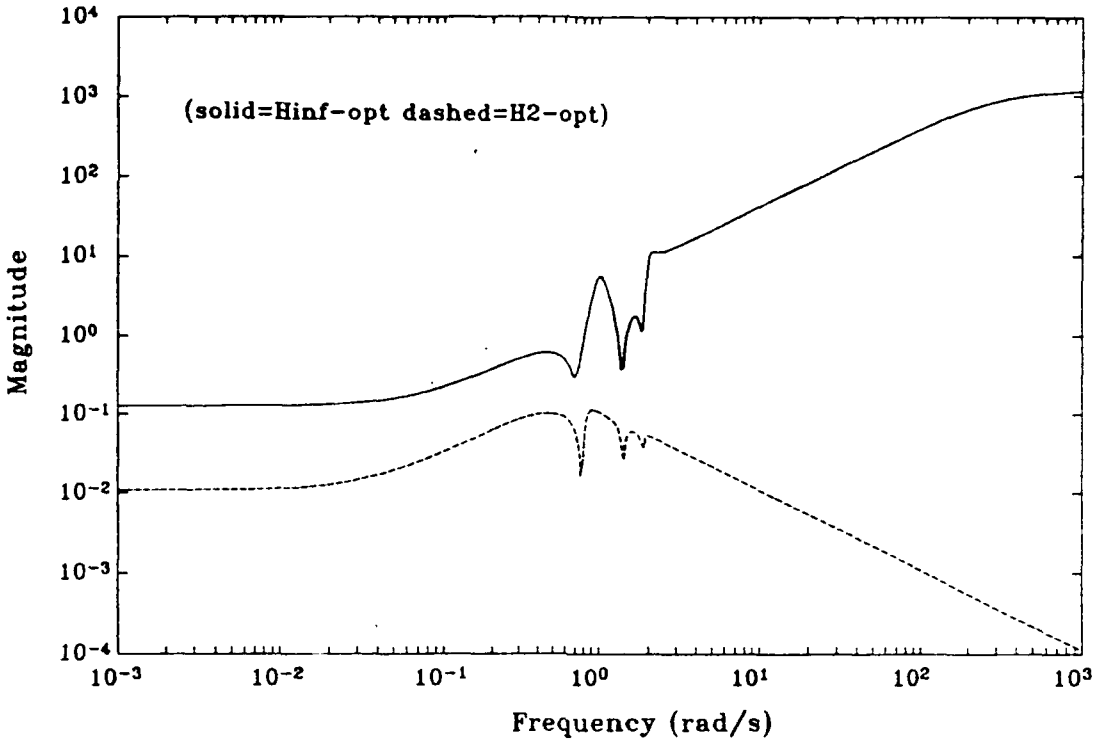

Figure 6.3 σ-Plot of the H_2 and H_∞ Optimal Controllers

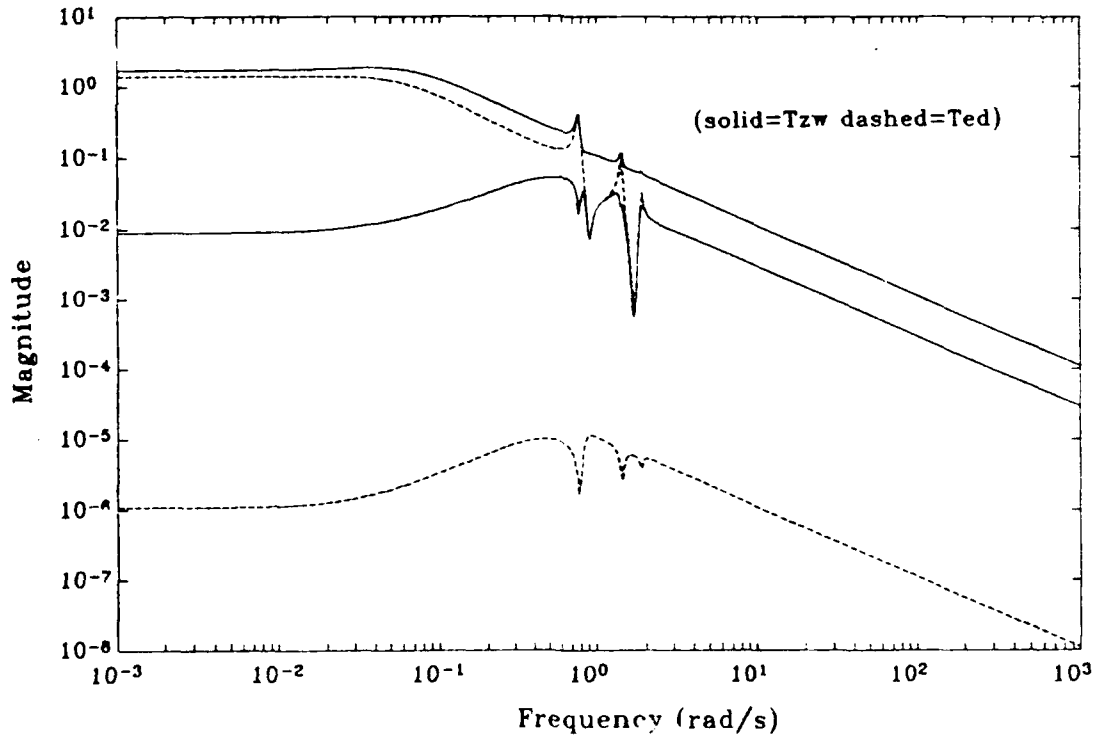

Figure 6.4 σ-Plot of the H_{2opt} T_{zw} and T_{ed}

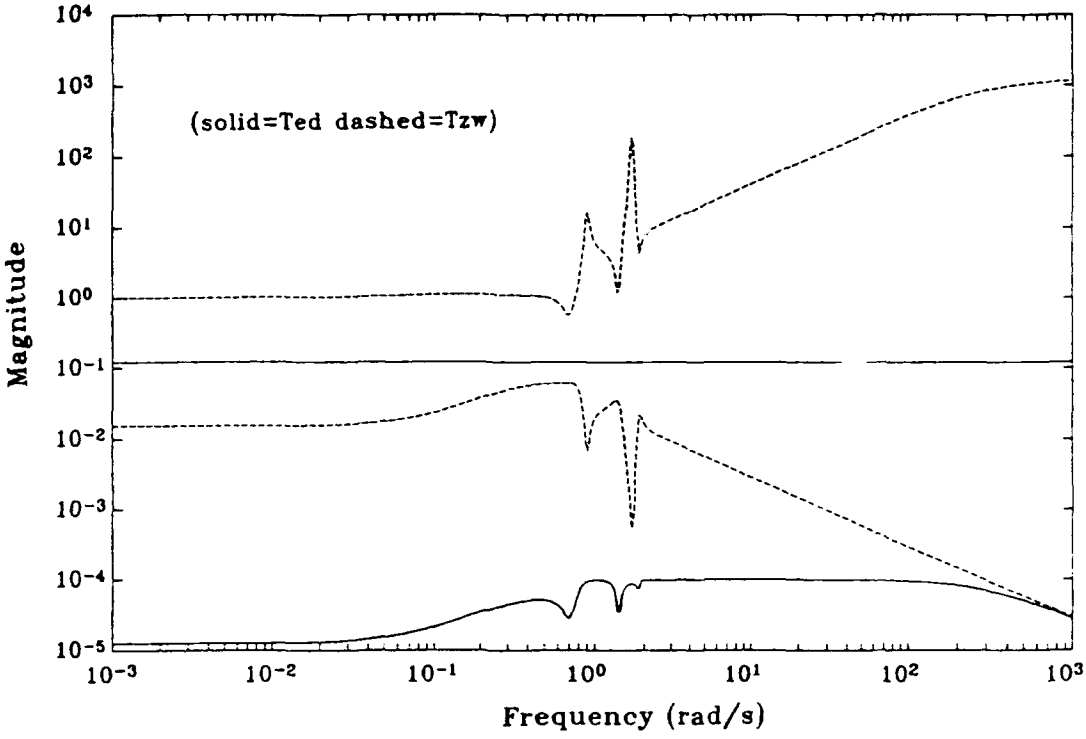

Figure 6.5 σ-Plot of the $H_{\infty opt}$ T_{zw} and T_{ed}

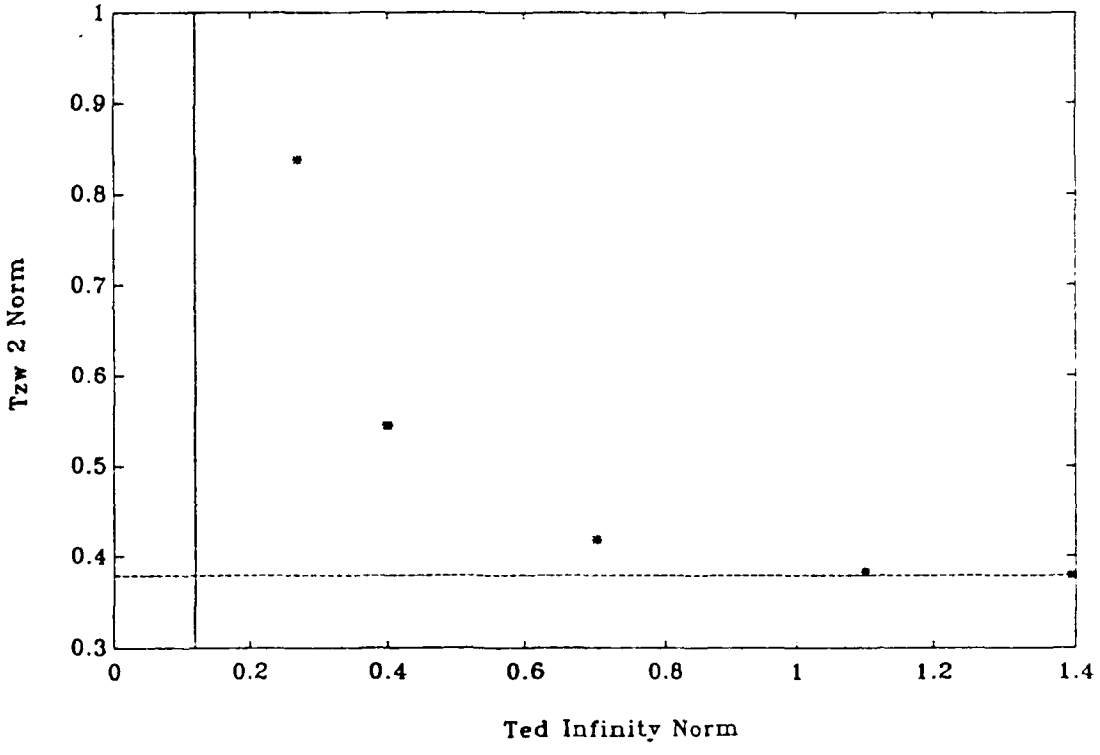

Figure 6.6 Mixed Controller Trade-off

Table 6.1 Mixed Solution to 2I2O

γ	$\|T_{ed}\|_\infty$	$\|T_{rw}\|_2$
.27	.27	.8381
.4	.4	.5444
.7	.7	.4180
1.1	1.1	.3824

Figure 6.7 shows the controllers transitioning from H_{2opt} to $H_{\infty opt}$ with the arrow pointing toward decreasing γ. Note the large change from γ = .27 to γ_o. In Figure 6.8, T_{ed} is shown progressing to the infinite bandwidth $H_{\infty opt}$ solution as γ is decreased. Note that while $\|T_{ed}\|_\infty$ is going down, the minimum singular value is going up. Thus, a trade-off is being made here, as well as between the 2-norm and ∞-norm.

In Figure 6.9, T_{zw} is shown progressing away from the H_{2opt} solution as γ is decreased. Note that the bandwidth increases here as γ is decreased.

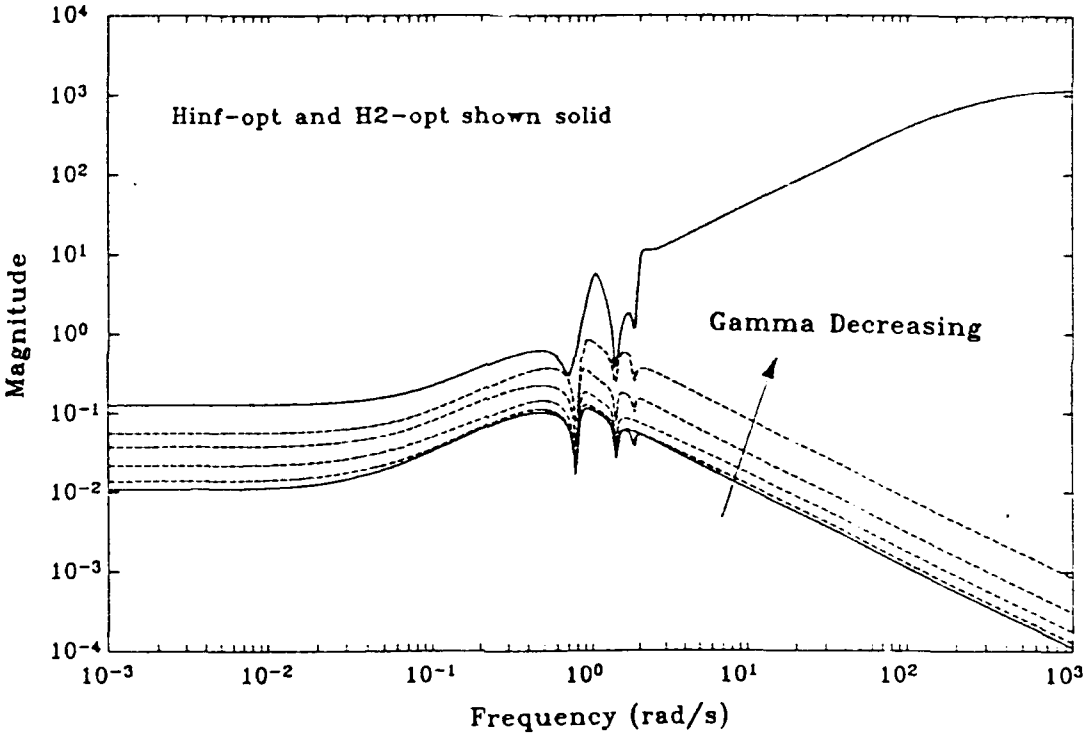

Figure 6.7 σ-Plot of the Mixed Controllers

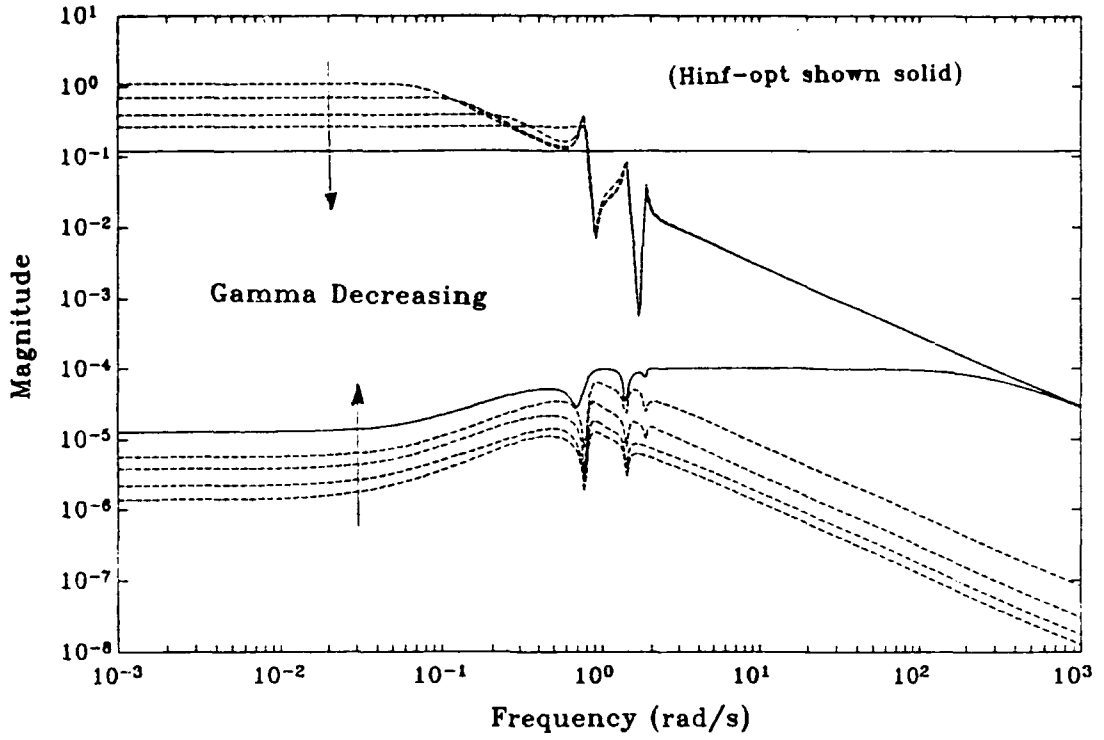

Figure 6.8 σ-Plot of T_{ed}

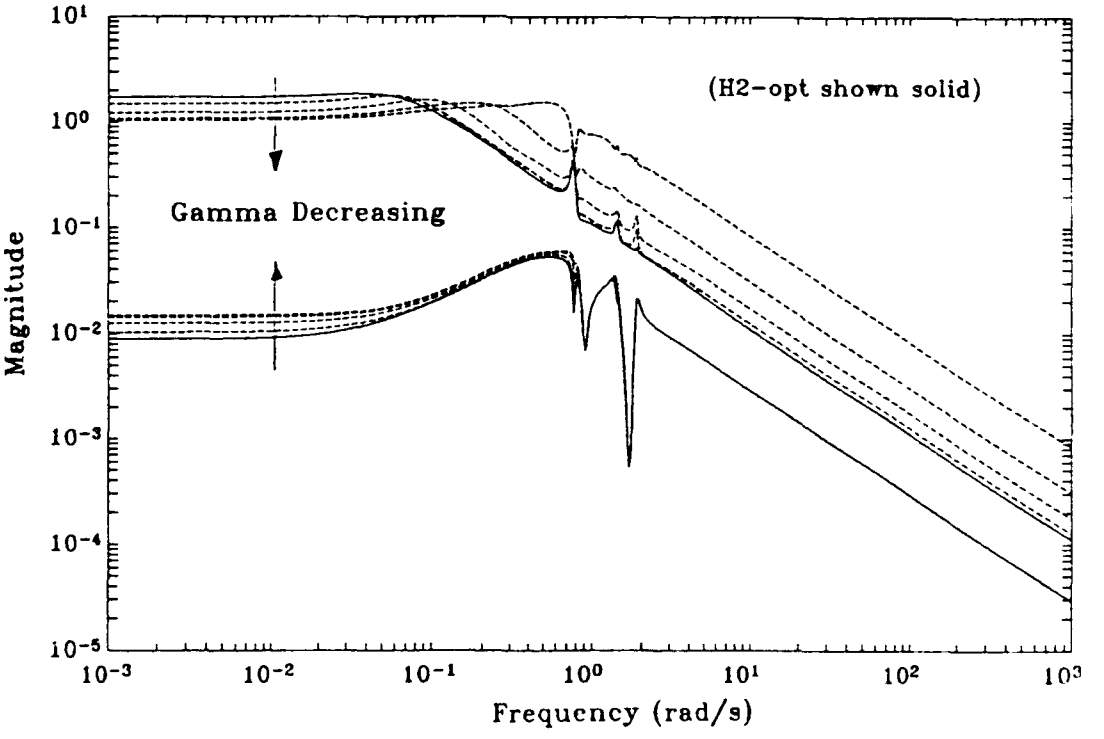

Figure 6.9 σ-Plot of T_{zw}

Looking at the γ = .27 case, Figure 6.10 shows T_{ed} and the Mixed controller (shifted up two decades for clarity). The controller peaks at .9 and 1.8 rad/s can be seen to correspond with dips in the maximum T_{ed} singular value at those frequencies. Notice the similarity the controller has to the minimum T_{ed} singular value plot, caused in this problem by the way the state and control penalties are structured. Figure 6.11 shows T_{zw} and the Mixed controller, but the relationships here are not so clear. Figure 6.12 and 6.13 show similar characteristics for γ = .7.

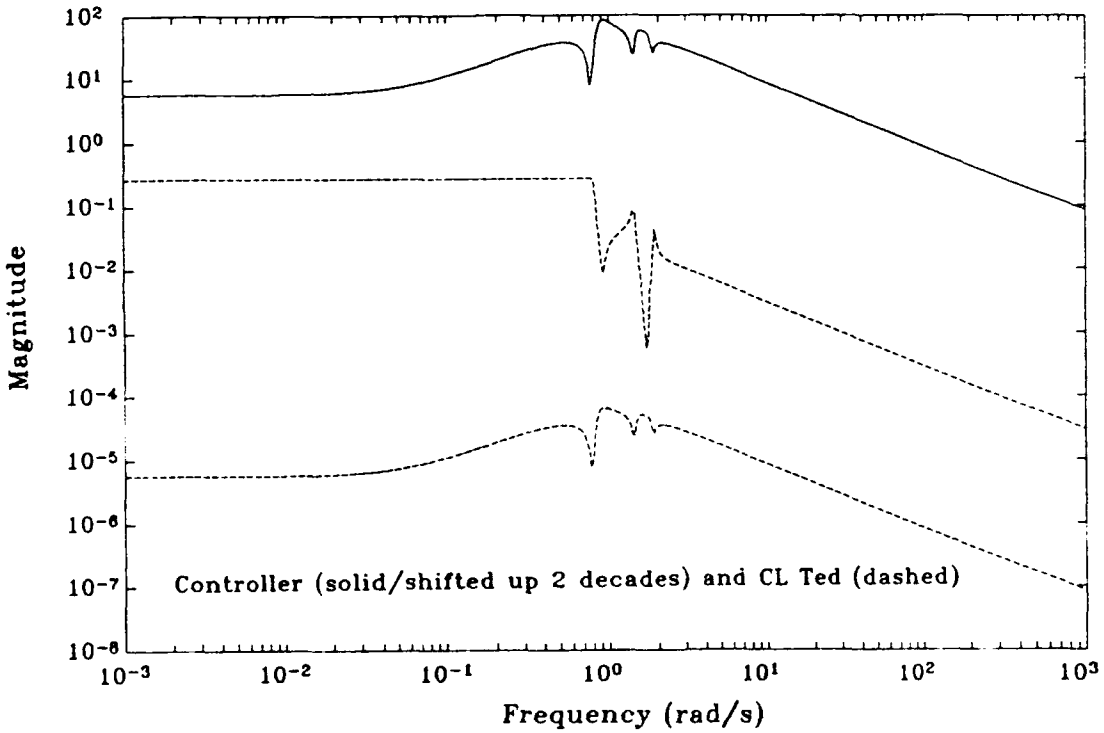

Figure 6.10 σ-Plot of Controller and T_{ed} (∞-norm = .27)

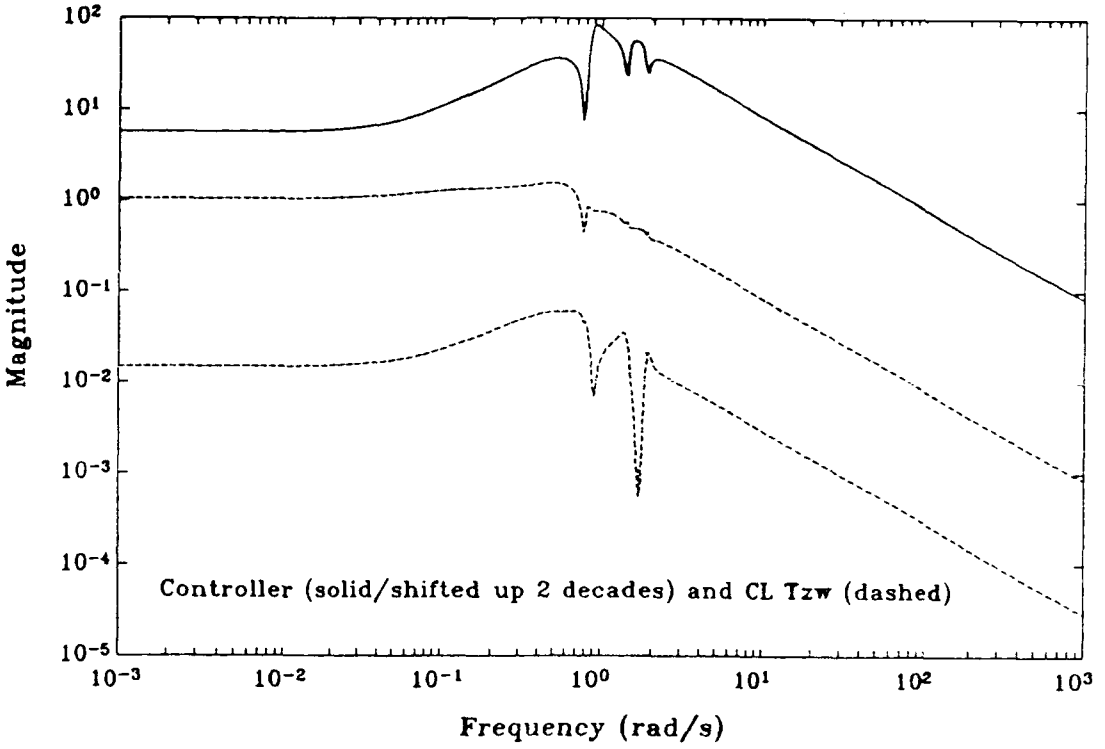

Figure 6.11 σ-Plot of Controller and T_{zw} (∞-norm = .27)

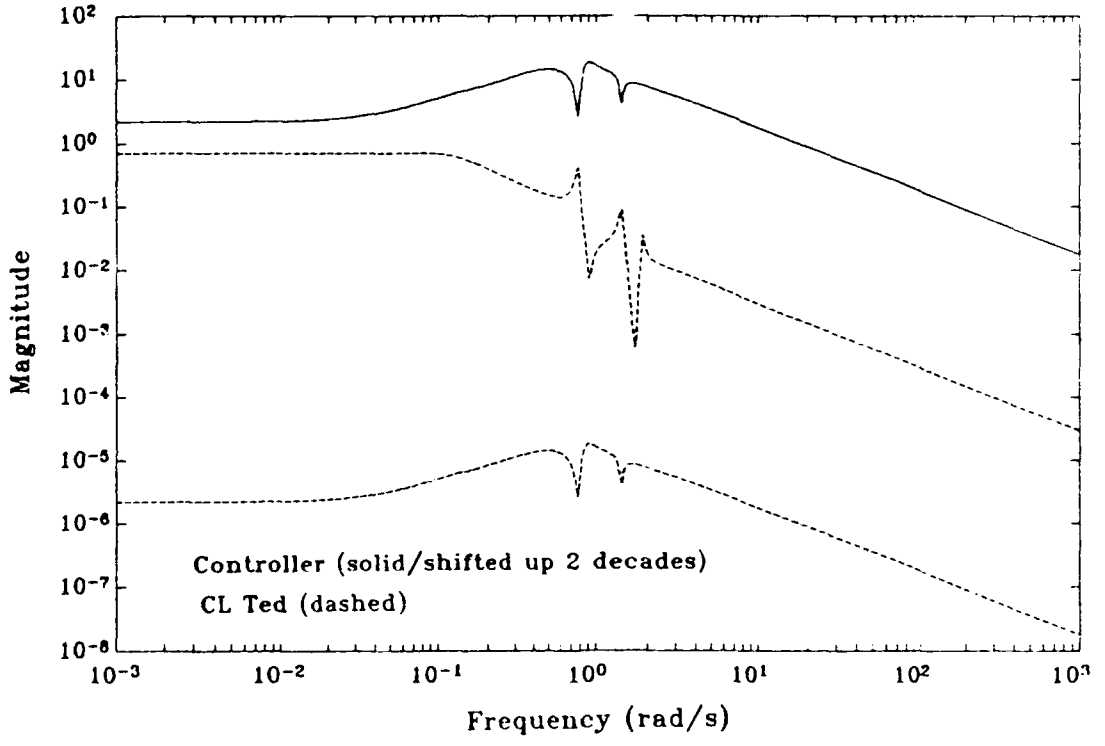

Figure 6.12 σ-Plot of Controller and T_{ed} (∞-norm = .7)

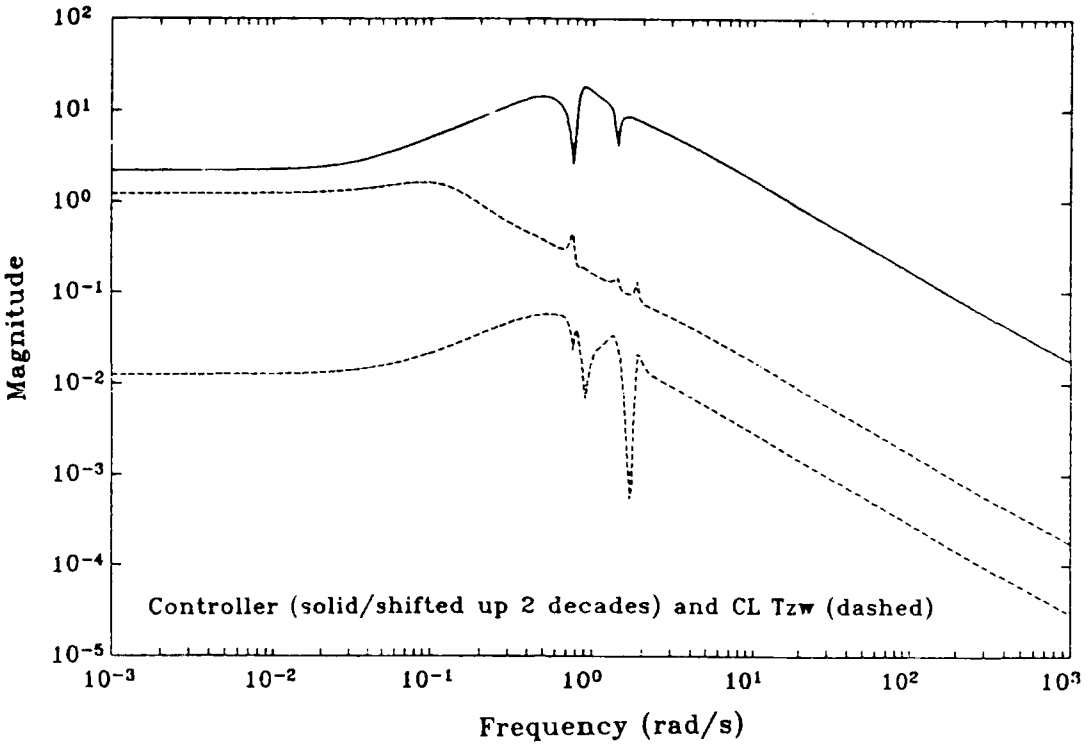

Figure 6.13 σ-Plot of Controller and T_{zw} (∞-norm = .7)

Thus, the Mixed Solution provides complete visibility into the ∞-norm versus 2-norm trade-off for the 2I2O system. This practical example again showed the solution to be on the ∞-norm boundary where $\|T_{ed}\|_\infty = \gamma$.

Chapter VII. Conclusions and Recommendations

7.1 Summary and Conclusions

The objective of this thesis was to apply a newly developed nonconservative mixed optimization solution to several example problems and compare this solution to the best previously available solutions. The final measure in the comparison was the 2-norm versus ∞-norm trade-off curve.

In Chapter 2, various aspects of control theory and the role of H_2 and H_∞ theory were discussed. Chapter 3 covered the procedure and analysis techniques required to obtain a Mixed Solution.

The 1I1O example was looked at in Chapter 4. The comparison in this case was done between the Mixed and H_∞ central solutions for a third order SISO system. The example showed that the Mixed Solution does converge to the H_{2opt} solution at γ_2 and to the $H_{\infty opt}$ solution at γ_o. For $\gamma_o < \gamma < \gamma_2$, the Mixed Solution is superior to the H_∞ central Solution because of the latter's conservative overbound. In this specific example, the difference peaked at the mid-range γ, and was approximately 5 percent of the 2-norm.

A 1I2O example was covered in Chapter 5. For this system, the Mixed Solution was compared with the Bernstein & Haddad Solution for an eighth order system. This particular example problem came from the original Bernstein & Haddad

paper demonstrating their solution and included the limitation that the H_∞ control penalty must be zero. The example showed that both the Mixed Solution and the Bernstein & Haddad solution converge to the same ($H_{2opt.}$) solution at γ_2. For $\gamma < \gamma_2$, the Mixed Solution is superior to the Bernstein & Haddad solution, again because of the latter's conservative overbound. As in the 1I1O comparison, the hallmark of the Mixed Solution appears to be the sharper corner to the roll-off that it makes on the T_{ed} plot.

Chapter 6 looked at a 2I2O eighth order example system. This system was chosen as an extension of the 1I2O Bernstein & Haddad system because of its practical motivation (actuators, sensors, and spinning masses). No comparison to previous results was possible in this case, because no other solution exists to this problem. The example again showed again that the Mixed Solution converges to the $H_{\infty\ opt.}$ or $H_{2\ opt}$ solution at their respective γ's. The example clearly showed the ∞-norm versus 2-norm trade that is possible.

7.2 Recommendations

Practical applications still need to be looked at in earnest. Several of the practical examples that were looked at could not be done with the software code used in this thesis, because either the problem would not numerically start, or once started would not converge. It is not known whether this is related to modeling, numerics, or software,

but this is definitely an area of further study.

As an adjunct to this, further refinements to the current numerical algorithm might help its robustness and speed. Perhaps a whole new algorithm could better find the solution.

For the current algorithm, finding a start point for a system greater than 1I1O is very time consuming because of numerous points that should work, but do not. A reliable method of finding start points would be a worthwhile investment.

Finally, the Mixed Solution has a large number of tunable parameters. The practical techniques of using these parameters to achieve desired results still needs to be investigated.

Bibliography

1. Ridgely, D.B., "A Non-Conservative Solution to the General Mixed H_2/H_∞ Optimization Problem," Phd Dissertation, Massachusetts Institute of Technology, Cambridge, MA, 1991.

2. Yeh, H., Banda, S.S., "Necessary and Sufficient Conditions for Mixed H_2 and H_∞ Optimal Control," Proceedings of the 29th Conference on Decision and Control, Honolulu, HI, Dec. 1990.

3. Black, K.M., "A New Algorithm for Solving a Mixed H_2/H_∞ Optimization Problem," Proceedings of the 1991 American Control Conference, Boston, MA, June 1991.

4. Wells, S.R., Ridgely, D.B., "Using Increased Order Controllers in Mixed H_2/H_∞ Optimization," submitted to the 1992 American Control Conference, Chicago, IL, 1992.

5. Bernstein, D.S., Haddad, W.M., "LQG Control with an H_∞ Performance Bound: A Ricatti Equation Approach," IEEE Transactions on Automatic Control, Vol. 34, No. 3, March 1989.

6. Mustafa, D., Glover, K., "Minimum Entropy H_∞ Control," Lecture Notes in Control and Information Sciences, Springer-Verlag, Berlin, 1990.

7. Doyle, J., Zhou, K., Bodenhemier, B., "Optimal Control with Mixed H_2 and H_∞ Performance Objectives," Proceedings of the American Control Conference, Pittsburgh, PA, June 1989.

8. Fox, R.L., Optimization Methods for Engineering Design, Addison-Wesley, Reading, MA, 1971.

Appendix A: Selected Software Items

This appendix contains the PRO-MATLAB user written routines utilized in this thesis and an example of an input file to the Fortran based DFP program.

BH.M algorithum for solving the Bernstein and Haddad problem:

```
g2=1/(gam*gam);
a=am;
b=bm;
c=cm;
v1=d1*d1';
v2=d2*d2';
r1=e1'*e1;
r2=e2'*e2;
r1inf=e1inf'*e1inf;
sig=b*inv(r2)*b';
sigbar=c'*inv(v2)*c;
%
% solve for q
%
f=a';
g=-(g2*r1inf-sigbar);
h=v1;
q=are(f,g,h);
%
%initialize p
%
%p=eye(n);
p=pchest;
%
% iterate between qhat and p equations
%
error=1;
while error>.001
%
f=(a+g2*q*r1inf-sig*p)';
g=-g2*r1inf;
h=q*sigbar*q;
qhat=are(f,g,h);
%
f=(a+g2*(q+qhat)*r1inf);
g=sig;
h=r1;
pold=p;
p=are(f,g,h);
```

```
%
error=norm(p-pold,'fro')
%
end
disp('converged')
%
% check answers
%
if abs(q'-q)>10^(-5)
disp('q not symetric')
end
%
if min (eig(q)) < 0
disp('q not positive definite')
min(eig(q))
end
%
if abs(qhat'-qhat)>10^(-5)
disp('qhat not positve definite')
end
%
if min(eig(qhat))<0
disp('qhat not positive definite')
end
%
if abs(p'-p)>10^(-5)
disp('p not symmetric')
end
%
if min (eig(p))<0
disp('p not positive definite')
min(eig(p))
end
%
% compute the controller
%
bc=q*c'*inv(r2);
cc=-inv(r2)*b'*p;
ac=a+b*cc-bc*c+g2*q*r1inf;
dc=0;
%
%compute cl system
%
[a,b,c,d]=lftf(pfwd,[8,2,1,4,1],ac,bc,cc,dc);
%
%compute norms
%
h=mynorm(a,b,c(1:2,:),zeros(2,2))
hinf=h(2)
h=mynorm(a,b,c(3:4,:),zeros(2,2))
h2=h(1)
```

BLACK.M algorithum for solving the Bernstein and Haddad problem using the K. Black technique:

```
g2=1/(gam*gam);
a=am;
b=bm;
c=cm;
v1=d1*d1';
v2=d2*d2';
r1=e1'*e1;
r2=e2'*e2;
r1inf=e1inf'*e1inf;
sig=b*inv(r2)*b';
sigbar=c'*inv(v2)*c;
%
% find gam = infinity p and qhat
%
f=a;
g=sig;
h=r1;
pzero=are(f,g,h);
z=a-sig*p;
x=sigbar;
qhatz=lyap(z,x);
%
% solve for q
f=a';
g=-(g2*r1inf-sigbar);
h=v1;
q=are(f,g,h);
%
% iterate between qhat and p equations
%
p=pzero;
qhatk=qhatz;
error=1;
k=0;
while error>.000001
%
k=k+1
%
f=(a+g2*(q+qhatk)*r1inf);
g=sig;
h=r1;
pold=p;
p=are(f,g,h);
%
z=a-sig*p+g2*(q+qhatk/2)*r1inf;
x=q*sigbar*q;
qhatk=lyap(z,x);
```

```
%
error=norm(p-pold,'fro')
%
end
disp('converged')
%
% check answers
%
if abs(q'-q)>10^(-5)
disp('q not symetric')
end
%
if min (eig(q)) < 0
disp('q not positive definite')
min(eig(q))
end
%
if abs(qhatk'-qhatk)>10^(-5)
disp('qhat not positve definite')
end
%
if min(eig(qhatk))<0
disp('qhat not positive definite')
end
%
if abs(p'-p)>10^(-5)
disp('p not symmetric')
end
%
if min (eig(p))<0
disp('p not positive definite')
min(eig(p))
end
%
% compute the controller
%
bc=q*c'*inv(r2);
cc=-inv(r2)*b'*p;
ac=a+b*cc-bc*c+g2*q*r1inf;
dc=0;
%
%compute cl system
%
[a,b,c,d]=lftf(pfwd,[8,2,1,4,1],ac,bc,cc,dc);
%
%compute norms
%
h=mynorm(a,b,c(1:2,:),zeros(2,2))
hinf=h(2)
h=mynorm(a,b,c(3:4,:),zeros(2,2))
h2=h(1)
```

BHD.M algorithum for solving the dual of the Bernstein and Haddad problem:

```
g2=1/(gam*gam);
a=am;
e1=ce;
c=cy;
d1=bw;
d2=dyw;
d1inf=bd;
d2inf=dyd;
b=bu;
e2=deu;
v1inf=d1inf*d1inf';
v1=d1*d1';
v2=d2*d2';
r1=e1'*e1;
r2=e2'*e2;
sig=b*inv(r2)*b';
sigbar=c'*inv(v2)*c,
%
% solve for q
%
f=a;
g=-(g2*v1inf-sig);
h=r1;
q=are(f,g,h);
%
%initialize p
%
%p=eye(n);
p=pchest;
%
% iterate between qhat and p equations
%
error=1;
while error>.001
%
f=a+g2*v1inf*q-p*sigbar;
g=-g2*v1inf*q;
h=q*sig*q;
qhat=are(f,g,h);
%
f=(a+g2*v1inf*(q+qhat))';
g=sigbar;
h=v1;
pold=p;
p=are(f,g,h);
%
error=norm(p-pold,'fro')
```

```
%
end
disp('converged')
%
% check answers
%
if abs(q'-q)>10^(-5)
disp('q not symetric')
end
%
if min (eig(q)) < 0
disp('q not positive definite')
min(eig(q))
end
%
if abs(qhat'-qhat)>10^(-5)
disp('qhat nct positve definite')
end
%
if min(eig(qhat))<0
disp('qhat not positive definite')
end
%
if abs(p'-p)>10^(-5)
disp('p not symmetric')
end
%
if min (eig(p))<0
disp('p not positive definite')
min(eig(p))
end
%
% compute the controller
%
bc=-p*c'*inv(v2);
cc=inv(r2)*b'*q;
ac=a+bc*c-b*cc+g2*v1inf*q;
dc=0;
%
%compute cl system
%
[a,b,c,d]=lftf(p2,[3,2,1,1,1],ac,bc,cc,dc);
%
%compute norms
%
h=mynorm(a,b(1:6,1),c,d);
hinf=h(2)
h=mynorm(a,b(1:6,2),c,d);
h2=h(1)
```

This is an example of an input file to the Fortran based DFP program. It contains all dimensions, state space matrices, numerical parameters, and an initial controller guess.

```
THIS IS THE  I.file     FOR THE DIRECT METHOD
THE SISO MIX NUMBER 1 PROBLEM GAMMA 3.5 MU .000000

THE DIMENSIONS ISTATE,NU,NY,ND,NE,NW,NZ
       8       1       1       2       2       2       2

THE PARAMETERS GAMMA AND MU (2D11.6)
  0.730D+00  0.100D+00

THE TOLERANCES OF: 1-D SEARCH, CHECKSTOP (2D11.6)
  0.100D-03  0.100D-04

THE A MATRIX (8F8.4)
   -0.16100E+00     0.10000E+01     0.00000E+00     0.00000E+00
    0.00000E+00     0.00000E+00     0.00000E+00     0.00000E+00
   -0.60040E+01     0.00000E+00     0.10000E+01     0.00000E+00
    0.00000E+00     0.00000E+00     0.00000E+00     0.00000E+00
   -0.58220E+00     0.00000E+00     0.00000E+00     0.10000E+01
    0.00000E+00     0.00000E+00     0.00000E+00     0.00000E+00
   -0.99835E+01     0.00000E+00     0.00000E+00     0.00000E+00
    0.10000E+01     0.00000E+00     0.00000E+00     0.00000E+00
   -0.40730E+00     0.00000E+00     0.00000E+00     0.00000E+00
    0.00000E+00     0.10000E+01     0.00000E+00     0.00000E+00
   -0.39820E+01     0.00000E+00     0.00000E+00     0.00000E+00
    0.00000E+00     0.00000E+00     0.10000E+01     0.00000E+00
    0.00000E+00     0.00000E+00     0.00000E+00     0.00000E+00
    0.00000E+00     0.00000E+00     0.00000E+00     0.10000E+01
    0.00000E+00     0.00000E+00     0.00000E+00     0.00000E+00
    0.00000E+00     0.00000E+00     0.00000E+00     0.00000E+00

THE BU MATRIX AS BU TRANSPOSE
    0.00000E+00     0.00000E+00     0.64000E-02     0.23500E-02
    0.71300E-01     0.10002E+01     0.10450E+00     0.99550E+00

THE BD MATRIX AS BD TRANSPOSE
    0.00000E+00     0.00000E+00     0.64000E-02     0.23500E-02
    0.71300E-01     0.10002E+01     0.10450E+00     0.99550E+00
    0.00000E+00     0.00000E+00     0.00000E+00     0.00000E+00
    0.00000E+00     0.00000E+00     0.00000E+00     0.00000E+00

THE BW MATRIX AS BW TRANSPOSE
    0.00000E+00     0.00000E+00     0.64000E-02     0.23500E-02
    0.71300E-01     0.10002E+01     0.10450E+00     0.99550E+00
    0.00000E+00     0.00000E+00     0.00000E+00     0.00000E+00
    0.00000E+00     0.00000E+00     0.00000E+00     0.00000E+00

THE CY MATRIX
    0.10000E+01     0.00000E+00     0.00000E+00     0.00000E+00
    0.00000E+00     0.00000E+00     0.00000E+00     0.00000E+00
```

```
THE CE MATRIX
    0.00000E+00     0.00000E+00     0.00000E+00     0.00000E+00
    0.55000E-03     0.11000E-01     0.13200E-02     0.18000E-01
    0.00000E+00     0.00000E+00     0.00000E+00     0.00000E+00
    0.00000E+00     0.00000E+00     0.00000E+00     0.00000E+00

THE CZ MATRIX
    0.00000E+00     0.00000E+00     0.00000E+00     0.00000E+00
    0.55000E-03     0.11000E-01     0.13200E-02     0.18000E-01
    0.00000E+00     0.00000E+00     0.00000E+00     0.00000E+00
    0.00000E+00     0.00000E+00     0.00000E+00     0.00000E+00

THE DYD MATRIX
    0.00000E+00     0.10000E+01

THE DYW MATRIX
    0.00000E+00     0.10000E+01

THE DEU MATRIX
    0.00000E+00
    1.00000E-04

THE DZU MATRIX
    0.00000E+00
    0.10000E+01

  THE AC MATRIX  (COLUMNS    1 -   4)
-0.17045507697D+01  0.10000000000D+01  0.00000000000D+00  0.00000000000D+00
-0.72062271373D+01  0.00000000000D+00  0.10000000000D+01  0.00000000000D+00
-0.97874078270D+01  0.51082188294D-02  0.69041782133D-02  0.99821823511D+00
-0.15856634151D+02  0.18756741014D-02  0.25351279377D-02 -0.65424179507D-03
-0.15640813718D+02  0.56908750396D-01  0.76916860407D-01 -0.19849974463D-01
-0.12892587618D+02  0.79831882393D+00  0.10789936014D+01 -0.27845644401D+00
-0.63547130042D+01  0.83407635573D-01  0.11273228489D+00 -0.29092879823D-01
-0.33964959280D+01  0.79456747572D+00  0.10739233455D+01 -0.27714796042D+00

  THE AC MATRIX  (COLUMNS    5 -   8)
 0.19953075890D-02  0.39906151780D-01  0.47887382136D-02  0.65300975640D-01
 0.22716649979D-02  0.45433299958D-01  0.54519959949D-02  0.74345399931D-01
-0.24804614306D-01 -0.44703834031D+00 -0.55536356870D-01 -0.73278478339D+00
 0.99793142253D+00 -0.23359553586D-01 -0.34977755986D-02 -0.38690133929D-01
-0.39626920718D+00 -0.63788925285D+01 -0.90654244797D+00 -0.12088672144D+02
-0.58756954262D+01 -0.10984769656D+03 -0.12477369584D+02 -0.17994886255D+03
-0.60422527221D+00 -0.11283546485D+02 -0.13849144072D+01 -0.17484681044D+02
-0.58592457757D+01 -0.10955472754D+03 -0.13440824044D+02 -0.17946852788D+03

  THE BC MATRIX
 0.15435507697D+01
 0.12022271373D+01
 0.91953201896D+01
 0.58695035337D+01
 0.15123359258D+02
 0.73653352902D+01
 0.61932664252D+01
 0.18585048340D+01

  THE CC MATRIX  (COLUMNS    1 -   4)
-0.15449433389D+01  0.79815919209D+00  0.10787778458D+01 -0.27840076386D+00

  THE CC MATRIX  (COLUMNS    5 -   8)
-0.58902951070D+01 -0.11014122311D+03 -0.13512533653D+02 -0.18042913911D+03
```

Appendix B. Data

Table B.1 CENTRAL H_∞ RESULTS (1I1O)

	γ	$\|Ted\|_2$	$\|Ted\|_\infty$
γ_0	2.1426	291.55	2.1426
	2.1500	27.601	2.1500
	2.1600	18.146	2.1599
	2.1700	14.55	2.1698
	2.1800	12.526	2.1796
	2.1900	11.190	2.1894
	2.2000	10.225	2.1991
	2.2100	9.4877	2.2088
	2.2200	8.9018	2.2184
	2.2300	8.4223	2.2280
	2.2400	8.0211	2.2375
	2.2500	7.6792	2.2470
	2.2600	7.3838	2.2564
	2.2700	7.1254	2.2658
	2.2800	6.8971	2.2751
	2.2900	6.6937	2.2844
	2.3000	6.5111	2.2936
	2.32	6.1961	2.3119
	2.34	5.9336	2.3299
	2.36	5.7109	2.3478
	2.38	5.5193	2.3655
	2.40	5.3527	2.3830
	2.42	5.2062	2.4003
	2.44	5.0764	2.4174
	2.46	4.9605	2.4343
	2.50	4.7625	2.4675

Table B.1 cont.

γ	$\|Ted\|_2$	$\|Ted\|_\infty$
2.55	4.5629	2.5080
2.60	4.4023	2.5474
2.65	4.2704	2.5856
2.70	4.1602	2.6228
2.75	4.0671	2.6589
2.80	3.9874	2.6939
2.85	3.9186	2.7280
2.90	3.8586	2.7610
2.95	3.8061	2.7931
3.00	3.7598	2.8243
3.10	3.6821	2.8840
3.20	3.6198	2.9403
3.30	3.5691	2.9935
3.40	3.5274	3.0436
3.50	3.4926	3.0909
3.70	3.4386	3.1779
3.90	3.3992	3.2555

Table B.2 MIXED RESULTS (1110)

	γ	$\|Ted\|_2$	$\|Ted\|_\infty$
γ_0	2.1426		
	2.15	27.6012	2.1502
	2.16	17.9685	2.1600
	2.17	14.3460	2.1701
	2.18	12.2802	2.1800
	2.19	10.9172	2.1900
	2.20	9.9325	2.2000
	2.21	9.1785	2.2100
	2.22	8.5782	2.2200
	2.23	8.0863	2.2300
	2.24	7.6743	2.2400
	2.25	7.3231	2.2500
	2.26	7.0209	2.2600
	2.27	6.7576	2.2700
	2.28	6.5193	2.2800
	2.29	6.3104	2.2900
	2.30	6.1423	2.3000
	2.32	5.8002	2.3200
	2.34	5.5319	2.3400
	2.36	5.3050	2.3600
	2.38	5.1100	2.3800
	2.40	4.9425	2.4000
	2.42	4.7945	2.4200
	2.44	4.6645	2.4400
	2.46	4.5489	2.4600
	2.50	4.3536	2.5000
	2.55	4.1601	2.5500
	2.60	4.0075	2.6000
	2.65	3.8850	2.6500
	2.70	3.7852	2.7000

Table B.2 cont.

γ	$\|Ted\|_2$	$\|Ted\|_\infty$
2.75	3.7030	2.7500
2.80	3.6345	2.8000
2.85	3.5770	2.8500
2.90	3.5280	2.9000
2.95	3.4863	2.9500
3.0	3.4506	3.0000
3.1	3.3936	3.0999
3.2	3.3520	3.1998
3.3	3.3203	3.3000
3.4	3.2969	3.4000
3.5	3.2798	3.4999
3.7	3.2594	3.6999
3.9	3.2502	3.9273

Table B.3 B & H Results (1I2O)

$\|T_{ew}\|_\infty$	$\|T_{zw}\|_2$
.2371	1.7908
.2574	1.3401
.2776	1.0675
.2977	.0936
.3179	.8011
.3382	.7327
.3585	.6837
.3787	.6464
.3988	.6168
.4188	.5926
.4386	.5722
.4582	.5548
.4776	.5397
.4967	.5263
.5156	.5145
.5342	.5039
.5525	.4944
.5706	.4858
.5883	.4781
.6058	.4710
.6411	.4583
.6478	.4561
.6488	.4558
.6526	.4546
.6593	.4525
.6631	.4513
.6640	.4510
.6677	4499

Table B.3 cont.

$\|T_{ew}\|_\infty$	$\|T_{zw}\|_2$
.6745	.4479
.7119	.4378
.7684	.4250
.8220	.4151
.8712	.4075
.9270	.4004
.9750	.3954
1.0254	.3910
1.0676	.3880
1.1099	.3855
1.1481	.3836
1.1839	.3821
1.2137	.3811
1.2400	.3804
1.2631	.3799
1.2830	.3795
1.3002	.3792
1.3140	.3790
1.3268	.3789
1.3376	.3788
1.3466	.3787
1.3542	.3787
1.3606	.3786
1.3659	.3786
1.3704	.3786
1.3741	.3786
1.3772	.3786
1.3797	.3786
1.3819	.3786